REPORT NO.
NASA-CR-54360
WESTINGHOUSE
WAED 66.63E
SEPTEMBER 1966

DEVELOPMENT AND EVALUATION OF MAGNETIC AND ELECTRICAL MATERIALS CAPABLE OF OPERATING IN THE 800° TO 1600°F TEMPERATURE RANGE

Seventh Quarterly Report

edited by
P. E. Kueser

prepared for

NATIONAL AERONAUTICS AND SPACE ADMINISTRATION
LEWIS RESEARCH CENTER
UNDER CONTRACT NAS3-6465

Westinghouse Electric Corporation
AEROSPACE ELECTRICAL DIVISION
LIMA, OHIO

Report No. 66.63E

March 1966

DEVELOPMENT AND EVALUATION OF MAGNETIC AND ELECTRICAL MATERIALS CAPABLE OF OPERATING IN THE 800° TO 1600°F TEMPERATURE RANGE

SEVENTH QUARTERLY REPORT
(JUNE 1, 1966 - AUGUST 31, 1966)

sponsored by

NATIONAL AERONAUTICS AND SPACE ADMINISTRATION
CONTRACT NAS3-6465

Project Management
NASA - Lewis Research Center
Space Power Systems Division
R. A. Lindberg

Prepared by:

P. E. Kueser, et al
Manager, NASA Materials Study
and Research Program

Approved by:

N. W. Bucci, Jr.
Manager, Engineering
Systems Research and
Development Department

Westinghouse Electric Corporation
Aerospace Electrical Division
Lima, Ohio

PREFACE

The work reported here was sponsored by the Space Power Systems Division of the NASA Lewis Research Center under Contract NAS3-6465. Mr. R. A. Lindberg of NASA has provided the Project Management for the program. His review and suggestions as well as those of Mr. T. A. Moss, also of NASA, are gratefully acknowledged. The Westinghouse Aerospace Electrical Division (WAED) is responsible for the over-all Technical Direction of the program. The Westinghouse Research and Development Center (WR&D) is conducting Tasks 1, 2, and 4 of Program I on Optimized Magnetic Materials for Application in the 1000° to 1200°F Range, the Investigation for Raising the Alpha to Gamma Transformation, and Creep Testing of Rotor Materials. Eitel-McCullough (EIMAC) is responsible for the Bore Seal Development, Task 1 of Program III. All other tasks are being conducted at the Westinghouse Aerospace Electrical Division (WAED).

In a program of this magnitude a large group of engineers and scientists are involved in its progress. An attempt to recognize those who are contributing directly, together with their area of endeavor, follows:

Program I - Magnetic Materials for High-Temperature Operation

Task 1 - Optimized Precipitation Hardened Magnetic Materials for Application in the 1000° to 1200°F Range

Dr. K. Detert (WR&D); J. W. Toth (WAED)

Task 2 - Investigation for Raising the Alpha to Gamma Transformation Temperature in Cobalt-Iron Alloys

Dr. K. Detert (WR&D); J. W. Toth (WAED)

Task 3 - Dispersion-Strengthened Magnetic Materials for Application in the 1200° to 1600°F Range

Dr. R. J. Towner (WAED)

Task 4 - Creep Testing

M. Spewock (WR&D); D. H. Lane (WAED)

Program II - High Temperature Capacitor Feasibility

R. E. Stapleton (WAED)

Program III - Bore Seal Development and Combined Material Investigation Under a Space Simulated Environment

Task 1 - Bore Seal Development

R. C. McRae, Dr. L. Reed, M. F. Parkman (EIMAC); J. W. Toth (WAED)

Tasks 2, 3, 4 - Stator and Bore Seal, Transformer and Solenoid

W. L. Grant, H. E. Keneipp, D. H. Lane, R. P. Shumate, J. W. Toth (WAED)

Dr. A. C. Beiler (WAED) and Dr. G. W. Wiener (WR&D) are acting as consultants on Program I.

SUMMARY

This is the seventh quarterly report on Contract NAS3-6465 for the Development and Evaluation of Magnetic and Electrical Materials Capable of Operating in the Temperature Range from 800° to 1600°F. Advanced space electric power systems are the area of eventual application.

Program I is directed at developing high-temperature magnetic materials with satisfactory strength for use in the solid rotors of electrical generators. The precipitation strengthened materials selected for evaluation from 15-pound ingots have resulted in alloys which have yield strength and tensile strength considerably higher than commercially available high-temperature rotor materials such as H-11 or cobalt-base Nivco alloys. Dispersion-strengthening on cobalt-iron and cobalt-base alloys has resulted in the identification of compositions which have better creep resistance and saturation magnetization at 1400°F than the precipitation hardened magnetic materials. These data together with that obtained on the precipitation strengthened alloys indicate that both types of mechanisms are important to the rotor materials of Advanced Space Electric Power Systems. The precipitation hardening providing the strength below approximately 1300°F and the dispersion strengthening mechanism above that temperature. Creep testing has continued on the Nivco alloy. Four specimens are still on test with the longest time approaching 9000 hours and the vacuum now at 1×10^{-9} torr with an extension of 0.95 percent at 1100°F and 37,500 psi.

Program II will determine the feasibility of high-temperature capacitors using high quality dielectric materials. The program has been completed with a satisfactory endurance test of 1000 hours. The change in the capacitor losses is the apparent result of a slight separation of the electrodes. This is believed to have been caused by the inter-electrode diffusion bonding between adjacent wafers.

Program III incorporates developments on alkali-metal compatible ceramic-to-metal seals and combinations of material designed into a stator with a bore seal, a transformer and a solenoid for investigations of compatibility under electrical and magnetic stresses at elevated temperature and under high vacuum. The endurance tests were completed on the stator, transformer, and solenoid at 1100°F hot spot temperature. At the end of the 5000-hour test the stator chamber pressure was at 3.5×10^{-9} torr. The transformer and solenoid test chambers also at a 1100°F hot spot temperature after 5000 hours was at 6.1×10^{-9} torr. The electrical conductor and

electrical insulation systems and all components showed no signs of deterioration during this test period.

TABLE OF CONTENTS

TABLE OF CONTENTS - Continued

TABLE OF CONTENTS - Concluded

LIST OF FIGURES

LIST OF FIGURES - Continued

LIST OF FIGURES - Concluded

LIST OF TABLES

SECTION I

INTRODUCTION

This is the seventh quarterly report on Contract NAS3-6465 for the Development and Evaluation of Magnetic and Electrical Materials Capable of Operating in the Temperature Range from 800° to 1600°F. The period of performance is from June 1, 1966 through August 31, 1966. The program consists of three Programs with their related tasks as follows:

Program I - Magnetic Materials for High-Temperature Operation

- Task 1 - Optimized Precipitation Hardened Magnetic Materials for Application in the 1000° to 1200°F Range
- Task 2 - Investigation for Raising the Alpha to Gamma Transformation Temperature in Cobalt-Iron Alloys (completed)
- Task 3 - Dispersion-Strengthened Magnetic Materials for Application in the 1200° to 1600°F Range
- Task 4 - Creep Testing

Program II - High-Temperature Capacitor Feasibility

Program III - Bore Seal Development and Combined Material Investigation Under a Space Simulated Environment

- Task 1 - Bore Seal Development
- Task 2 - Stator and Bore Seal
- Task 3 - Transformer
- Task 4 - Solenoid

In Program I, limitations in magnetic material performance at elevated temperature have been recognized from Contract NAS3-4162 and the development of materials incorporating improved magnetic and mechanical properties is being pursued. In most cases, high-strength compromises the magnetic properties; therefore, a balance between these two variables is sought.

Program II is directed at determining the feasibility of applying high-quality dielectric materials and their processes to a high-temperature (1100° F) capacitor which is lightweight and suitable for static power conditioning apparatus used in space applications.

Program III incorporates development on ceramic-to-metal seals and on combinations of materials previously evaluated under Contract NAS3-4162 into a stator with a bore seal, a transformer, and a solenoid for investigations of compatibility under electrical and magnetic stress at elevated temperature and high vacuum.

The three Programs will be reported consecutively in Sections II, III, and IV. Section II and Section IV are further divided into their respective tasks. Each task is reported separately and includes a summary of technical progress, a discussion, and the program for the next quarter so the reader may obtain an understanding of each task.

The first through the sixth quarterly reports were issued as NASA-CR-54354, through 54359. These reports are extensively referenced in this report and fully titled in Section V. Other references identified by number in the discussion of each task are contained in Section V. These are identified in Section V by the program and task for which the reference is applicable.

SECTION II

PROGRAM I - MAGNETIC MATERIALS FOR HIGH-TEMPERATURE OPERATION

Program I is directed at improvement and further understanding of magnetic materials suitable for application in the rotor of a generator or motor in advanced space electric power systems.

Task 1 is concerned with precipitation-hardened magnetic materials in the 1000° to 1200°F range. These materials are of the iron-cobalt-nickel ternary system. The two specific areas of interest are the iron and cobalt corners of the ternary system.

Task 2 is a small research investigation for determining the feasibility of raising the alpha to gamma transformation temperature in the iron-cobalt system; thereby increasing the useful magnetic temperature of this system. This investigation is completed and the final results were given in the third quarterly report. Selected alloy additions of three to five weight percent increased the transformation temperature approximately 9°F (5°C) for each weight percent added. Magnetic saturation was lowered by each addition. If only a 45°F increase in alpha to gamma transformation temperature is desired, at a slight sacrifice in magnetic saturation, several alloying agents are satisfactory.

Task 3 is directed at applying dispersion-strengthening mechanisms to magnetic materials to achieve useful and relatively invariant mechanical and magnetic properties in the 1200° to 1600°F range. Because both variables are influenced differently by particle size and spacing, a compromise is sought thereby tailoring the materials to the need of dynamic electric machines.

Task 4 is a creep program on Nivco alloy (approximately 72 percent cobalt, 23 percent nickel, and certain other elements) which will generate 5000- and 10,000-hour design data in a vacuum environment (1×10^{-6} torr or less). This material represents a presently available magnetic material with the highest useful application temperature for stressed applications.

A. TASK 1 - OPTIMIZED PRECIPITATION HARDENED MAGNETIC MATERIALS FOR APPLICATIONS IN THE 1000° TO 1200°F RANGE

1. Summary of Technical Progress

a) The evaluation of the final alloys, martensitic alloy 1-A-S-2 (Fe-12Ni-30Co-3Ta-1W-0.4Al-0.4Ti) and cobalt-base alloy 1-B-S-1 (Co-15Ni-5Fe-1.3Al-5Ta-0.2Zr), was started during this quarter.

b) Change in electrical resistivity, coercive force, and hardness were measured during isothermal aging to 1000 hours. The results indicate that sufficient stability can be expected up to 1022°F (550°C) in the martensitic alloy and to 1292°F (700°C) in the cobalt-base alloy.

c) The yield strength and tensile strength of these alloys were measured at room temperature and at 1112°F (600°C). The high-temperature strength was considerably higher than comparable commercially available high-temperature rotor materials such as H-11 alloy and cobalt-base Nivco alloy.

d) The a-c and d-c magnetic properties were determined on ring specimens at room temperature and elevated temperature. The magnetic properties were considerably better than H-11 alloy or Nivco alloy.

2. Discussion

The objective of this program is to find and evaluate precipitation hardened alloy compositions which display high creep strength and useful ferromagnetic properties at temperatures in the range of 1000° to 1200°F.

The target ultimate tensile strength for the alloy at 1100°F is 125,000 psi or better. The target stress to produce 0.4 percent creep strain in 1000 hours at 1100°F is 76,000 psi or greater. The 10,000-hour stress target at 1100°F is 80 to 90 percent of that at 1000 hours. The target magnetic saturation for the developmental alloy is 13,000 gauss or better at 1100°F and a coercive force less than 25 oersteds.

An alloy screening program was conducted as the first step in attaining this goal. The purpose of the screening program was to find a

certain region of alloy composition where the combination of desirable mechanical and magnetic properties could be attained. Vickers hardness tests, coercivity measurements and saturation measurements after a suitable heat treatment, and dilatometer tests were conducted to provide pertinent data and to determine the thermal stability of the alloy structure. Details of the test methods and test results were reported in the first five quarterly reports.

The reasons for selecting martensitic alloy 1-A-S-2 (Fe-12Ni-30Co-3Ta-1W-0.4Al-0.4Ti) and cobalt-base alloy 1-B-S-1 (Co-15Ni-5Fe-1.3Al-5Ta-0.2Zr) were outlined in the sixth quarterly report. The alloys were vacuum induction melted as 15-pound ingots to provide sufficient material for tensile, creep, and magnetic tests.

The chemical analyses and processing of the ingots into 60-mil sheet were reported in the sixth quarterly report.

a. EXPERIMENTAL PROCEDURE

The dilatometer technique used in determining the thermal expansion of specimens from the final alloys was described in the first quarterly report. The method used in obtaining tensile data on sheet specimens was reported in the sixth quarterly report.

In order to produce the laminations for the magnetic test rings, 60-mil-thick sheet was annealed for one hour at 1922°F (1050°C) in helium and then cross rolled to 44-mil thickness to obtain the required 3-1/2-inch-wide strip. At this stage the martensitic alloy strips were annealed at 1832°F (1000°C) for one hour in a helium atmosphere. The 44-mil strips were then straight rolled in the original rolling direction to a thickness of 26 mils. The strips were then annealed for one hour at 2012°F (1100°C) in helium and cold rolled to the final thickness of 25 mils. Rings having an outer diameter of three inches and an inner diameter of 2.5 inches were punched from the strip. Nine rings from martensitic alloy 1-A-S-2 were aged three hours at 1022°F in helium before testing. Ten rings punched from the cobalt-base alloy 1-B-S-1 were annealed one hour at 2012°F (1100°C) and aged one hour at 1382°F (750°C) in helium before magnetic testing.

The laminations were stacked and wound with Anadur insulated nickel-clad silver wire. The d-c and a-c properties were de-

termined according to a modified testing procedure specified in ASTM A341 and A343.

The major part of this quarterly report concerns a kinetics study of the precipitation process as manifested by a change in properties. Change in hardness, coercive force, and electrical resistivity were measured during isothermal aging at several temperatures for periods to 1000 hours. Prior to testing, the martensitic alloys were given a one-hour homogenization and austenitizing anneal at 1832°F (1000°C) in a helium-flushed tube furnace. The samples were brought to room temperature in the water-cooled portion of the furnace. The cooling rate was a moderate 54°F (30°C) per minute. The subsequent aging was done in neutral salt baths containing the appropriate mixture of nitrites and nitrates or chlorides according to the required aging temperature. This was described in the second quarterly report. The temperature of the baths was maintained within 9°F (5°C). The properties were always measured at room temperature; therefore, the isothermal aging was interrupted for the test. Previous experience had shown that this interruption for the test did not produce any noticeable difference in the rate of change or in the absolute values of properties when measured at the same time and temperature (refs. 1 and 2).

This result was confirmed by a few spot checks. In some cases, different test samples were used for measuring the change of properties at various times. The measured values coincided within the limit of accuracy in spite of the fact that the time sequence for the test was different. These checks on different samples also confirmed reproducibility in the case of martensitic alloys. However, reproducibility in different samples of cobalt-base alloy was poor because of inhomogeneities in the alloy.

Hardness was measured as the Vickers hardness number under a load of 50 kg. The accuracy was two percent. The coercive force was measured in a Foerster "Koerzimeter" as previously outlined (second quarterly report) with an accuracy of two percent. The electric resistivity was measured on strips about 2.5-mm wide, 0.5-mm thick, and 150-mm long by the standard four-blade resistance method. The temperature was kept constant at 77°F (25°C) within ± 0.18°F (0.1°C) by means of a coolant loop and a heater attached to a thermostat. The accuracy

in determining specific resistivity was two percent, with the limitation set by the cross section measurements.

b. RESULTS

The data obtained from tensile tests are shown in table II-1. The ferritic alloys have considerably higher strength at 1112°F (600°C) than the cobalt-base alloys. However, they are brittle at room temperature. These data also show the effect of a different heat treatment on the tensile strength of cobalt-base alloy 1-B-S-1. Test data from commercially available alloys of similar type such as H-11 alloy, 15 percent nickel maraging steel, and Nivco alloy are also listed in table II-1 for comparison (ref. 3). One can see the improvement of high temperature strength obtained in the experimental alloys. Alloy 1-B-S-1 tested at 1100°F after aging one hour at 1380°F and ten hours at 1200°F shows a ten percent improvement in strength over Nivco alloy. Table II-2 and II-3 show the magnetic test data. These data are also compared to data obtained previously (ref. 3) on alloys such as H-11 and Nivco. Again, one sees that considerable improvement of the high temperature properties has been achieved in the experimental alloys.

Test results of property changes during isothermal aging are shown in figures II-1 through II-6. The plot of hardness change for alloy 1-A-S-2 in figure II-1 shows that sufficient overaging to drop the room temperature hardness below 500 VHN occurs only at temperatures in excess of 1022°F (550°C). The measured change of coercive force (figure II-2) indicates a considerable increase (~60 oersteds) at an aging time of 1000 hours at 1022°F (550° C). The electrical resistivity decreases (figure II-3) during aging as one expects for a precipitation process. If a noticeable amount of reverted austenite had formed, one would expect the electrical resistivity to increase again after prolonged aging as had been observed in 15 percent nickel maraging steel (figure II-4). One may therefore conclude that no measurable amount of reverted austenite formed in the present martensitic alloy during aging as high as 1202°F (650°C) within the measured periods of time.

The plot of change of hardness for the cobalt-base alloy 1-B-S-1 in figure II-5 shows that sufficient overaging to drop the room temperature hardness below 300 VHN occurs within 1000 hours only at temperatures of 1292°F (700°C) or higher. The plot of the

TABLE II-1. Tensile Test Data of 300 Gram Vacuum Arc Melted Martensitic Alloys 1-A-S-1 and 1-A-S-2, and Cobalt Alloys 1-B-S-1 and 1-B-S-2

Alloy Number	Nominal Alloy Composition (weight percent)	Room Temperature Hardness 50 kg Load VHN	Temperature °F	Temperature °C	0.2% Yield Strength (psi)	Ultimate Tensile Strength (psi)	Uniform Elongation (percent)	Reduction of Area (percent)
Martensitic Alloys								
1-A-S-1[a]	Fe-15Ni-30Co-1W-3Ta-0.3Al-0.4Ti-0.003Zr-0.001B	-	77	25	Specimen failed at 182 000 psi with no elongation			
1-A-S-2[a]	Fe-12Ni-30Co-1W-3Ta-0.4Al-0.4Ti-0.003Zr-0.001B	-	77	25	Specimen failed at 182 000 psi with no elongation			
1-A-S-1[a]	Fe-15Ni-30Co-1W-3Ta-0.3Al-0.4Ti-0.003Zr-0.001B	674	1112	600	139 000	165 200	6.0	4.8
1-A-S-1[a]	Fe-15Ni-30Co-1W-3Ta-0.3Al-0.4Ti-0.003Zr-0.001B	669	1112	600	130 000	164 800	9.0	20.8
1-A S-2[a]	Fe-12Ni-30Co-1W-3Ta-0.4Al-0.4Ti-0.003Zr-0.001B	671	1112	600	141 700	169 000	2.0	0.8
1-A-S-2[a]	Fe-12Ni-30Co-1W-3Ta-0.4Al-0.4Ti-0.003Zr-0.001B	666	1112	600	158 700	171 000	3.5	2.4
For Comparison:								
H-11 Alloy[b]	Fe-5Cr-1.3Mo-0.5V-0.4C	-	77	25	180 000	215 000	15.2	29.0
H-11 Alloy[b]	Fe-5Cr-1.3Mo-0.5V-0.4C	-	800	427	144 000	174 000	15.0	40.0
15%Ni Maraging Steel[c]	Fe-9Co-15Ni-5Mo-0.7Al-0.7Ti	613	77	25	282 000	296 000	4.9	31.7
15%Ni Maraging Steel[c]	Fe-9Co-15Ni-5Mo-0.7Al-0.7Ti	619	1112	600	110 000	117 000	10.5	61.5
Cobalt-Base Alloys								
1-B-S-1[d]	Co-15Ni-5Fe-5Ta-1.25Al-0.2Zr-0.001B	316	77	25	105 500	152 800	33.0	39.4
1-B-S-1[d]	Co-15Ni-5Fe-5Ta-1.25Al-0.2Zr-0.001B	318	77	25	108 500	153 600	33.0	39.4
1-B-S-2[d]	Co-15Ni-5Fe-5Ta-1.25Al-0.1Zr-0.1Be-0.001B	321	77	25	105 400	154 700	33.6	42.5
1-B-S-2[d]	Co-15Ni-5Fe-5Ta-1.25Al-0.1Zr-0.1Be-0.001B	319	77	25	104 200	153 600	33.8	41.7
1-B-S-1[d]	Co-15Ni-5Fe-5Ta-1.25Al-0.2Zr-0.001B	323	1112	600	88 700	125 600	19.0	24.8
1-B-S-1[d]	Co-15Ni-5Fe-5Ta-1.25Al-0.2Zr-0.001B	329	1112	600	87 100	126 800	18.0	20.8
1-B-S-2[d]	Co-15Ni-5Fe-5Ta-1.25Al-0.1Zr-0.1Be-0.001B	325	1112	600	89 500	123 800	19.5	32.0
1-B-S-2[d]	Co-15Ni-5Fe-5Ta-1.25Al-0.1Zr-0.1Be-0.001B	322	1112	600	86 400	122 800	20.5	37.6
1-B-S-1[e]	Co-15Ni-5Fe-5Ta-1.25Al-0.2Zr-0.001B	351	77	25	114 300	166 400	23.6	39.3
1-B-S-1[e]	Co-15Ni-5Fe-5Ta-1.25Al-0.2Zr-0.001B	358	1112	600	99 200	132 000	13.6	20.5
1-B-S-1[e]	Co-15Ni-5Fe-5Ta-1.25Al-0.2Zr-0.001B	354	1202	650	85 900	117 300	10.0	14.2
For Comparison:								
Nivco Alloy[b]	Co-23Ni-1Zr-2Ti	-	77	25	112 400	165 400	30.7	43.6
Nivco Alloy[b]	Co-23Ni-1Zr-2Ti	-	1100	593	89 900	124 600	24.3	47.0

(a) Sheet specimens annealed one hour at 1832°F(1000°C) and aged one hour at 1112°F(600°C) before testing.
(b) Round bar specimens. Data from Magnetic Materials Topical Report by P. E. Kueser et al, NASA-CR-54091, Contract NAS3-4162.
(c) Sheet specimens; source same as note (b).
(d) Sheet specimens annealed one hour at 1832°F(1000°C) and aged one hour at 1382°F(750°C) before testing.
(e) Sheet specimens annealed one hour at 1832°F(1000°C); then aged one hour at 1382°F(750°C) and 10 hours at 1202°F(650°C) before testing.

TABLE II-2. Magnetic Properties of Ferritic Alloy 1-A-S-2[a]

DC Properties							
Alloy Number	Test Temperature (°F)	Test Temperature (°C)	Induction at Magnetizing Force Indicated (kilogauss) 10 Oe	100 Oe	250 Oe	Coercive Force from 200 Oe (oersteds)	Residual Induction at Magnetizing Force of 200 Oe (kilogauss)
1-A-S-2	77	25	--	14.4	18.2	27.3	9.07
1-A-S-2	1004	540	--	14.0	16.8	20.1	8.25
1-A-S-2	1103	595	--	13.6	16.2	22.2	8.20
For Comparison							
H-11 Alloy[b]	77	25	--	16.2	17.9	23.1	11.75
H-11 Alloy[b]	1103	595	--	12.5	13.0	14.1	7.35

AC Properties								
Alloy Number	Induction (kilogauss)	Frequency (cps)	Core Loss (watts per pound)	Apparent Core Loss (exciting volt-amps per pound)	Core Loss (watts per pound)	Apparent Core Loss (exciting volt-amps per pound)	Core Loss (watts per pound)	Apparent Core Loss (exciting volt-amps per pound)
			At 77°F (25°C)		At 1004°F (540°C)		At 1103°F (595°C)	
1-A-S-2	10	60	19.73	38.04	14.90	32.75	15.59	32.25
1-A-S-2	15	60	31.20	139.0	19.77	182.0	19.99	195.0
1-A-S-2	10	400	156.0	276.0	110.0	233.0	111.0	241.0
1-A-S-2	15	400	252.0	940.0	162.0	950.0	162.0	1010.0
For Comparison								
H-11 Alloy[b]	10	400	115.0	179.0	--	--	87.0	185.0

(a) Test specimen consisted of 0.025 inch thick rings (3 inch O.D. by 2-1/2 inch I.D.) which had been annealed one hour at 2012°F(1100°C) cold rolled (5% reduction) and then aged 3 hours at 1022°F(550°C) before testing.

(b) Data from Magnetic Materials Topical Report by P. E. Kueser et al, NASA-CR-54091, Contract NAS3-4162, 1964.

TABLE II-3. Magnetic Properties of Cobalt-Base Alloy 1-B-S-2[a]

DC Properties

Alloy Number	Test Temperature (°F)	Test Temperature (°C)	Induction at Magnetizing Force Indicated (kilogauss) 10 Oe	100 Oe	250 Oe	Coercive Force from 200 Oe (oersteds)	Residual Induction at Magnetizing Force of 200 Oe (kilogauss)
1-B-S-2	77	25	9.6	12.8	14.0	2.43	5.8
1-B-S-2	1004	540	8.8	10.9	12.0	0.88	7.8
1-B-S-2	1103	595	8.3	10.3	11.3	0.72	7.8
1-B-S-2	1202	650	8.3	10.3	11.3	0.72	8.3
For Comparison							
Nivco Alloy[b]	77	25	1.0	10.9	13.6	35.5	8.0
Nivco Alloy[b]	1103	595	2.0	10.3	11.6	20.9	7.8

AC Properties

Alloy Number	Induction (kilogauss)	Frequency (cps)	Core Loss (watts per pound)	Apparent Core Loss (exciting volt-amps per pound)	Core Loss (watts per pound)	Apparent Core Loss (exciting volt-amps per pound)	Core Loss (watts per pound)	Apparent Core Loss (exciting volt-amps per pound)	Core Loss (watts per pound)	Apparent Core Loss (exciting volt-amps per pound)
			At 77°F (25°C)		At 1004°F (540°C)		At 1103°F (595°C)		At 1202°F (650°C)	
1-B-S-2	6	60	1.31	2.72	0.67	1.29	0.56	0.86	0.55	0.86
1-B-S-2	6	400	16.80	23.74	8.10	11.25	7.98	9.12	7.74	8.66
For Comparison										
Nivco Alloy[b]	6	400	80.0	149.0	--	--	41.3	77.0	--	--

(a) Test specimen consisted of 0.025 inch thick rings (3 inch O.D. by 2-1/2 inch I.D.) which had been annealed one hour at 2012°F (1100°C) and then aged one hour at 1382°F (750°C).

(b) Data from Magnetic Materials Topical Report by P. E. Kueser et al, NASA-CR-54091, Contract NAS3-4162, 1964.

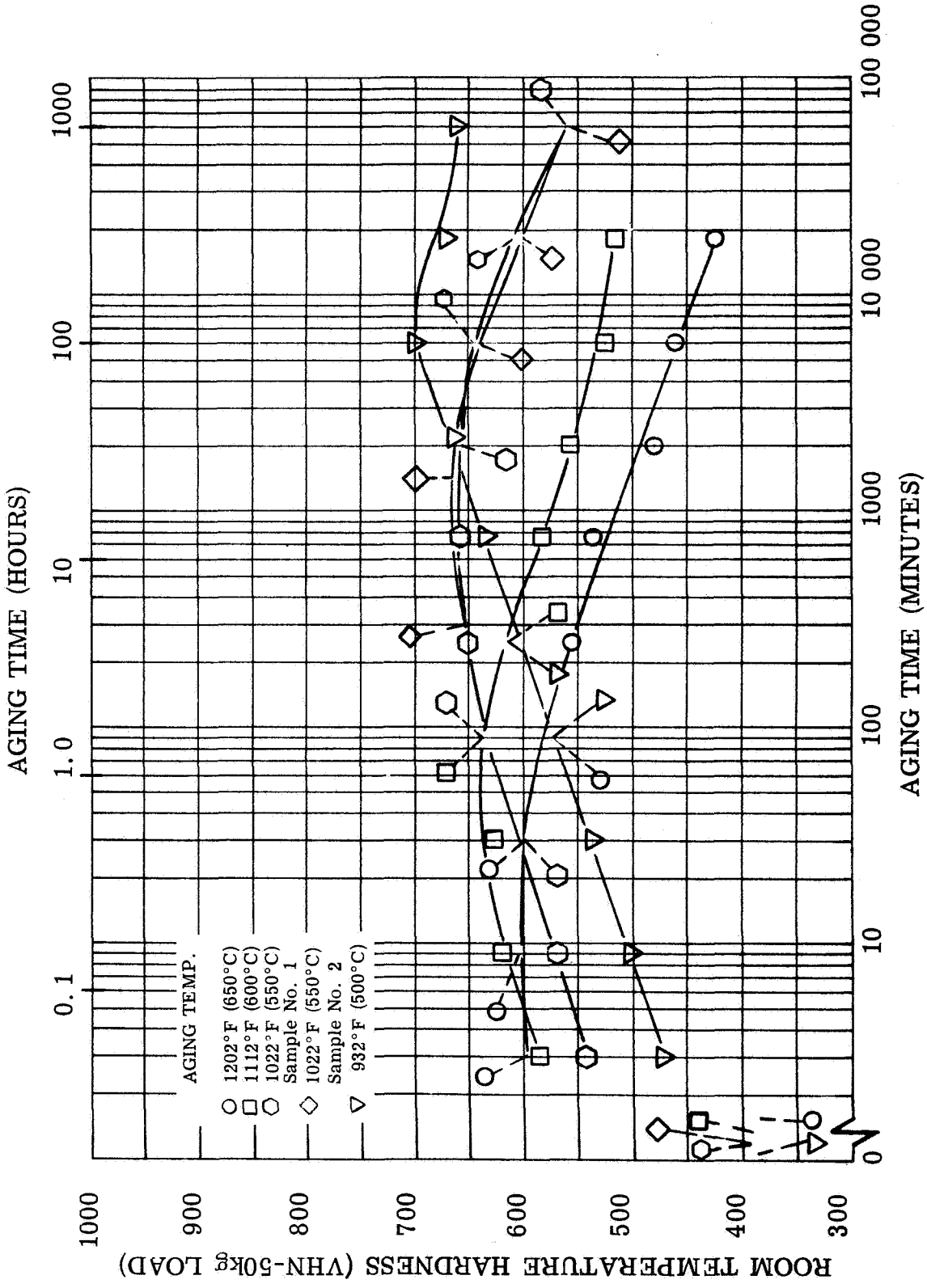

FIGURE II-1. Change in Room Temperature Hardness of Alloy 1-A-S-2 (Fe-12Ni-30Co-1W-3Ta-0.4Al-0.4Ti-0.003Zr-0.001B) During Isothermal Aging at Various Temperatures

Figure II-1. Hardness of Alloy 1-A-S-2 During Isothermal Aging at Various Temperatures

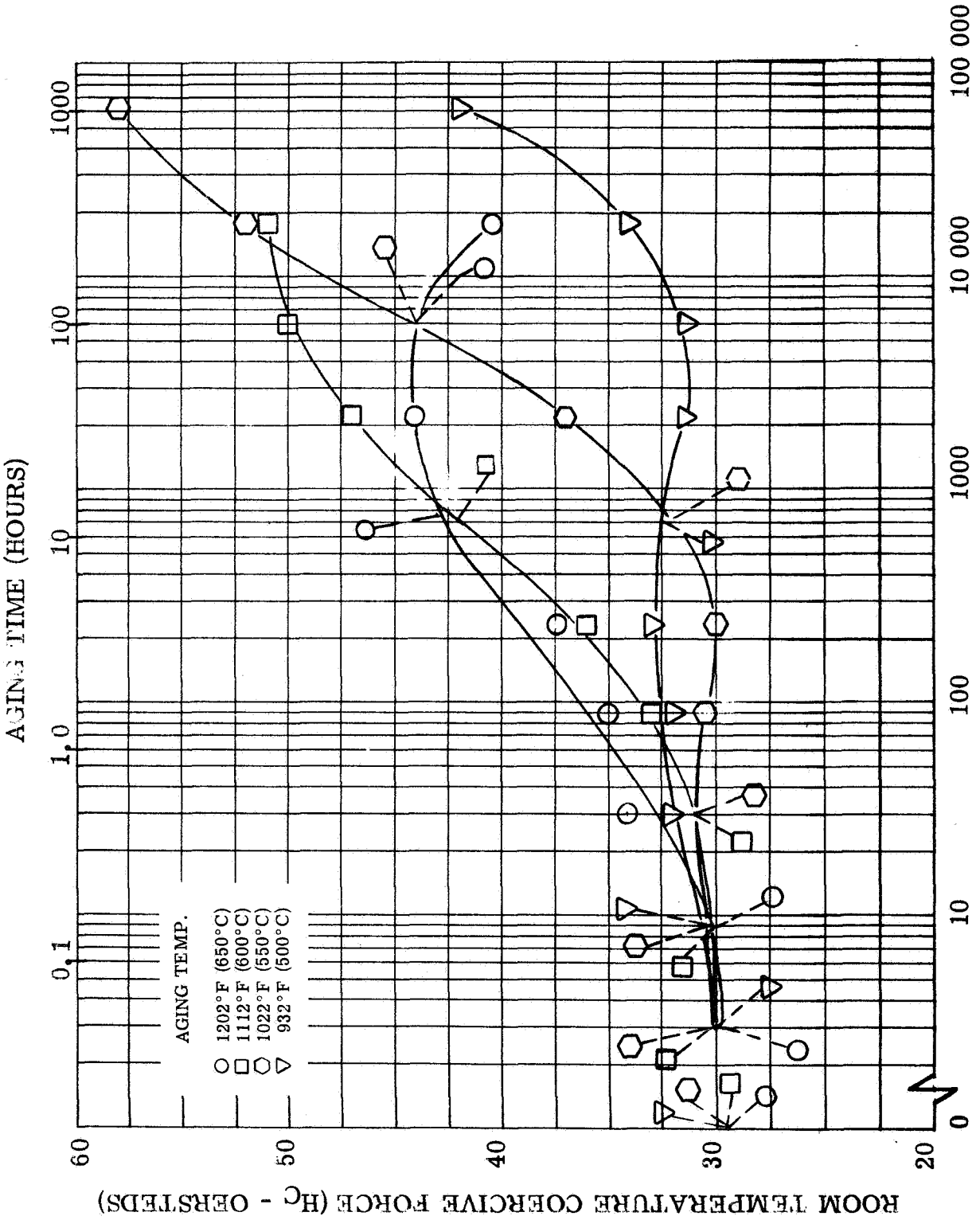

FIGURE II-2. Change in Room Temperature Coercive Force of Alloy 1-A-S-2 (Fe-12Ni-30Co-1W-3Ta-0.4Al-0.4Ti-0.003Zr-0.001B) During Isothermal Aging at Various Temperatures

Figure II-2. Coercive Force of Alloy 1-A-S-2 During Isothermal Aging at Various Temperatures

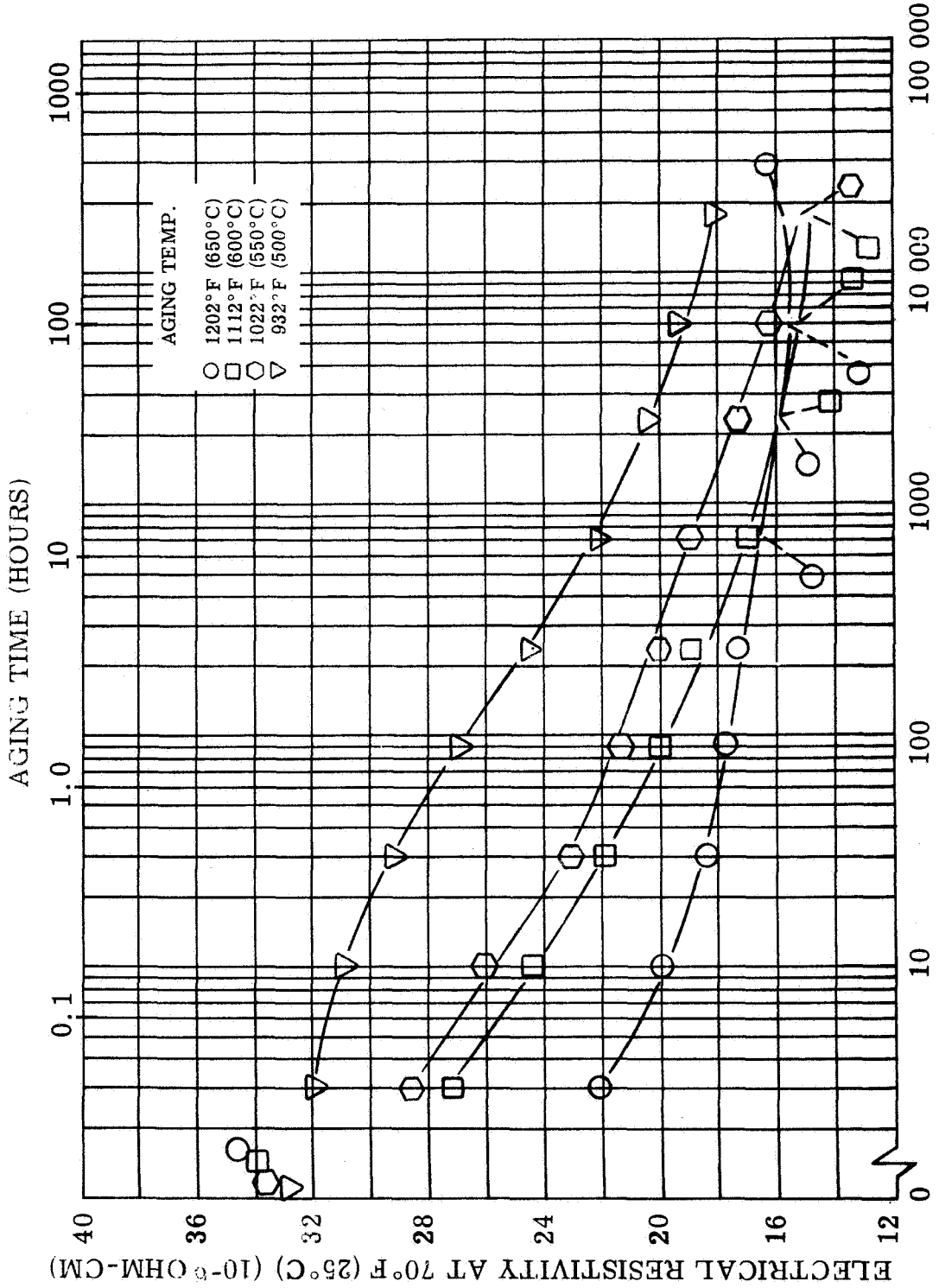

FIGURE II-3. Change in Room Temperature Electrical Resistivity of Alloy 1-A-S-2 (Fe-12Ni-30Co-1W-3Ta-0.4Al-0.4Ti-0.003Zr-0.001B) During Isothermal Aging at Various Temperatures

Figure II-3. Electrical Resistivity of Alloy 1-A-S-2 During Isothermal Aging at Various Temperatures

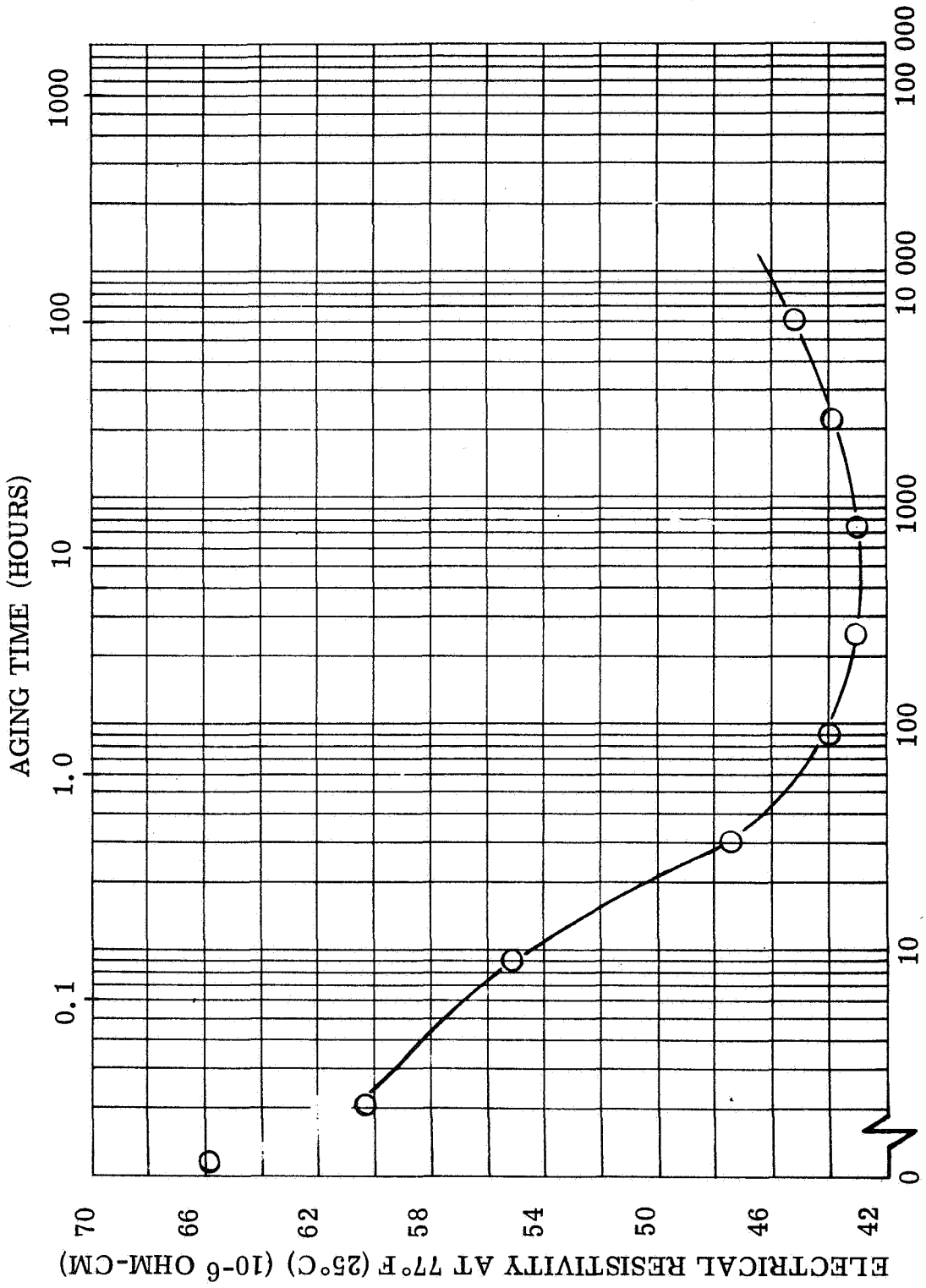

FIGURE II-4. Change in Room Temperature Electrical Resistivity of 15% Ni Maraging Steel (Fe-9Co-15Ni-5Mo-0.7Al-0.7Ti) During Isothermal Aging at 1112°F (600°C)

Figure II-4. Electrical Resistivity of 15% Ni Maraging Steel During Isothermal Aging at 1112°F (600°C)

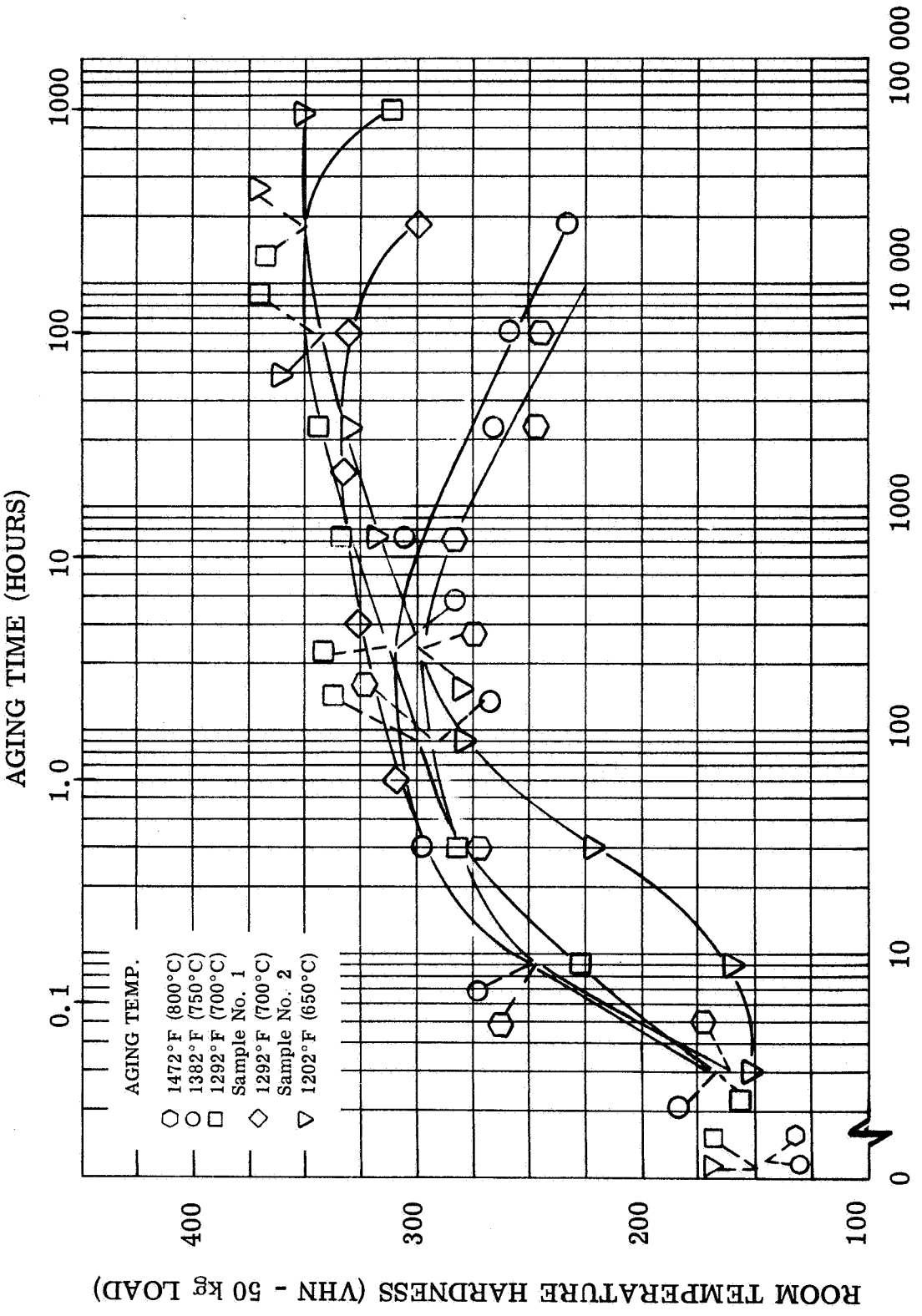

FIGURE II-5. Change in Room Temperature Hardness of Alloy 1-B-S-1 (Co-15Ni-5Fe-5Ta-1.25Al-0.2Zr-0.001B) During Isothermal Aging at Various Temperatures

Figure II-5. Hardness of Alloy 1-B-S-1 During Isothermal Aging at Various Temperatures

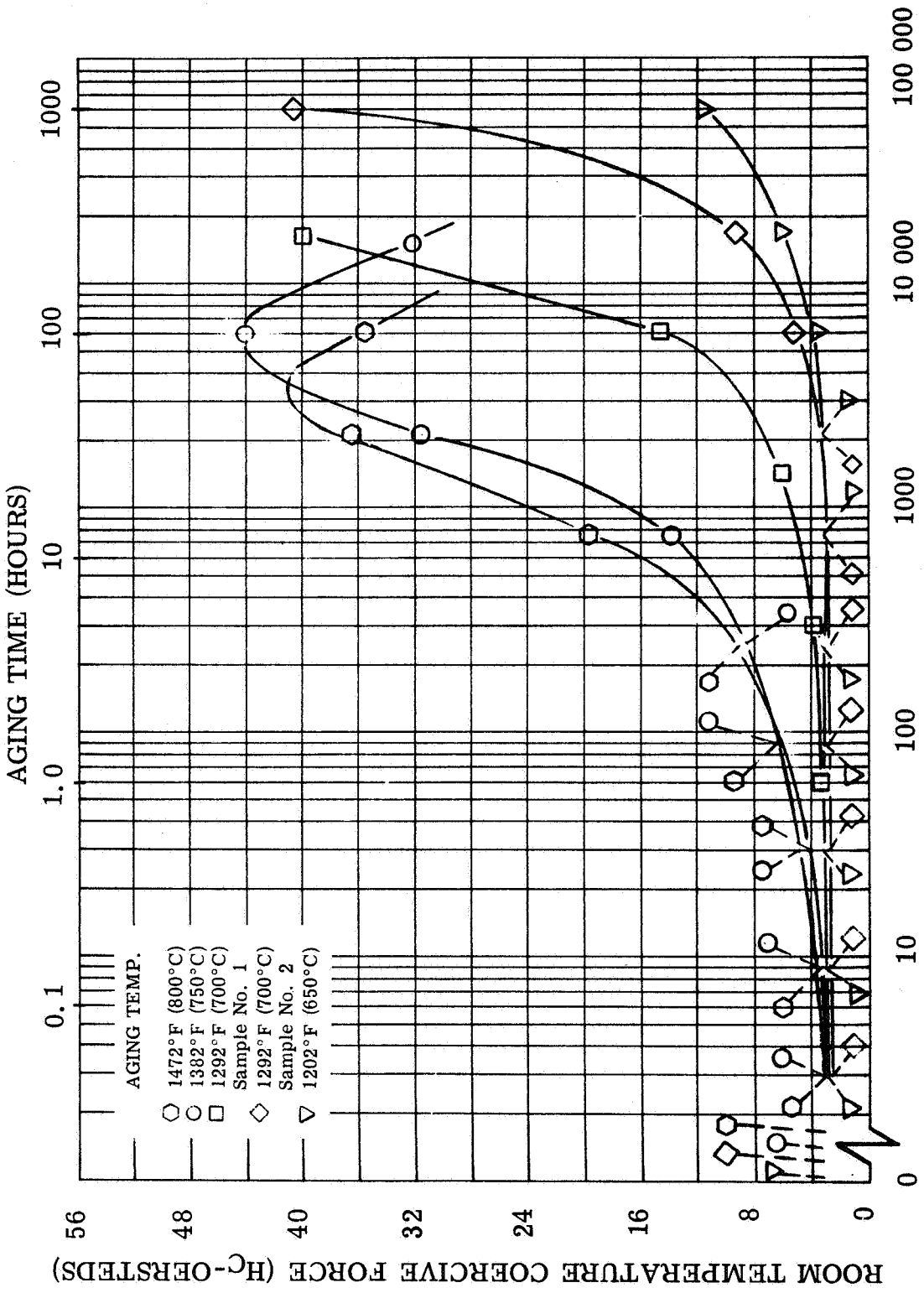

FIGURE II-6. Change in Room Temperature Coercive Force of Alloy 1-B-S-1 (Co-15Ni-5Fe-5Ta-1.25Al-0.2Zr-0.001B) During Isothermal Aging at Various Temperatures

Figure II-6. Coercive Force of Alloy 1-B-S-1 During Isothermal Aging at Various Temperatures

change in coercive force (figure II-6) shows that a strong increase of coercive force is also associated with overaging in the cobalt alloys. After 1000 hours at 1292°F (700°C) the room temperature coercive force was higher than 40 oersteds. The coercive force values were substantially lower when measured at higher temperatures (table II-4). The change of electrical resistivity of alloy 1-B-S-1, plotted in figure II-7, shows a decrease which is probably due to a precipitation process. At aging temperatures below 1202°F (650°C) the resistivity increased slightly before it dropped. This increase of resistivity was observed previously in cobalt-base alloys with γ' precipitate (ref. 4). It occurs also in nickel alloys with additions which produce γ' precipitate (refs. 5 and 6). This increase of resistivity is associated with a pre-precipitation stage with a kind of zone formation. One notices that an increase of electrical resistivity occurred with long aging times at temperatures higher than 1292°F (700°C). Such a phenomenon has also been observed in similar alloys with γ' precipitate (ref. 4). This resistivity increase occurs at aging times when the coercive force reaches its maximum and the hardness is already decreasing with aging time. The cause of this behavior of change of electrical resistivity is not yet understood. It is perhaps associated with a transition of the precipitate from a metastable γ' phase into a more stable phase. Such transition has been reported in nickel alloys with additions of Al+Ti and Al+Ti+Nb (refs. 7 and 8).

TABLE II-4. Coercive Force of Samples of Alloy 1-B-S-1 at Long Aging Times

Alloy Number	Aging Time and Temperature	Coercive Force (oersteds)	
		At Room Temperature	At 1112°F (600°C)
1-B-S-1	1000 hours at 1292°F (700°C)	41.0	19.0
1-B-S-1	300 hours at 1382°F (750°C)	32.5	20.0

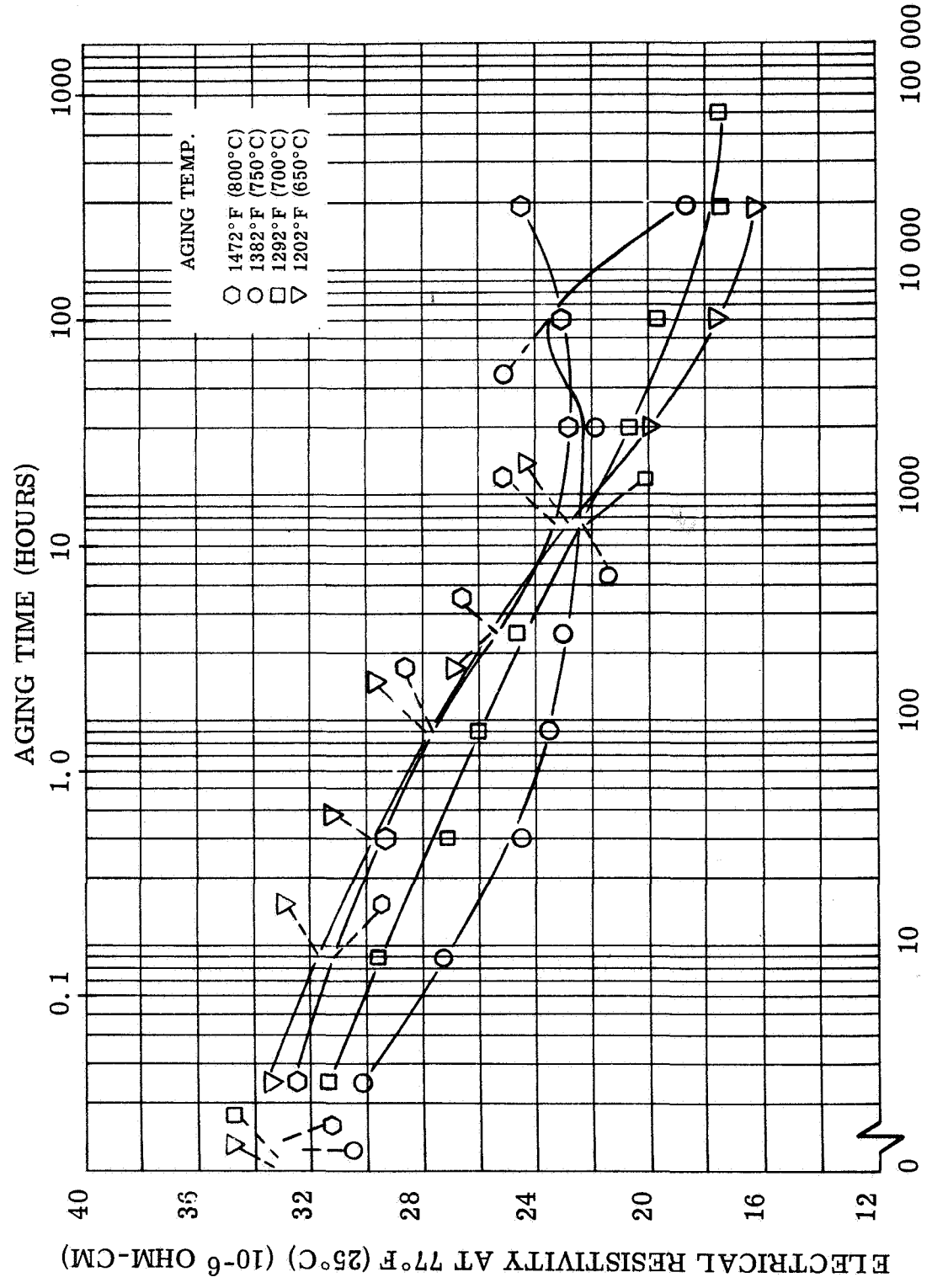

FIGURE II-7. Change in Room Temperature Electrical Resistivity of Alloy 1-B-S-1 (Co-15Ni-5Fe-5Ta-1.25Al-0.2Zr-0.001B) During Isothermal Aging at Various Temperatures

Figure II-7. Electrical Resistivity of Alloy 1-B-S-1 During Isothermal Aging at Various Temperatures

Such a transition can be observed in alloy 1-B-S-1 containing Al+Ta after aging at 1472°F (800°C) for 200 hours (see figure II-7). A light micrograph and electron micrograph replica showed that in addition to the grain boundary precipitate the matrix contains two types of precipitate within the grains. Fine cubes representing the γ' phase form first. There are also larger needle-like precipitate particles which have been identified as a hexagonal phase with $a_0 = 9.41$ Å, $c = 15.50$ Å which is in agreement with the hexagonal phase Co_3Ta found by Dragsdorf and Forgeny (ref. 9). It is interesting to note that this phase is hexagonal with the linear dimensions of the crystal lattice unit cell almost twice as large as the η phase Ni_3Ti, which occurs in Ni alloys with Al+Ti addition when the transition from γ' into η occurs. The unit cell of hexagonal Co_3Ta is also twice as large as the hexagonal Laves phase Co_2Ta of the $MgZn_2$ type.

Further studies of this transition phenomena appear necessary. It may well be that in the observed overaging at temperatures above 1292°F (700°C), the increase of coercive force and the irregularity of the resistivity change at long aging times, depend on this transition of the precipitate phase rather than on the growth of the original γ' particles. If this is the case one should be able to suppress this transition by increasing the aluminum to tantalum ratio and hence increase the thermal stability of this alloy.

An effort was made to evaluate the measured change of properties of alloy 1-A-S-2 by regression analysis. It was believed that a computer program which was available at the Westinghouse Research & Development Center (ref. 10) could be utilized. The change of electrical resistivity was analyzed with a good approximation and high degree of significance by a relation of the form:

$$\ln \Delta R = a_0 + n \ln t \qquad (1)$$

where $\Delta R = R - R_0$; the change of resistivity from value R_0 after aging time t. The constant terms a_0 and n, derived from the analysis, are listed in table II-5. This relation is similar to the expression found previously for the change of electrical resistivity in maraging steel by other investigators (refs. 1 and 11).

Differentiating equation (1) with respect to time and rearranging gives:

$$\frac{d(\Delta R)}{dt} = \frac{n}{t} \cdot \Delta R \qquad (2)$$

A rate expression of the type,

$$\frac{d(\Delta R)}{dt} = K\Delta R^p, \qquad (3)$$

is often used in restricted type of rate expressions. It is easier to handle mathematically than more complicated functions and provides an acceptable fit in many cases where p is defined as the empirical order of reaction and K is the rate constant. By applying equation (3) and obtained a fit to the data shown in Figure II-7, the order of reaction found was 14. Experiencing reactions higher than the third order are highly unlikely.

A comparison of the more vigorous expression given by equation (2) with the restricted type given by equation (3) is of interest. It shows that the kinetics of the reaction is of the first order, (p = 1) with the rate constant K being replaced in equation (3) by n/t which is in effect a rate constant varying inversely with time.

TABLE II-5. The Constant Terms for the Analytical Expressions of Change In Electrical Resistivity of Alloy 1-A-S-2

$$(\ln \Delta R = a_0 + n \ln t)$$

Temperature		Constant	
(°F)	(°C)	a_0	n
1202	650	2.55 ± 0.04	0.05 ± 0.007
1112	600	2.00 ± 0.09	0.11 ± 0.015
1022	550	1.75 ± 0.12	0.13 ± 0.02
932	500	0.087 ± 0.2	0.31 ± 0.038

The change of hardness in the ferritic alloys was also evaluated analytically as a polynominal function. An equation of the form:

$$H = a_0 + a_1 \ln t + a_2 (\ln t)^2 \qquad (4)$$

appeared to give a good fit in the main portion of the curve. However, the deviation increased with the longest time values so that an extrapolation of equation (4) would be meaningless.

c. APPLICATION CONSIDERATIONS

The determination of operating characteristics on both the ferritic base (1-A-S-2) and cobalt-base (1-B-S-1) alloys is of value in appreciating potential changes in the magnetic and mechanical behavior which these alloys may undergo due to diffusion kinetics.

An analysis of the time to reach the first coercive force inflection point (figure II-2) or time to reach maximum hardness is the ferritic alloy (figure II-1) suggests that these time periods (tm) obey an Arrhenius type relationship.

$$t_m = t_{mo} \quad \exp Q/RT,$$

where T is absolute temperature, R is the universal gas constant, t_{mo} is a constant, and Q is the activation energy produced by a diffusion-controlled, precipitation process. The activation energy observed in the ferritic alloy was approximately 65 K cal/mole value as found by reviewing figure II-8. This is in basic agreement with bulk diffusion of iron, nickel or cobalt in the alloy. Using a 65 K cal/mole value, table II-6 estimates the times at which the coercive force inflection point and the maximum hardness will occur at several temperatures for alloy 1-A-S-2. The coercive force inflection point was selected since it indicates the time at which the rate of change in coercive force is the greatest. This occurs prior to the time when the precipitate size equals the size of the magnetic domain wall. Maximum coercive force values are obtained for this alloy when this precipitate size is attained. Maximum hardness occurs earlier and suggests that the alloy will begin overaging almost an order of magnitude in time before the coercive force inflection point is reached.

The utilization of this method for the cobalt-base alloy 1-B-S-1

TABLE II-6. Estimated Time to Reach Coercive Force Inflection Point or Maximum Hardness at the Indicated Temperature for Alloy 1-A-S-2

Temperature (°C)	Temperature (°F)	Time at Which Coercive Force Inflection is Reached (hours)	Time at Which Maximum Hardness is Reached (hours)
450	842	25,000	2,500
500	932	1,000	133
550	1022	133	13
600	1112	8	0.8

was not as straight forward because inhomogenities in the alloy caused variations in the rate of changes in properties from sample to sample. Applying an activation energy of 70 K cal/mole to the long time data, an approximate fit is observed between adjacent points. Using this value for activation energy and applying it to an Arrhenius type relationship as before, table II-7 shows the estimated times at several temperatures when maximum hardness or the first coercive force inflection point will be reached.

The values observed in tables II-6 and II-7 are meant to alert the designer to conditions where more thorough data may be required to fully identify long-term performance of the alloys selected for the design. The times shown in the tables estimate when a change in material properties is expected. These times should not be considered as an operational limit.

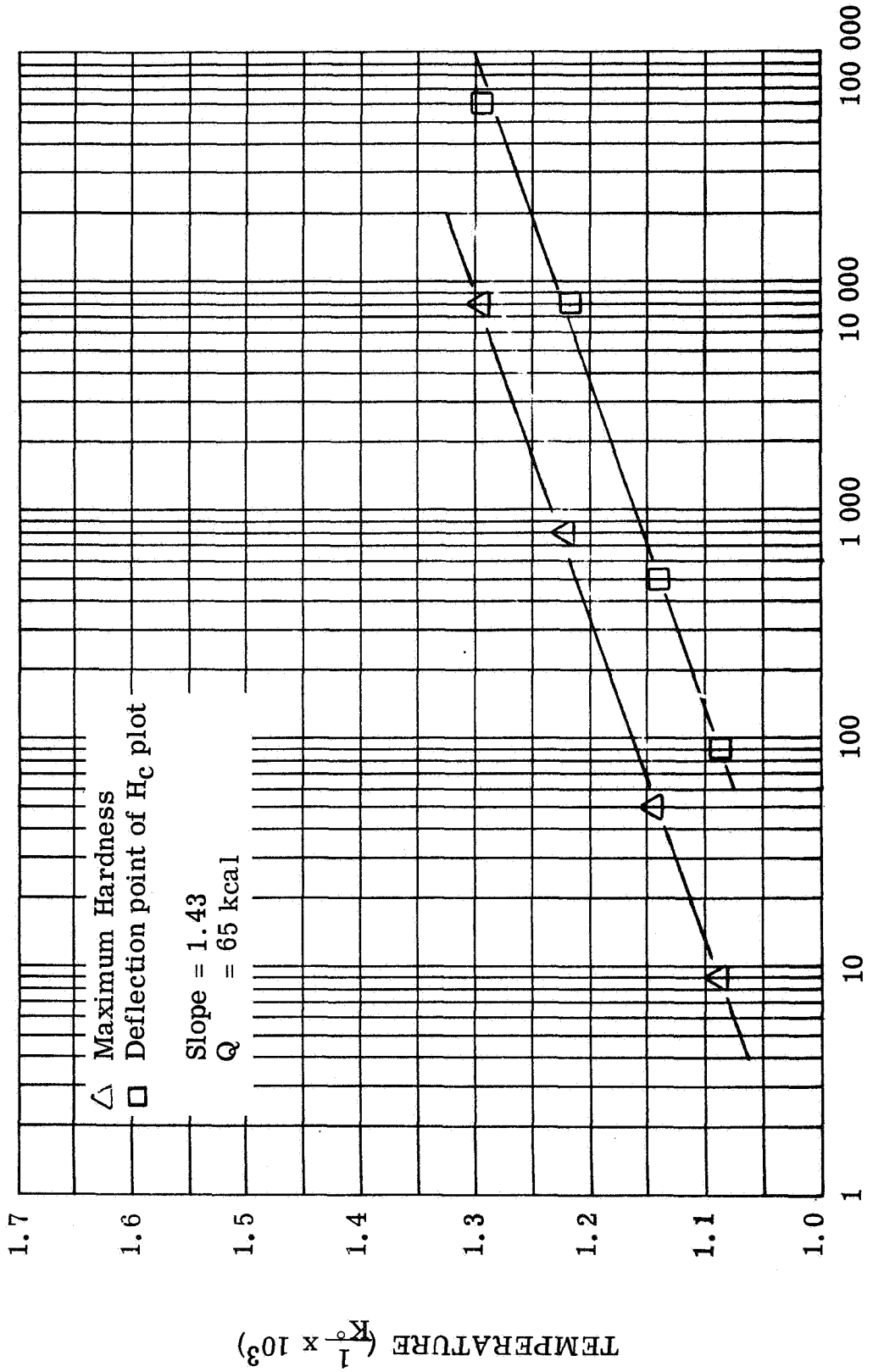

FIGURE II-8. Time-Temperature Plot of Hardness and Coercive Force of Alloy 1-A-S-2 (Fe-12Ni-30Co-1W-3Ta-0.4Al-0.4Ti-0.003Zr-0.001B)

Figure II-8. Time-Temperature Plot of Hardness and Coercive Force of Alloy 1-A-S-2

TABLE II-7. Estimated Time to Reach Coercive Force Inflection Point or Maximum Hardness at the Indicated Temperature for Alloy 1-B-S-1

Temperature (°C)	Temperature (°F)	Time at Which Coercive Force Inflection is Reached (hours)	Time at Which Maximum Hardness is Reached (hours)
550	1022	300,000	75,000
600	1112	30,000	7,500
650	1202	4,150	1,000
700	1282	835	166

d. CONCLUSION

The results of the studies on the final alloys have shown that the magnetic properties are superior to those of the commercially available materials. The high temperature mechanical properties in short-time tests are considerably better than the commercial alloys. This is demonstrated in figure II-9 showing yield stress as a function of temperature. The stability of the structure is greatly improved. The results have also shown that for application as creep resistant alloys, minor adjustment of the chemistry and heat treatment may become necessary to control creep at the grain boundaries. More adjustments may be required to keep the coercive force under a certain specified limit. In order to maintain a specific ductility at room temperature, in the case of the ferritic alloys, a certain variation of the composition from the alloy 1-A-S-2 may become necessary.

With all these adjustments completed one may still project a temperature limit for the ferritic alloy of above 1022°F (550°C) with a yield stress at this temperature of more than 130,000 psi, and an induction of at least 14 kG at 100 oersteds. The

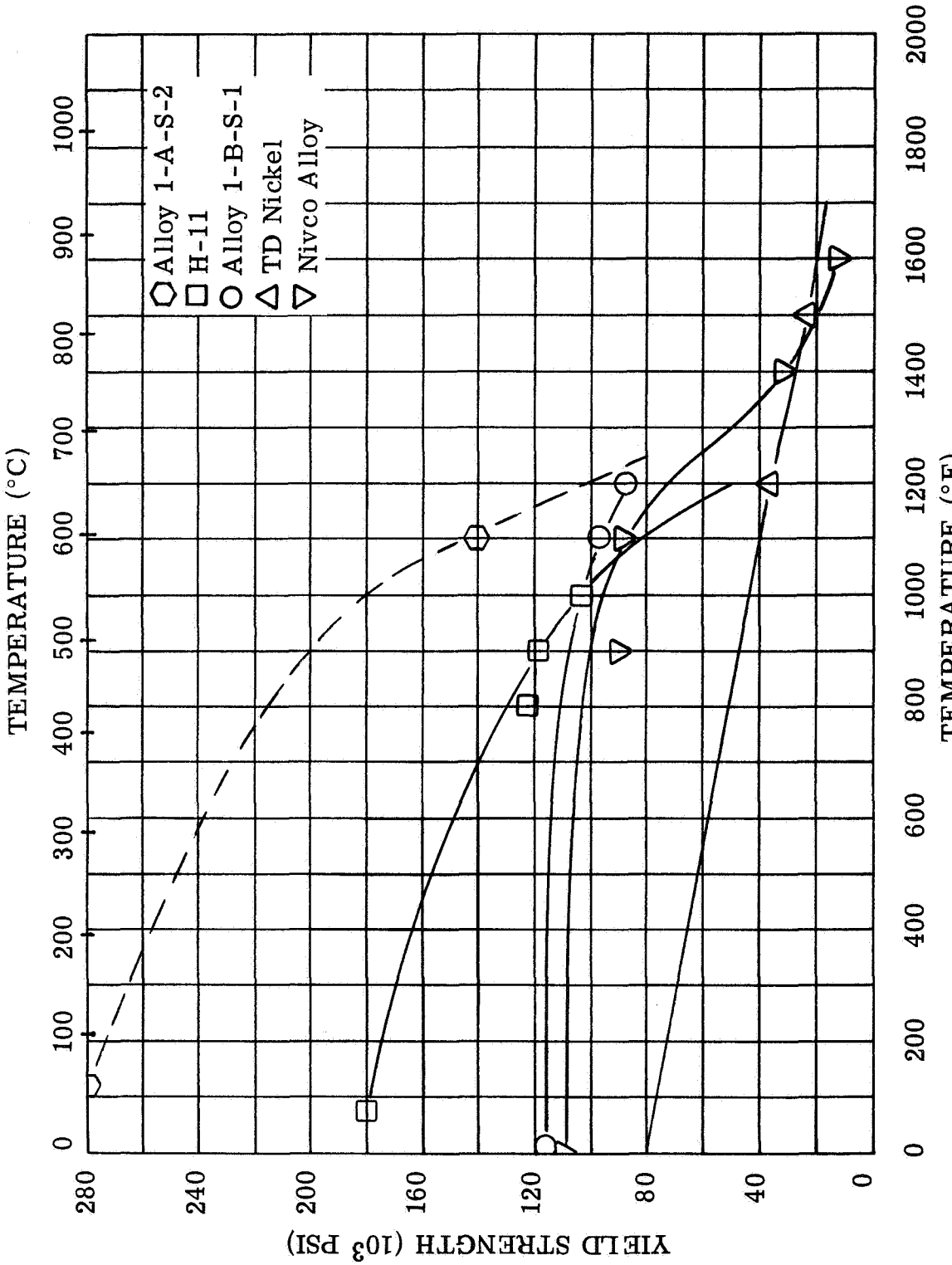

FIGURE II-9. Comparison of Yield Strength as a Function of Temperature of Experimental Alloys 1-A-S-2 and 1-B-S-1 and Commercial H-11, Nivco, and TD Nickel Alloys

Figure II-9. Comparison of Yield Strength as a Function of Temperature of Experimental Alloys and Commercial Alloys

temperature limit of the cobalt-base alloy will be above 1292°F (700°C) with a yield stress at 1202°F (650°C) higher than 85,000 psi, and the induction at 1202°F (650°C) will be at least 10 kG when a field of 100 oersteds is applied.

3. Program for the Next Quarter

Creep testing of the final cobalt-base and martensitic type alloys will be started.

B. TASK 2 - INVESTIGATION FOR RAISING THE ALPHA TO GAMMA TRANSFORMATION TEMPERATURE IN COBALT-IRON ALLOYS

Work on this task is complete and will be reported in the Final Topical Report.

C. TASK 3 - DISPERSION-STRENGTHENED MAGNETIC MATERIALS FOR APPLICATION IN THE 1200° TO 1600°F RANGE

1. Summary of Technical Progress

a) The chemical analyses of seven extrusions made from powder on the initial evaluation phase (first phase) of this task were in generally good agreement with the chemical analyses of the powders (as reported by the powder suppliers), and the intended compositions (as defined by the Westinghouse compositional target limits).

b) The total oxygen contents of five oxide dispersion-strengthened extrusions measured by vacuum fusion were in quite good agreement with the combined oxygen values calculated from the Al_2O_3, BeO, and ThO_2 contents. This provided additional evidence (beyond the x-ray diffraction identification of constituents previously reported) that, where internal oxidation and subsequent hydrogen reduction treatments had been applied to the powders, oxidation of the aluminum and beryllium alloy additions was substantially complete, and oxides of cobalt and iron had been reduced.

c) As part of the intermediate evaluation (second phase) of this task, short term (100 hour maximum) vacuum creep tests were completed at 1400°F on hot-extruded compositions previously identified as having the best combination of tensile and magnetic properties in the 1200° to 1600°F range. Five cobalt-base and two iron + 27 w/o cobalt-base compositions were tested under 10,000 psi stress. The lowest creep strain, 0.17 percent after 100 hours, was obtained on the Fe + 24.8 w/o Co + 1.1 w/o B + 3.2 w/o Zr material. Testing was also conducted on four cobalt-base and one iron + 27 w/o cobalt-base materials at 15,000 psi. The Co + 1.1 w/o B + 4.4 w/o Cb composition had the lowest creep strain, 0.92 percent in 100 hours. Several dispersion-strengthened compositions had better creep resistance and saturation magnetization, B_S, values at 1400°F than Nivco alloy, the best precipitation-hardened magnetic material presently available for applications above 1000°F.

d) Four composite powders for the intermediate evaluation

phase of this task were received, two from Chas. Pfizer and two from Sherritt Gordon Mines. The following compositions were obtained from each supplier: Co + 4 v/o ThO_2 and Co + 7.5 v/o ThO_2. These are in the process of being extruded and evaluated.

e) A shorter internal oxidation time (1/2 hour rather than 2 hours at 1830°F) was applied to a Co + Be prealloyed atomized powder in an attempt to produce a still finer beryllia dispersoid. The BeO dispersoid in cobalt appeared to be more thermally stable at 1600°F than Al_2O_3 dispersoids, based on examination of earlier extrusions conducted with the optical microscope.

2. Discussion

The purpose of this project is to determine the feasibility of making soft-magnetic materials having relatively low values of coercive force at 1200° to 1600°F which are dispersion-strengthened to provide satisfactory creep resistance. Such a material is needed for solid rotor applications. As a goal, the material should have the following properties at some temperature between 1200° and 1600°F, preferably at 1600°F.

Saturation magnetization, B_S - 12,000 gauss minimum
Coercive force, H_C - 25 oersteds maximum
Creep strain in 10,000 hours at 10,000 psi - 0.4 percent maximum.

In pursuit of this goal, dispersion-strengthened cobalt-base and iron + 27 w/o cobalt-base extrusions were made from (a) prealloyed atomized powders containing boride compound particles, (b) internally oxidized powders containing alumina or beryllia, and (c) composite powders containing both a metal phase and a refractory oxide phase (alumina or thoria) within each powder particle. Also, dispersion-strengthened cobalt-base extrusions containing thoria were purchased from two suppliers. The initial evaluation phase of this project included determination of saturation magnetization, coercive force, and tensile properties of extrusions at room temperature and in the 1200° to 1600°F range. The intermediate and final evaluation phases of this project will be conducted on the best candidate compositional systems developed in the first phase. Changes in powder processing conditions and application of secondary working treatments to extruded material will be made on a selective basis to those materials having thermally stable dispersoids and the best combinations of mechanical and magnetic properties.

Westinghouse Electric Corporation

[illegible] Electrical Division
[illegible]

Box [illegible]
Telephone [illegible]

October 9, 1967

SUBJECT: NASA Contract NAS3-6465

Enclosed is the Seventh Quarterly Report on NASA Contract NAS3-6465, sponsored by the Space Power Systems Division at the Lewis Research Center.

This program is directed at the development and evaluation of magnetic and electrical materials capable of operating in the temperature range from 800-1600°F in a space environment.

Any comment or suggestions you may have will be appreciated. These should be directed to the undersigned.

Yours truly,

WESTINGHOUSE ELECTRIC CORPORATION
AEROSPACE ELECTRICAL DIVISION

P. E. Kueser, Manager
NASA Materials Study Program

ds

a. INITIAL EVALUATION

(1) Chemical Analyses of Extrusions

Chemical analyses have been determined to date on a total of seven extrusions made from powder. There has been generally good agreement between the chemical analyses of the extrusions (as determined by Westinghouse), the chemical analyses of the powders (as reported by the powder suppliers), and the intended compositions (as defined by the Westinghouse compositional target limits). The results are presented in table II-8.

The third quarterly report gave the chemical analyses of all 18 prealloyed atomized powders obtained for the initial evaluation phase of the program (phase I), including the powders which subsequently were given internal oxidation treatments by Westinghouse, and the chemical analyses of two composite powders which were available at that time. In regard to the prealloyed atomized powder target specifications, it was stated that the chemical analyses reported by the two suppliers, Hoeganaes Sponge Iron Corporation and Domtar Chemicals Limited, indicated that Mn, Si, and C were high in the cobalt-base powders. It was necessary in some instances for the supplier to add intentionally manganese and silicon, usually in amounts of approximately 0.25 percent each, in order to increase fluidity and achieve proper flow of the molten metal through the atomizing nozzle, as discussed in the third quarterly report. In the iron + 27 w/o cobalt-base atomized powders, the carbon contents tended to be higher than the specifications.

No detrimental effects on magnetic or mechanical properties have been identified with the fact that the impurity contents of some of the extrusions in table II-8 were slightly higher than the original goals.

The concentrations of the alloying elements in the extrusions in table II-8 were generally close to the intended values. However, the beryllium content of the extrusion made from the internally oxidized powder No. 9 was analyzed by Westinghouse to be 0.69 w/o compared with 1.94 w/o for the original powder before oxidation, as reported by Domtar Chemicals Limited. No reason has been found to date to explain this anomaly.

TABLE II-8. Chemical Analyses of Powders and Extrusions

Powder or Extrusion No.	Powder Supplier	Intended Composition or Analysis	Mn	Si	C	S	
a. Prealloyed Atomized Powders							
5.	Hoeganaes	Intended Composition[a]	0.04 max.	0.04 max.	0.020 max.	0.006 max.	0.
		Powder Analysis[b]	0.19	0.04	0.043	0.007	<0.
		Extrusion Analysis[c]	0.02[d]	0.10	0.048	0.006	<0.
13.	Hoeganaes	Intended Composition[a]	0.50 max.	0.25 max.	0.020 max.	0.025 max.	0.
		Powder Analysis[b]	0.11	0.22	0.023	0.011	<0.
		Extrusion Analysis[c]	0.30	0.23	0.048	0.007	0.
b. Internally Oxidized Powders							
8.	Hoeganaes	Intended Composition[a][e]	0.04 max.	0.04 max.	0.020 max.	0.006 max.	0.
		Powder Analysis[b][e]	0.22	0.27	0.009	0.004	<0.
		Extrusion Analysis[c][f]	0.5[d]	0.18	0.013	0.005	<0.
9	Domtar	Intended Composition[a][e]	0.04 max.	0.04 max.	0.020 max.	0.006 max.	0.
		Powder Analysis[b][e]	<0.05	0.012	0.028	<0.002	0.
		Extrusion Analysis[c][f]	0.02[d]	0.10	0.047	0.002	0.
18.	Domtar	Intended Composition[a][e]	0.50 max.	0.25 max.	0.020 max.	0.025 max.	0.
		Powder Analysis[b][e]	<0.1	0.08	0.026	<0.002	<0.
		Extrusion Analysis[c][f]	0.04	0.14	0.026	0.008	0.
c. Composite Powders							
3.	Pfizer	Intended Composition[a]	0.04 max.	0.04 max.	0.020 max.	0.006 max.	0.
		Powder Analysis[b]	--	--	--	--	--
		Extrusion Analysis[c]	0.02[d]	<0.02	0.019	0.011	<0.
11.	Pfizer	Intended Composition[a]	0.50 max.	0.25 max.	0.020 max.	0.025 max.	0.
		Powder Analysis[b]	--	--	--	--	--
		Extrusion Analysis[c]	0.21	<0.02	0.044	0.017	<0.

Notes: (a) Westinghouse target limits.
(b) Analysis reported by powder supplier.
(c) Analysis made by Westinghouse.
(d) Emission spectrographic semi-quantitative analysis.
(e) Before internal oxidation treatment.
(f) After internal oxidation treatment.
(g) Includes 0.04 percent soluble aluminum and 2.74 percent insoluble aluminum.
(h) Determined by vacuum fusion using platinum bath at 3542°F(1950°C).

ELEMENT (weight percent)							
P	Ni	Cr	Co	Fe	B	Ti	Zr
10 max.	0.70 max.	--	94.8	--	1.0±0.2	--	--
05	0.58	0.02	93.11	0.21	1.1	--	--
01	0.8(d)	0.2(d)	--	0.4(d)	1.14	<0.01(d)	<0.02(d)
15 max.	0.70 max.	--	25.6±1.5	69.2±2.0	1.0±0.2	--	4.2±0.8
05	0.12	0.064	24.75	69.73	1.1	--	3.24
05	0.09	0.026	24.4	69.5	1.33	0.03(d)	3.40
10 max.	0.70 max.	--	97.5	--	--	--	--
05	0.29	0.022	95.59	0.97	--	--	--
01	0.7(d)	0.1(d)	--	1(d)	0.01(d)	0.4(d)	0.5(d)
10 max.	0.70 max.	--	98.7	--	--	--	--
10	0.48	0.07	97.7	Not detected	--	--	--
04	1(d)	0.2(d)	--	0.6(d)	0.01(d)	<0.01(d)	<0.02(d)
15 max.	0.70 max.	--	26.6±1.5	72.0±2.0	--	--	--
05	<0.05	<0.1	27.9	70.0	--	--	--
06	0.8(d)	0.1(d)	27.3	--	0.02(d)	<0.01(d)	0.3(d)
10 max.	0.70 max.	0.10 max.	Remainder	--	--	--	--
--	--	--	--	--	--	--	--
01	0.3(d)	<0.05(d)	--	0.06(d)	0.02(d)	<0.01(d)	<0.02(d)
15 max.	0.70 max.	0.10 max.	23.7±1.5	64.2±2.0	--	--	--
--	--	--	--	--	--	--	--
01	0.2(d)	<0.05(d)	23.5	--	0.01(d)	<0.01(d)	<0.02(d)

TABLE II-8. Chemical Analyses of Powders and Extrusions (Continue

Powder or Extrusion No.	Powder Supplier	Intended Composition or Analysis	Cb	Al	Al_2O_3
a. Prealloyed Atomized Powders					
5.	Hoeganaes	Intended Composition[a]	4.2±0.8	--	--
		Powder Analysis[b]	4.38	--	--
		Extrusion Analysis[c]	4.03	0.01[d]	--
13.	Hoeganaes	Intended Composition[a]	--	--	--
		Powder Analysis[b]	--	--	--
		Extrusion Analysis[c]	--	0.2[d]	--
b. Internally Oxidized Powders					
8.	Hoeganaes	Intended Composition[a][e]	--	2.5±0.5	--
		Powder Analysis[b][e]	--	2.46	4.64
		Extrusion Analysis[c][f]	--	2.78[g]	5.18
9	Domtar	Intended Composition[a][e]	--	--	--
		Powder Analysis[b][e]	--	--	--
		Extrusion Analysis[c][f]	--	0.2[d]	--
18.	Domtar	Intended Composition[a][e]	--	--	--
		Powder Analysis[b][e]	--	--	--
		Extrusion Analysis[c][f]	--	0.05[d]	--
c. Composite Powders					
3.	Pfizer	Intended Composition[a]			
		Powder Analysis[b]	--	--	--
		Extrusion Analysis[c]	--	--	--
			--	0.3[d]	--
11.	Pfizer	Intended Composition[a]			
		Powder Analysis[b]	--	--	--
		Extrusion Analysis[c]	--	--	--
			--	0.3[d]	--

Notes: (a) Westinghouse target limits.
(b) Analysis reported by powder supplier.
(c) Analysis made by Westinghouse.
(d) Emission spectrographic semi-quantitative analysis.
(e) Before internal oxidation treatment.
(f) After internal oxidation treatment.
(g) Includes 0.04 percent soluble aluminum and 2.74 percent insoluble aluminum.
(h) Determined by vacuum fusion using platinum bath at 3542°F(1950°C).

ELEMENT (weight percent)							
Be	BeO	ThO_2	O[h]	N	Cu	Ca	Mg
--	--	--	--	--	--	--	--
--	--	--	--	--	--	--	--
--	--	--	0.13	0.0008	0.3[d]	<0.01[d]	0.01[d]
--	--	--	--	--	--	--	--
--	--	--	--	--	--	--	--
0.001[d]	--	--	0.185	0.066	0.2[d]	<0.01[d]	<0.01[d]
--	--	--	--	--	--	--	--
--	--	--	--	--	--	--	--
--	--	--	2.24	0.0006	0.2[d]	<0.01[d]	0.01[d]
1.3±0.3	--	--	--	--	--	--	--
1.94	5.38	--	--	--	--	--	--
0.69	1.91	--	0.85	0.0012	0.2[d]	<0.01[d]	<0.01[d]
1.4±0.3	--	--	--	--	--	--	--
1.4	3.9	--	--	--	--	--	--
1.14	3.16	--	1.55	<0.0005	0.2[d]	0.2[d]	<0.01[d]
--	--	11.2±1.5	--	--	--	--	--
--	--	--	--	--	--	--	--
--	--	11.2	1.31	<0.0005	0.2[d]	0.5[d]	0.01[d]
--	--	12.1±1.5	--	--	--	--	--
--	--	--	--	--	--	--	--
--	--	12.5	1.52	0.0032	0.1[d]	0.5[d]	0.08[d]

The estimates of the usual precisions of the analyses for the various elements performed by Westinghouse on the extrusions were as follows:

Element	Percent	Element	Percent	Element	Percent
Mn	±0.01	B	±0.03	O	±0.1 for samples containing Al_2O_3, BeO, or ThO_2
Si	±0.02	Cb	±0.05		
C	±0.002	Al	±0.04		
S	±0.002	Be	±0.03	O	±0.02 for samples without Al_2O_3, BeO, or ThO_2
P	±0.001	ThO_2	±0.2		
Co	±0.15	N	±0.0005		

The precision of the values obtained by emission spectrographic semi-quantitative analysis were estimated to be 0.3 to 3 times the amounts reported.

The precisions of the analyses on the powders estimated by the powder suppliers were given in the third quarterly report.

Table II-9 gives the oxide and oxygen contents of extrusions. The total oxygen contents of five oxide dispersion-strengthened extrusions measured by vacuum fusion were in quite good agreement with the combined oxygen values calculated from the Al_2O_3, BeO, and ThO_2 contents. In the case of the internally oxidized powders Nos. 8, 9, and 18, the difference between the measured and calculated oxygen contents was greater (and indicated a deficiency of oxygen) than for the composite powders No. 3 and 11. However, the good agreement between the measured and calculated oxygen values for the internally oxidized materials provided additional evidence (beyond the x-ray diffraction identification of oxide constituents described in the sixth quarterly report) that, where internal oxidation and subsequent hydrogen reduction treatments had been applied to powders, the oxidation of the aluminum and beryllium alloy additions was substantially complete, and oxides of cobalt and iron had been reduced.

TABLE II-9. Oxygen Contents of Oxide Dispersion-Strengthened Extrusions

Powder or Extrusion No.	Intended Composition (weight percent)	Oxide Forming Element (weight percent)	Oxide (weight percent)	Calculated Oxygen (O) Combined as Oxide (weight percent)	Measured Total Oxygen (O) (weight percent)	Difference Between Measured and Calculated Oxygen (O) (weight percent)
a. Internally Oxidized Powders (Extruded)						
8.	Co + 4.7Al_2O_3	2.74Al[a]	5.18Al_2O_3[b]	2.44	2.24	-0.20 (deficiency)
9.	Co + 3.6BeO	0.69Be[c]	1.91BeO[d]	1.22	0.85	-0.37 (deficiency)
18.	Fe-26.0Co + 3.9BeO	1.14Be[c]	3.16BeO[e]	2.02	1.55	-0.47 (deficiency)
b. Composite Powders (Extruded)						
3.	Co + 11.2ThO_2 (Pfizer)	--	11.2ThO_2[f]	1.36	1.31	-0.05 (deficiency)
11.	Fe + 23.7Co + 12.1 ThO_2 (Pfizer)	--	12.5ThO_2[f]	1.51	1.52	+0.01 (excess)

Notes: (a) Determined as insoluble Al. The soluble Al was 0.04 percent.
(b) Equivalent to 2.74 percent insoluble Al.
(c) Determined as total Be.
(d) Equivalent to 0.69 percent total Be.
(e) Equivalent to 1.14 percent total Be.
(f) Determined as ThO_2 by X-ray flourescence.

b. INTERMEDIATE EVALUATION

The first phase included compositions which represented a wide range of particle sizes and interparticle spacings of the dispersoid. Saturation magnetization was independent of particle size, as expected. As mentioned earlier, all compositions were found to have sufficiently low values of coercive force (below 25 oersteds) at 1200° to 1600°F whether the dispersoid was fine (submicron range) or coarse (micron range). The coercive force was somewhat less for materials containing coarse rather than fine dispersed particles, in accordance with theory. However, as a result of these observations, the particle size effect on coercive force at 1200° to 1600°F was determined to be of secondary importance. Therefore, it is unnecessary to investigate further the effect of coarsening the dispersoid on the magnetic properties (coercive force) in this second phase of the program. Of primary importance was the effect of particle size and the other dispersoid parameters on creep resistance. It is desirable, of course, to have small dispersed particles and small interparticle spacing in order to develop high strength and creep resistance, as shown by both experience and theory.

One investigation involving changes in powder processing and fabricating conditions has been already completed and was described in the fifth and sixth quarterly reports. The powders for these extrusions were processed in the normal manner except that the temperature was held to 1600°F maximum. By contrast, the normal billet preheat for conventional hydraulic extrusion was one hour at 2000°F. The purpose of this work was to investigate the effect of lower processing temperatures, 1600°F maximum, on coercive force and tensile properties. A Dynapak Machine was employed to enable extrusions to be made by a high energy rate process at a lower temperature (1600°F billet) than used for conventional hydraulic extrusion (2000°F). The boride dispersed particles and the grain size in the one cobalt-base and two iron + 27 w/o cobalt-base compositions were smaller in the Dynapak extrusions, and led to higher strengths in the specimens tensile tested at 1200°F (after aging 100 hours at 1200°F). The lack of improvement in strength at 1600°F (after aging the specimens 100 hours at 1600°F) was attributed to the coarsening of the boride particles at that temperature.

(1) Vacuum Creep Tests

An investigation of vacuum creep properties (100 hour maximum) at 1400°F of seven dispersion-strengthened compositions in the hot-extruded condition (no secondary working) was conducted at the 10,000 psi stress level. These materials were selected for creep testing on the basis of their 1200°F and, especially, 1600°F tensile properties. (It was necessary to re-extrude the Fe + 27 w/o Co-base compositions to obtain sufficient material for creep specimens.) After screening out the less creep resistant compositions, five were selected for additional testing at 15,000 psi stress. This cursory creep investigation was necessary to develop preliminary information concerning the combination of magnetic properties and creep resistance that had been achieved, since creep properties rather than tensile properties are more important in the solid rotor application. The dimensions of the creep specimen are shown in figure II-10.

The short term vacuum creep properties of several of the experimental dispersion-strengthened compositions in the hot-extruded condition listed in table II-10 were superior to precipitation-hardened Nivco alloy at 1400°F. The Co + 1.1 w/o B + 4.4 w/o Cb composition was the most creep resistant. Concerning the Fe + Co-base materials, the extrusion made from prealloyed atomized powder No. 13 which was dispersion-strengthened with ZrO_2 and $(Fe, Co)_2B$ had the best creep properties. The Fe + 27 w/o Co-base materials containing a BeO dispersion had lower creep resistance.

It should be noted that the coercive force values at 1400°F of the dispersion-strengthened extrusions were all lower than 17 oersteds. Furthermore, the saturation magnetization values were substantially higher than that of Nivco alloy.

(2) New Compositions

(a) Prealloyed Atomized Powder

The following new prealloyed atomized powder composition was ordered, but has not been received: Fe + 24.8 w/o Co + 8.3 w/o Zr. The zirconium will be oxidized to form a ZrO_2 dispersoid. It was

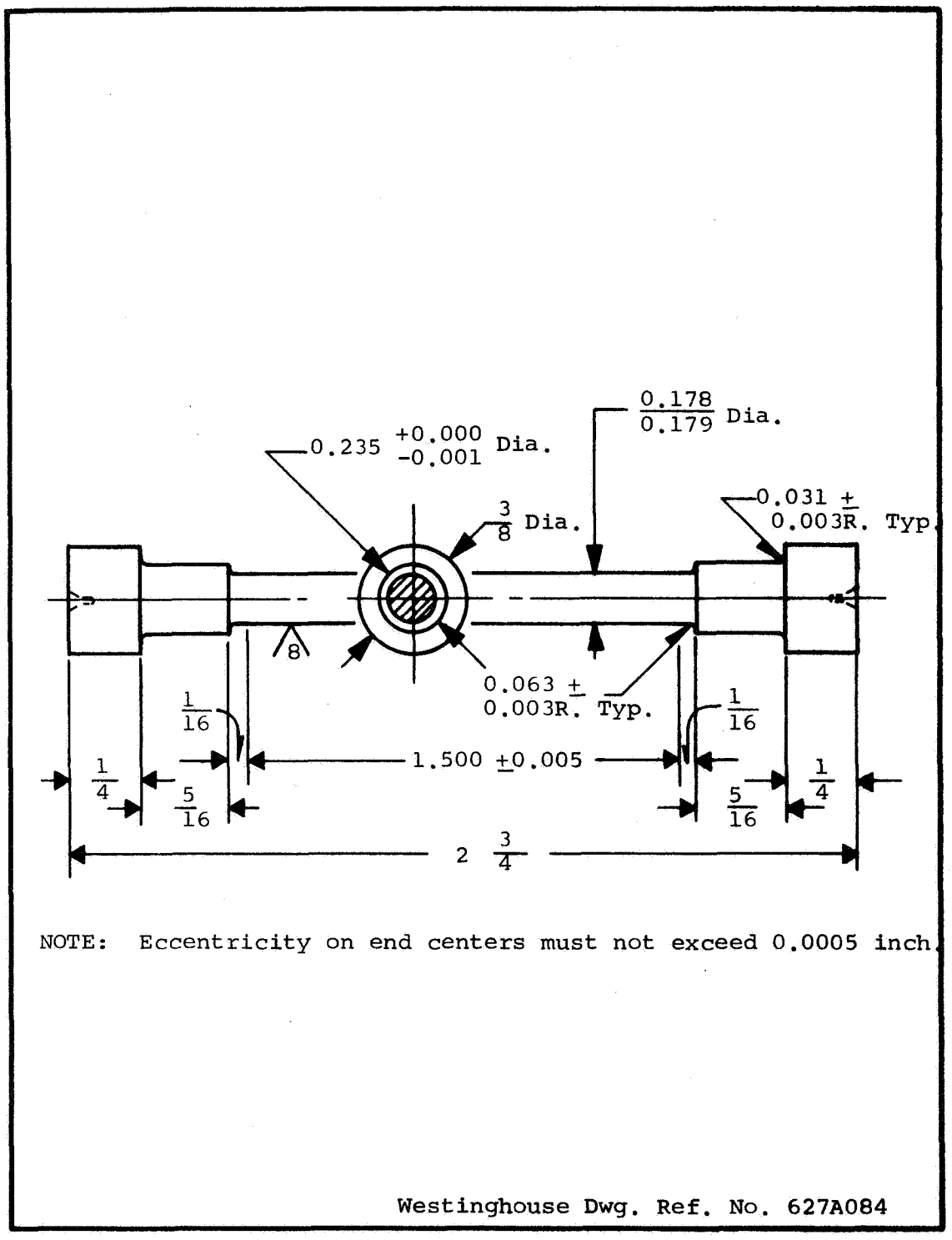

FIGURE II-10. Vacuum Creep Specimen

TABLE II-10. Properties of Dispersion-Strengthened Extrusions

Powder or Extrusion No	Nominal Composition (weight percent)	At 1400°F			
		Coercive Force, H_c (oersteds)	Saturation Magnetization B_S (kilogauss)	Short Term Vacuum Creep Properti Creep Strain in 100 Hours (percent) At 10,000 psi stress	At 15,000 psi st
a. Prealloyed Atomized Powders (Extruded)					
5.	Co+1.1B+4.4Cb	8.0	10.1	0.21	0.92
13.	Fe+24.8Co+1.1B+3.2Zr	6.4	15.0	0.17	Failed in 64 hou 16.7% strain
b. Internally Oxidized Powders (Extruded)					
8.	Co+4.7Al_2O_3	8.0	12.6	0.40	Failed in 10.8 h 2.6% strain
9.	Co+3.6BeO	6.4	12.9	Failed in 11.8 hours, 2.7% strain	---
18.	Fe+26.0Co+3.9BeO	4.9	16.4	Failed during loading, 6.5% strain	---
c. Composite Powders (Extruded)					
3.	Co+11.2ThO_2 (0.01-0.06 μ)	16.8	12.8	0.24	Failed in 0.15 h 0.33% strain
3.	Co+11.2ThO_2 (0.01-0.06 μ)	10.3	12.9	0.21	Failed in 7.5 ho 0.40% strain
d. Comparison Alloy					
	Nivco 5/8 in. Diam Forged and Heat Treated Bar	5.5	8.1	(3,000 psi stress to produce 0.2 perce creep strain in 100 hours at 1400°F.)(c (4,000 psi stress to produce 0.4 perce creep strain in 100 hours at 1400°F.)(c	

Notes: (a) All experimental alloy specimens aged 100 hours at 1400°F in vacuum (pressure of 1 x 10^{-5} torr or le (pressure of 1 x 10^{-6} torr or less).
(b) All experimental alloy specimens aged 100 hours at the test temperature in vacuum (pressure of 1 x 1 testing in vacuum (pressure of 1 x 10^{-5} torr).
(c) Approximate values obtained by extrapolation of vacuum creep data on Larson-Miller plot.
(d) Average of two tests. Other tensile test values represent one test.
(e) No tensile tests made at 1400°F. Values are average of 1200°F and 1600°F test results.
(f) Failed before reading 0.2 percent offset.

				At 1200°F			At 1600°F		
	Tensile Properties[e]			Tensile Properties[b]			Tensile Properties[b]		
a) ss	Ultimate Tensile Strength (1000 psi)	Yield Strength 0.2% Offset (1000 psi)	Elongation In 4D (percent)	Ultimate Tensile Strength (1000 psi)	Yield Strength 0.2% Offset (1000 psi)	Elongation In 4D (percent)	Ultimate Tensile Strength (1000 psi)	Yield Strength 0.2% Offset (1000 psi)	Elongation In 4D (percent)
	61	32	45	80	42	23	41	23	66
	40	21	61	62	32	40	19	10	82
rs,	30	21	16	38	30	17	21	12	15
	34	21	35	54[d]	35[d]	41[d]	13	7	28
	30	17	30	48	31	24	12	4	36
rs,	19	19	2	26	26	4	13	(f)	0
s,	25	20	6	30	24	8	20	16	3
	49	36	43	97	74	30	25	9.5	124

) before creep testing in vacuum

5 torr or less) before tensile

mentioned in the fifth quarterly report that a somewhat similar composition, extruded atomized powder No. 13, of lower zirconium content and containing boron was dispersion-strengthened by ZrO_2 particles and coarser boride particles. The new composition is of higher zirconium content, but without boron. The $(Fe, Co)_2B$ phase, which was less thermally stable than ZrO_2 in extruded powder No. 13, will have been replaced entirely by ZrO_2. The increased amount of ZrO_2 should provide a greater dispersion-strengthening effect.

(b) Composite Powders

Further work was initiated to investigate magnetic and mechanical properties as a function of the volume percent of dispersoid, while holding the dispersoid particle size constant, in extrusions of powder manufactured by two different methods. Specifically, four pound quantities each of cobalt-base composite powders containing nominally 4.0 and 7.5 volume percent thoria dispersoid (0.01-0.06 micron thoria) were obtained from Chas. Pfizer and Sherritt Gordon Mines for fabrication into rod to be tested in the hot-extruded and secondary worked conditions. The powder manufacturing methods were described in the second quarterly report. Previous evaluation of the Co + 10 v/o ThO_2 powder compositions obtained from both these suppliers showed a promising combination of magnetic and tensile properties at 1200° to 1600°F, and vacuum creep properties at 1400°F. The lower thoria contents of the new powders will provide even higher values of saturation magnetization (less dilution by the non-magnetic phase), higher tensile elongations, and lower notch sensitivity.

Information on chemical analyses submitted by Chas. Pfizer and Sherritt Gordon Mines for their powders are given in table II-11. It should be pointed out that the Westinghouse Specifications for Composite Powders which accompanied the Purchase Orders stated that the purity of the cobalt and thoria shall be 99.5 percent or greater, and that the supplier shall report the major impurities anticipated in the composite powder.

TABLE II-11. Chemical Analyses of Composite Powders[a]

Element	Composite Powder No. 13			Composite Powder No. 14		
	Westinghouse Spec. Target Limits (weight percent)	Chas. Pfizer Lot No. RX 2073-A Analysis (weight percent)	Sherritt Gordon Lot No. 1006 Analysis (weight percent)	Westinghouse Spec. Target Limits (weight percent)	Chas. Pfizer Lot No. RX 2073-B Analysis (weight percent)	Sherritt Gordon Lot No. 1007 Analysis (weight percent)
Mn	0.04 max.	--	--	0.04 max.	--	--
Si	0.04 max.	--	--	0.04 max.	--	--
C	0.020 max.	--	0.035	0.020 max.	--	0.040
S	0.006 max.	0.010[b]	0.032	0.006 max.	0.010[b]	0.032
P	0.010 max.	--	--	0.010 max.	--	--
Ni	0.70 max.	0.030[b]	0.09	0.70 max.	0.030[b]	0.08
Cr	0.10 max.	--	--	0.10 max.	--	--
Fe	--	0.050[b]	--	--	0.050[b]	--
ThO_2	4.52±0.50	--	4.2	8.41±0.50	--	8.6
Co	Remainder	96.1	95.5	Remainder	91.9	91.1

Notes:

(a) Reported by the powder supplier.

(b) Analysis of cobalt used in making composite powder.

The target limits for the various elements in table II-11 were what the supplier worked toward in his processing, and should be considered goals rather than rigid limits for acceptance or rejection. The materials will be analyzed by Westinghouse at a later date.

Thorium oxide powder was supplied by Westinghouse to Chas. Pfizer and Sherritt Gordon Mines for making composite powder Nos. 13 and 14. The thorium oxide was purchased through Henley and Co., Inc., New York, New York from Thorium Limited, London, England. The particle size was designated 100 to 300 angstrom by Thorium Limited, and they reported its impurity analysis to be as follows:

Cerium Oxide, Ce_2O_3	3 ppm
Other Rare Earth Oxides	5 ppm
Sodium Oxide, Na_2O	50 ppm
Calcium Oxide, CaO	250 ppm
Iron Oxide, Fe_2O_3	13 ppm
Heavy Metal Oxides, PbO	10 ppm

Photomicrographs of earlier composite powders from Chas. Pfizer and Sherritt Gordon Mines were presented in the third quarterly report. The new powders, Nos. 13 and 14, from the respective suppliers had the same general particle size, shape, and type of microstructure as the earlier powders when observed under the optical microscope.

Sintered compacts of the two composite powders, Nos. 13 and 14, from Chas. Pfizer were extruded to rod, but no magnetic or tensile properties have been determined to date. The composite powders from Sherritt Gordon Mines are in the process of being extruded. A delay in making and obtaining the properties of these extrusions was encountered, because the delivery of thorium oxide to Westinghouse by the supplier took longer than expected. Therefore, the composite powder suppliers did not receive the thorium oxide to use in the powder manufacture as early as scheduled.

(c) New Processing Conditions

As described in the fifth quarterly report, the Co + Be prealloyed atomized powder No. 9 was given an internal oxidation treatment for two hours at 1830°F followed by hydrogen reduction, isostatic pressing, hydrogen sintering, and extrusion. The BeO dispersion produced in the cobalt was found to be more stable and resistant to coarsening at 1600°F than Al_2O_3 dispersed in cobalt. This conclusion was reached after all extruded materials containing BeO and Al_2O_3 dispersed in cobalt had been reviewed. These included Co + Al_2O_3 extrusions fabricated from composite powders as well as internally oxidized powder, as follows:

Powder No.	Intended Composition (weight percent)
a. Internally Oxidized Powders (Extruded)	
8	Co + 4.7 alpha-Al_2O_3
9	Co + 3.6BeO
b. Composite Powders (Extruded)	
1	Co + 4.75 gamma-Al_2O_3 (0.01-0.06μ), Chas. Pfizer
2	Co + 4.75 alpha-Al_2O_3 (0.1-0.6μ), Chas. Pfizer

The basis for evaluating thermal stability was a comparison of microstructures of the original as-extruded rod with those of broken tensile specimens which had been tested at 1600°F after aging 100 hours at 1600°F in vacuum.

Since the BeO dispersoid was more stable than Al_2O_3, the Co + Be powder was selected and a shorter internal oxidation time (1/2 hour at 1830°F) applied in an attempt to achieve a still finer dispersoid of BeO in cobalt, and a smaller interparticle spacing. The

tensile and creep properties would be expected to be improved as a result.

Examination of the microstructure of the sintered compact showed that a finer BeO dispersoid did appear to be achieved as a result of the 1/2 hour internal oxidation treatment applied to the powder in comparison with the two hour treatment. An examination of the microstructure of the rod extruded from the compact will be made shortly.

3. Program for the Next Quarter

a) Proceed with the processing of powders into extrusions for the intermediate evaluation phase of the program.

b) Determine magnetic and tensile properties at room temperature and in the 1200° to 1600°F range.

c) Initiate exploratory secondary working treatments (cycles of swaging with 10 percent reductions per pass and intermediate and final annealing at the swaging temperature) on cobalt-base and iron + 27 w/o cobalt-base compositions having the finer and more thermally stable dispersoids, and the best combination of magnetic and mechanical properties in the hot-extruded condition.

D. TASK 4 - CREEP TESTING

1. Summary of Technical Progress

During the past quarter, testing continued on Nivco alloy heat 10-NO2V-1099. The status of each test is summarized as follows.

a) Specimen No. 3 was removed from test after 5000 hours at 1150°F and a stress of 30,000 psi. Total strain was 5.32 percent while the pressure at test termination was 2.7×10^{-9} torr.

b) A new sample, specimen No. 6, was placed on test at 55,000 psi at temperature of 1000°F. Test time amounts to 114 hours at a pressure of 1.8×10^{-7} torr.

c) The status of the remaining specimens are summarized below.

Specimen Number	Temp. (°F)	Stress (psi)	Time (hours)	Capsule Pressure (torr)	Strain (percent)
2	1100	37 500	8489	1.0×10^{-9}	0.95
4	1050	50 000	5037	2.3×10^{-9}	0.96
5	1150	25 000	4959	6.7×10^{-9}	2.60

2. Discussion

An unanticipated pressure rise occurred in two of the test capsules (No. 2 and No. 5) during the last quarter. However, in both cases, the rise in pressure was followed by a rapid decrease to values well below the previous pressures. It is felt that both increases in pressure were the result of localized specimen outgassing.

The strain time plots for each specimen are shown in figures II-11, II-12, and II-13. A summary of the creep test data for specimen No. 3, which has been taken off of test, is presented in table II-12.

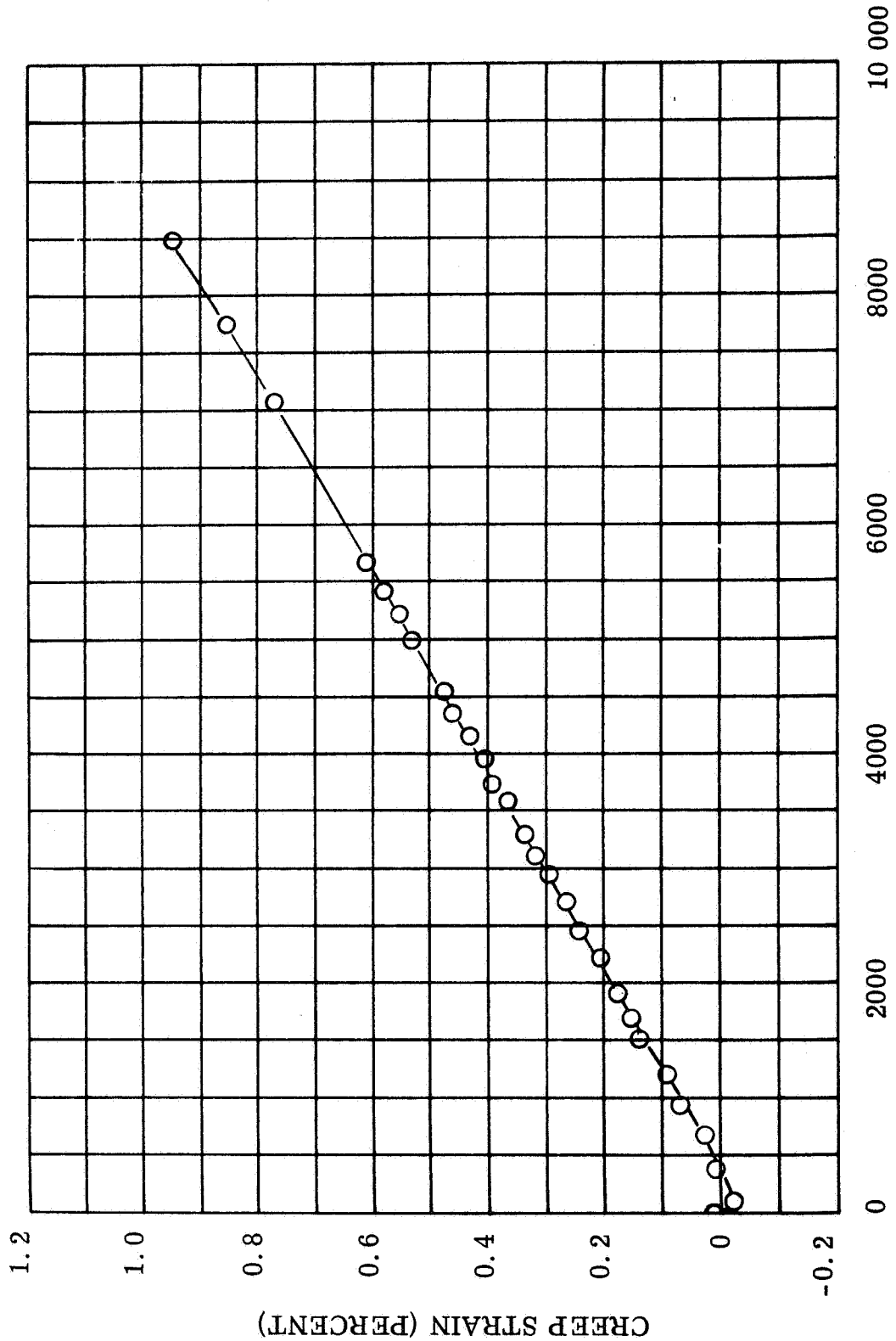

FIGURE II-11. Creep, Nivco heat 10-NO2V-1099, Tested in Vacuum at 1100°F and 37 500 psi Pressure at Beginning of the Test 9.0×10^{-7} torr Present Pressure 1×10^{-9} torr (Specimen #2)

Figure II-11. Creep Nivco Bar 1100°F

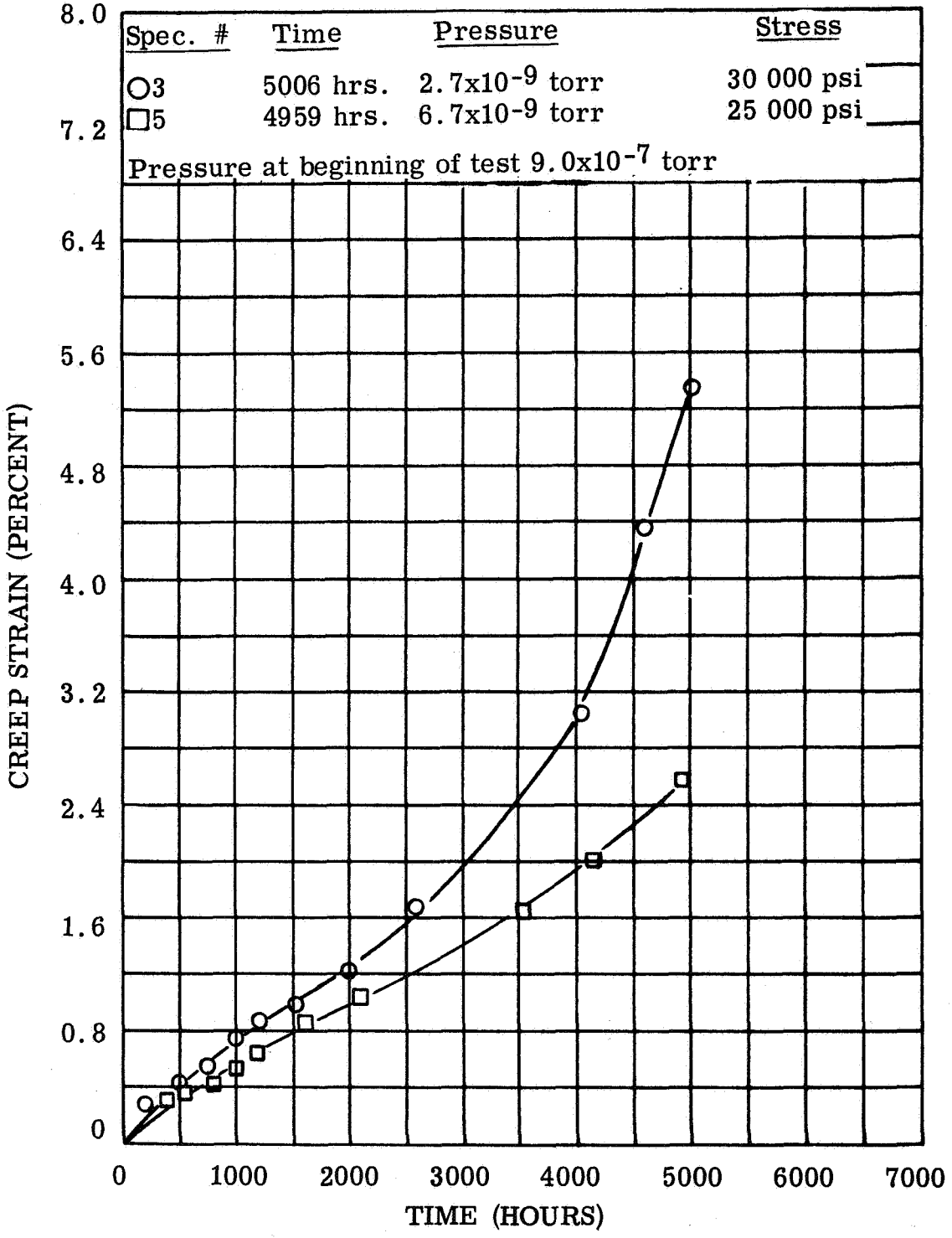

FIGURE II-12. Creep, Nivco heat 10-NO2V-1099, Tested in Vacuum at 1150°F and 25 000 psi and 30 000 psi

Figure II-12. Creep Nivco Bar 1150°F

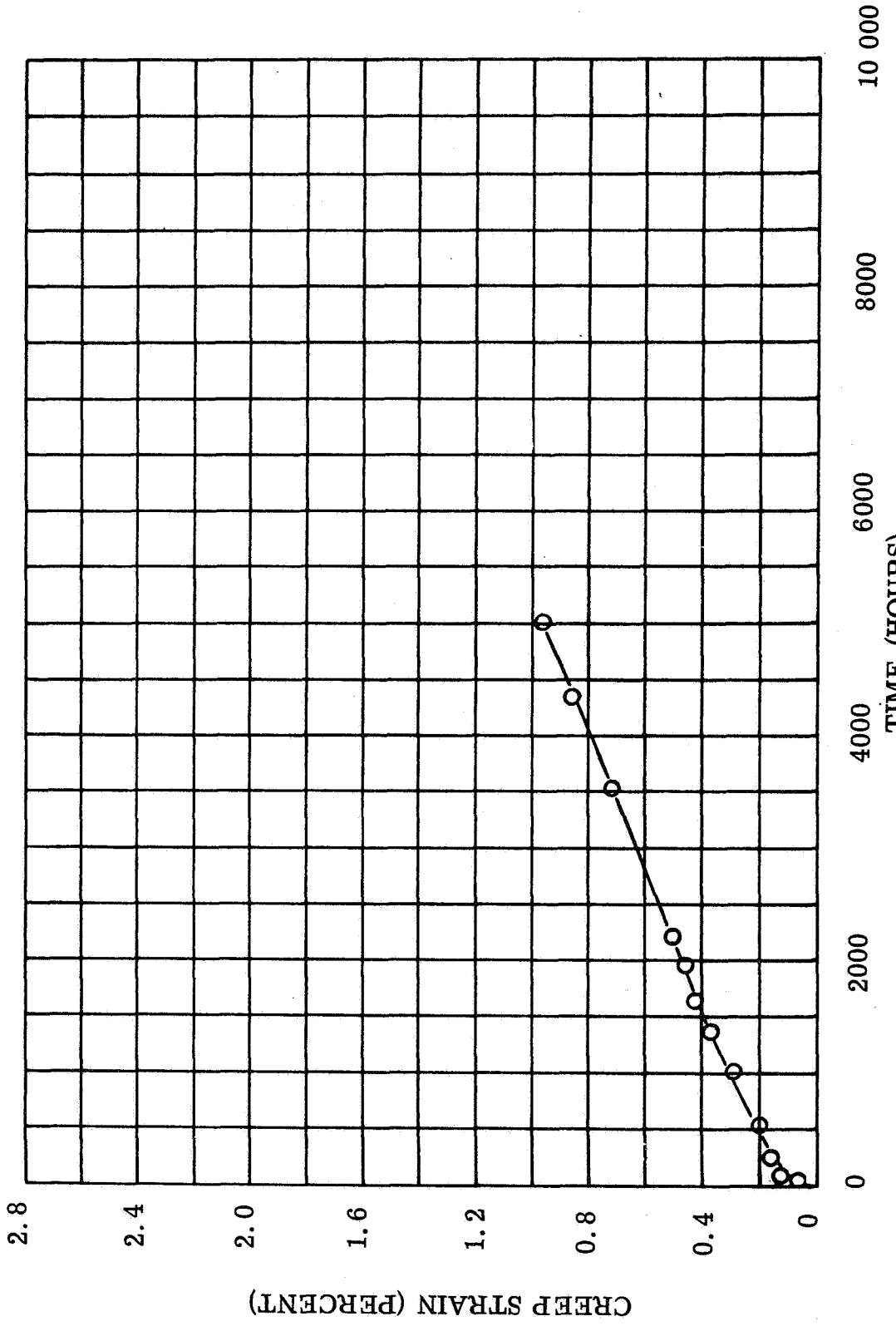

FIGURE II-13. Creep, Nivco heat 10-NO2V-1099, Tested in Vacuum at 1050°F and 50 000 psi. Pressure at Beginning of the Test 9.0×10^{-7} torr Present Pressure 1×10^{-9} torr (Specimen #4)

Figure II-13. Creep Nivco Bar 1050°F

3. Program for the Next Quarter

Testing will continue on specimens Nos. 4, 5, and 6 while specimen No. 2 will be removed from test when the total time reaches 10,000 hours.

TABLE II-12. Creep Data For Nivco Heat 10-NO2V-1099

Specimen	3
Temperature (°F)	1150
Stress (psi)	30,000
Duration of Test (hours)	5006
Total Creep Strain (percent)	5.32
Time to Cause 0.2 Percent Creep Strain (hours)	150
Time to Cause 0.4 Percent Creep Strain (hours)	460
Time to Cause 1.0 Percent Creep Strain (hours)	1550
Plastic Strain Obtained on Loading Specimen (percent)	0
Test Atmosphere	Vacuum
Minimum Creep Rate Percent Per Hour	0.00054
See Strain-Time Plot in Figure	II-12
Heat No.	10-NO2V-1099

SECTION III

PROGRAM II - HIGH TEMPERATURE CAPACITOR FEASIBILITY

This program will study the feasibility of building a lightweight capacitor suitable for operation up to 1100°F. It will utilize high-purity dielectric materials and specialized fabrication methods. The ultimate application is in lightweight, high-temperature, power conditioning-equipment suitable for space application.

A. SUMMARY OF TECHNICAL PROGRESS

1) The 250-hour life test at 1100°F in vacuum on a five wafer pyrolytic boron nitride capacitor was successfully extended to a total of 1120 hours at increased d-c energizing voltages (from 500 to 750 and 1000 V d-c/mil). At the completion of the test the capacitor losses were low ($\tan\delta < 0.0035$ at 1 kc/sec) and the capacitance had decreased 2.85 percent.

2) Analysis of electrical data and examination of the capacitor after testing indicates that the change in electrical properties with time can be largely accounted for by an added series capacitance resulting from a slight separation ($\sim$680 Å) of the electrodes from the wafer surfaces. It is believed this interface region was produced by interelectrode diffusion bonding between adjacent wafers.

3) Based on these assumptions, it appears that the observed instabilities in electrical properties are not associated with increased losses within the bulk of the dielectric but are primarily caused by interfacial phenomenon at the dielectric/electrode surfaces. Further improvements in capacitor fabrication techniques should, therefore, insure more reliable capacitor performance for extended periods of time at 1100°F with the dielectric stressed at maximum energizing voltages ($\geq$1000 V d-c/mil).

B. DISCUSSION

The overall objective of this program is to determine the feasibility of fabricating high-temperature capacitors which are compact, lightweight and suitable for operation in static power conditioning apparatus for space applications. A group of specific capacitor capabilities has been established as program objectives. These include:

1) Volume Parameter ($mF \cdot volts/in^3$): 50 to 150

2) Dissipation Factor ($\tan\delta$) at 1100°F: 0.005 to 0.03 maximum (60 cps to 50 kc/sec).

3) Capacitance change: ±5% (room temperature to 1100°F).

Feasibility will be demonstrated if these goals are achieved and the capacitor will be capable of operating in the 800° to 1100°F temperature range without supplemental cooling. Furthermore, a high-temperature capacitor meeting these requirements will be competitive in terms of size, weight, and electrical properties with more conventional capacitors designed for much lower operating temperatures.

Six quarterly reports have been issued on this program with detailed discussions of the results. The following summarizes these results:

1) Fixturing and methods have been developed for slicing, lapping and polishing thin wafers of pyrolytic boron nitride (Boralloy), polycrystalline Al_2O_3 (Lucalox and hot pressed Linde A), single-crystal sapphire, and hot-pressed polycrystalline BeO. Pyrolytic boron nitride has been successfully made into wafers one-inch square with thicknesses as thin as 0.5 mils (12 microns). The minimum thickness that can be reliably achieved with the other materials is in the range from 3 to 5 mils (75 to 125 microns).

2) Electrical data (capacitance, tan δ, d-c resistance), obtained over the temperature range from room temperature to 1100°F in vacuum for each of these thin wafer materials and the d-c breakdown strength, were measured at room temperature and 1100°F for several different materials. Test capacitors were prepared with sputtered high-purity platinum alloy electrodes using a CVC Plasma-Vac sputtering system.

3) The electrical data has been analyzed and compared for each candidate material. The results show that pyrolytic boron nitride will be the most promising high-temperature capacitor

material. Measured values obtained for a pyrolytic boron nitride capacitor with one mil thick dielectric are:

a) Tan δ at 1100°F: 0.0009 (1 kc/sec)

b) Capacitance change from room temperature to 1100°F: -1.5%

c) DC electric strength: Room temperature - 10,000 volts/mil; 1100°F - 7,000 volts/mil

The above indicates that the program objectives can be exceeded by a substantial margin using this material. In addition, a "figure of merit" was determined for each candidate material in order to assign a quantitative number to relative fabricabilities combined with electrical properties. The selection of pyrolytic boron nitride for a high-temperature capacitor was clearly indicated by this type of comparison.

4) A prototype multi-layered capacitor was fabricated with one mil thick pyrolytic boron nitride and "wrap around" sputtered electrodes to achieve parallel electrical interconnection in a three-wafer stacked configuration. Design feasibility has been demonstrated based on 1100°F electrical data in vacuum.

5) Satisfactory pyrolytic boron nitride wafers as thin as 0.4 mils have been made and tested. Sputtered thin-film electrodes of platinum and rhodium have been evaluated together with process controls necessary to achieve thickness reproducibility. An evaluation of rectangular versus tabbed wafer geometries has been made and the results and analysis of the data obtained for a five wafer multi-layer capacitor has been presented.

6) Two pyrolytic boron nitride multi-layer capacitors (nine wafers, average wafer thickness 0.76 mils and five wafers average wafer thickness 0.98 mils) were life tested at 1100°F in vacuum (10^{-7} to 10^{-9} torr). The five wafer unit has successfully completed 250 hours at 500 V d-c (in excess of 500 volts/mil electrical stress) with a capacitance change of less than 1.5 percent.

This report includes the results and analysis of an extended life test (from 250 to 1120 hours) on the five wafer pyrolytic boron nitride capacitor at 1100°F in vacuum with voltage stresses up to 1000 V d-c/mil.

1. Analysis of 1120 Hour Life Test Data

a. ELECTRICAL MEASUREMENTS

Figures III-1 to III-6 show a detailed presentation of all the electrical data obtained during the extended life test (to 1120 hours) on a five wafer multi-layer pyrolytic boron nitride capacitor (refer to sixth quarterly report for capacitor fabrication details). This test was continued beyond the planned 250 hour test time because of satisfactory performance to 250 hours. In addition, longer test times at increased energizing voltages would help to identify potential probelm areas for projected 10,000 hour applications.

Figure III-1 shows the change in tan δ and capacitance as functions of time. In general, it appears that for d-c energizing voltages up to and including 750 volts (750 V d-c/mil) the rates of change of capacitance and tan δ are essentially constant and relatively small in magnitude. These conditions appear to hold for times up to 477 hours. The d-c voltage was then increased to 1000 volts (1000 V d-c/mil) for an additional 643 hours. It is evident that tan δ increased and the capacitance decreased at greater rates after 477 hours or for the next 643 hours at 1000 V d-c.

The change in the RC product (megohms x microfarads) with time and higher energizing voltages is shown in figure III-2. An initial increase was observed after 259 hours but from 259 to 477 hours a decrease occurred indicating a decrease in insulation resistance or increase in the d-c conductivity. However, from 477 to 1120 hours (at 1000 V d-c) the RC product again increased. This may be the result of electrode polarization (depletion of charge carriers at the electrodes) or to a decrease in surface conductivity due to evaporation of condensed surface contaminants.

Figures III-3 and III-4 show tan δ and capacitance as functions of temperature (to 1100°F) and the change in magnitude of these parameters with time at constant temperature (to 1120 hours) at 10 kc/sec. A permanent increase in tan δ and decrease in capacitance is evident after the capacitor was cooled to 72°F. It should also be noted that after 259 hours of test time were completed, power to the vacuum furnace was inadvertantly interrupted on several occasions. This caused the furnace temperature to drop rapidly to temperatures in the 500° to 200°F range.

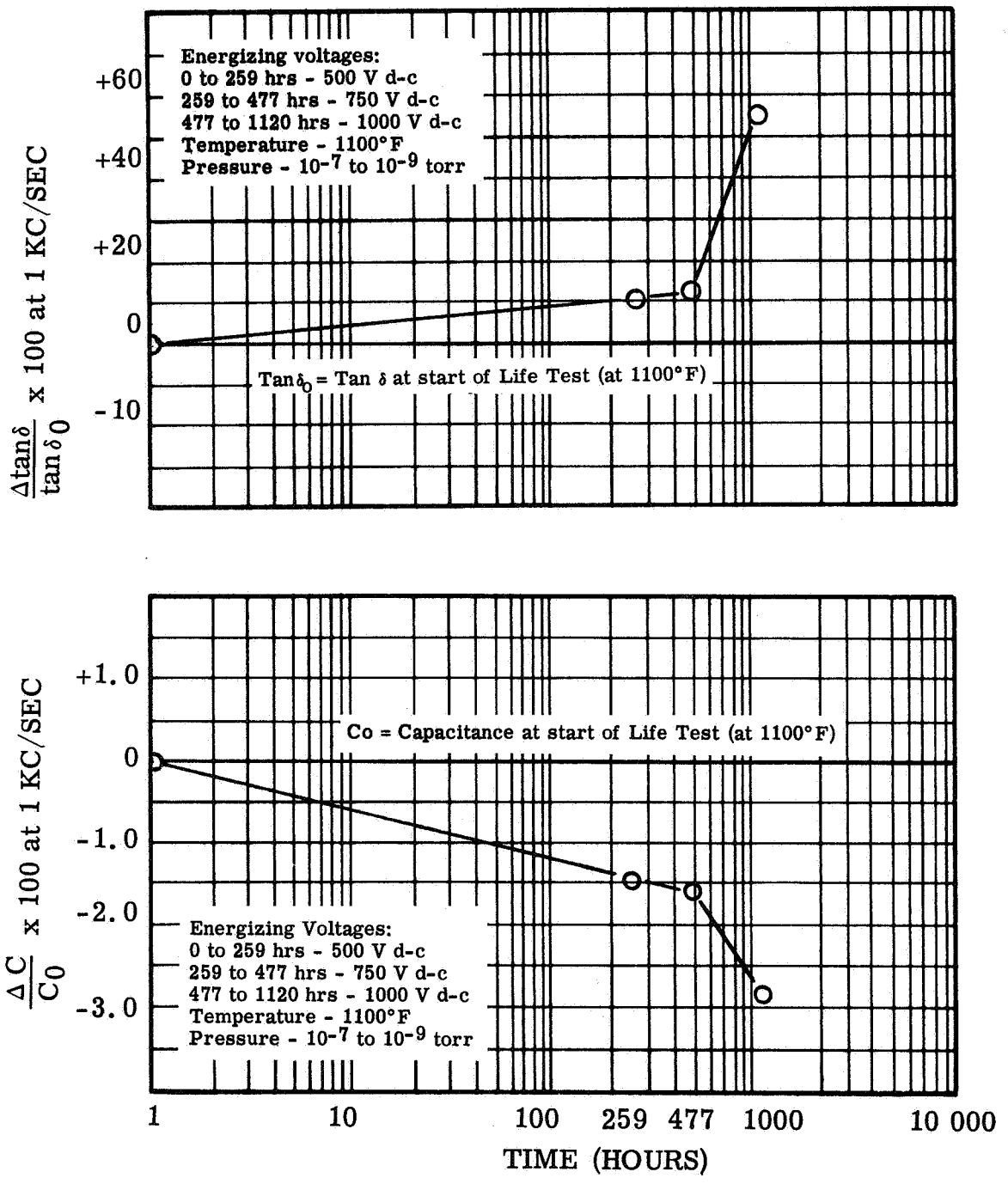

FIGURE III-1. Change in the Ratios of $\frac{\Delta \tan \delta}{\tan \delta_0}$ x 100 and $\frac{\Delta C}{C_0}$ x 100 as a Function of Time and Increased DC Energizing Voltages for a Five Wafer Multi-Layer Pyrolytic Boron Nitride Capacitor in Vacuum at 1100°F

Figure III-1. Change in Tan δ and Capacitance vs. Time

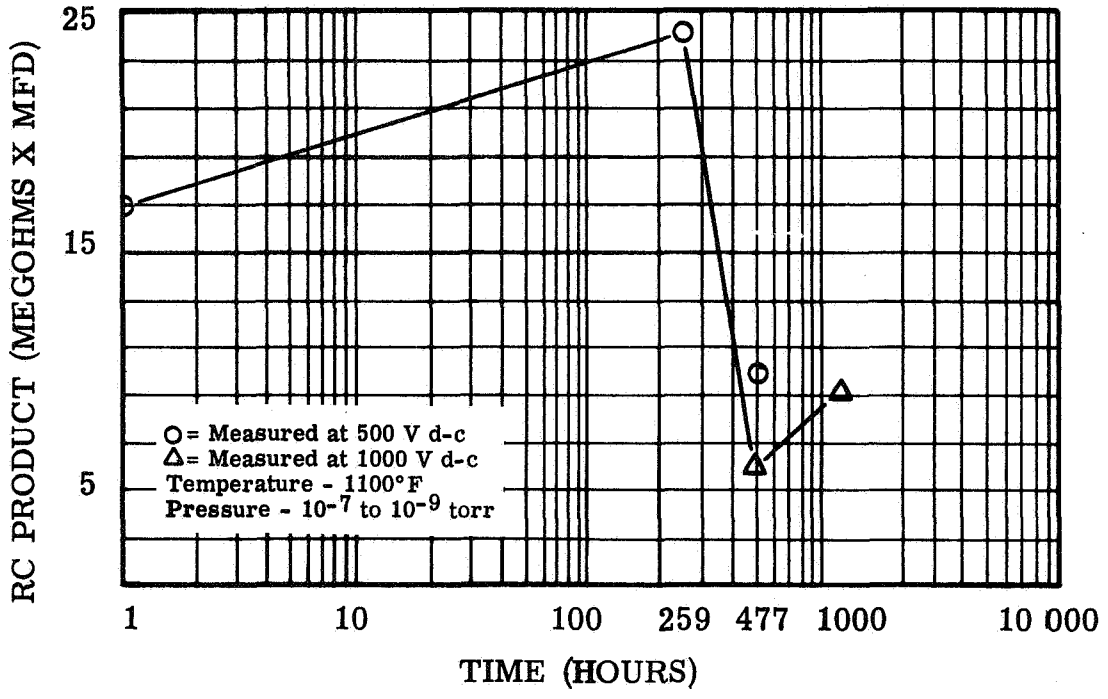

FIGURE III-2. Change in RC Product (Megohms x Microfarads) as a Function of Time and Increased DC Energizing Voltages for a Five Wafer Multi-Layer Pyrolytic Boron Nitride Capacitor In Vacuum at 1100°F

Figure III-2. Change in RC Product vs. Time

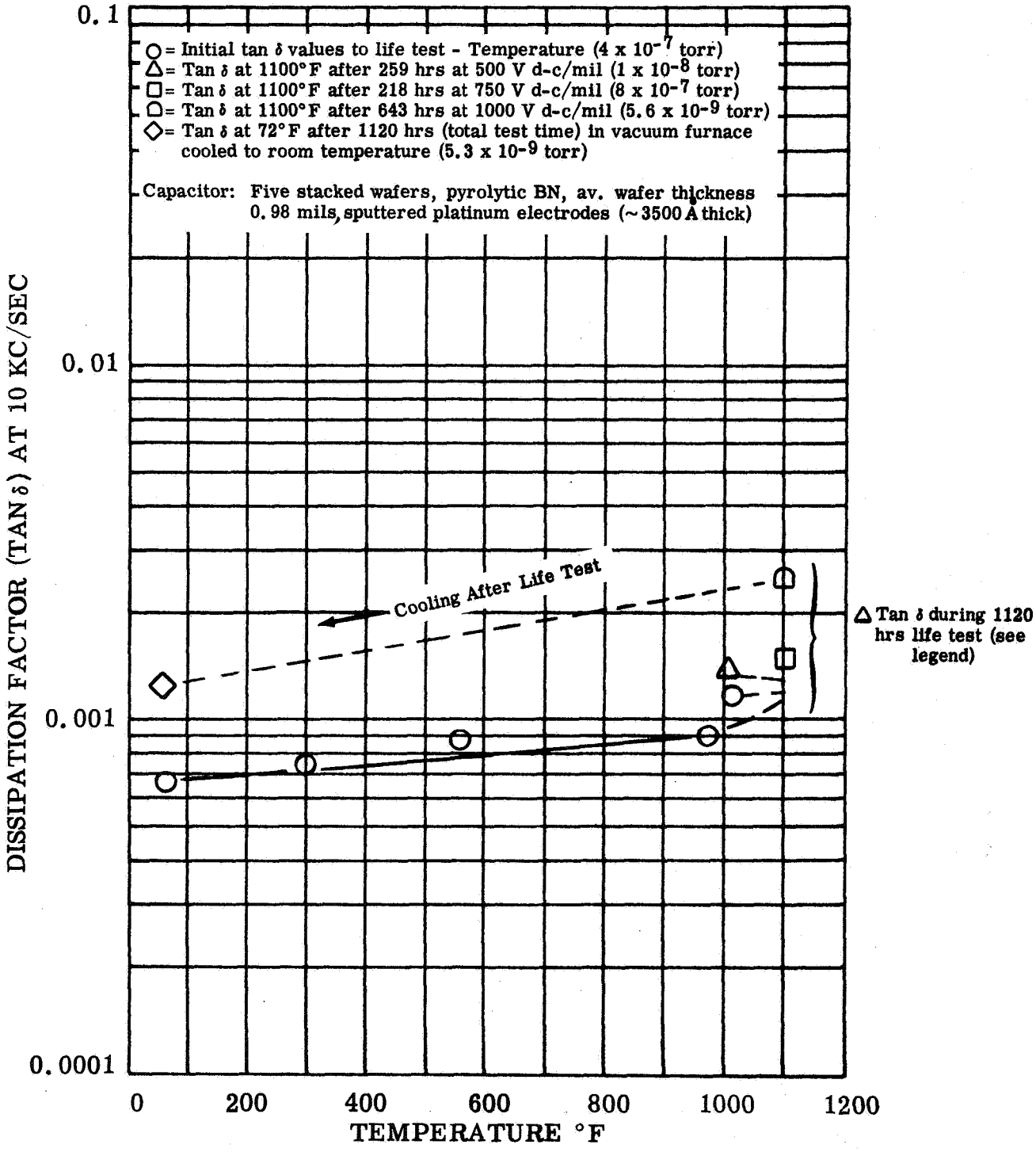

FIGURE III-3. Tan δ Versus Temperature and Change in Tan δ Versus Time and Increase DC Energizing Voltages at Constant Temperature (1100°F) in Vacuum for a Five Wafer Multi-Layer Pyrolytic Boron Nitride Capacitor

Figure III-3. Tan δ vs. Temperature and Time

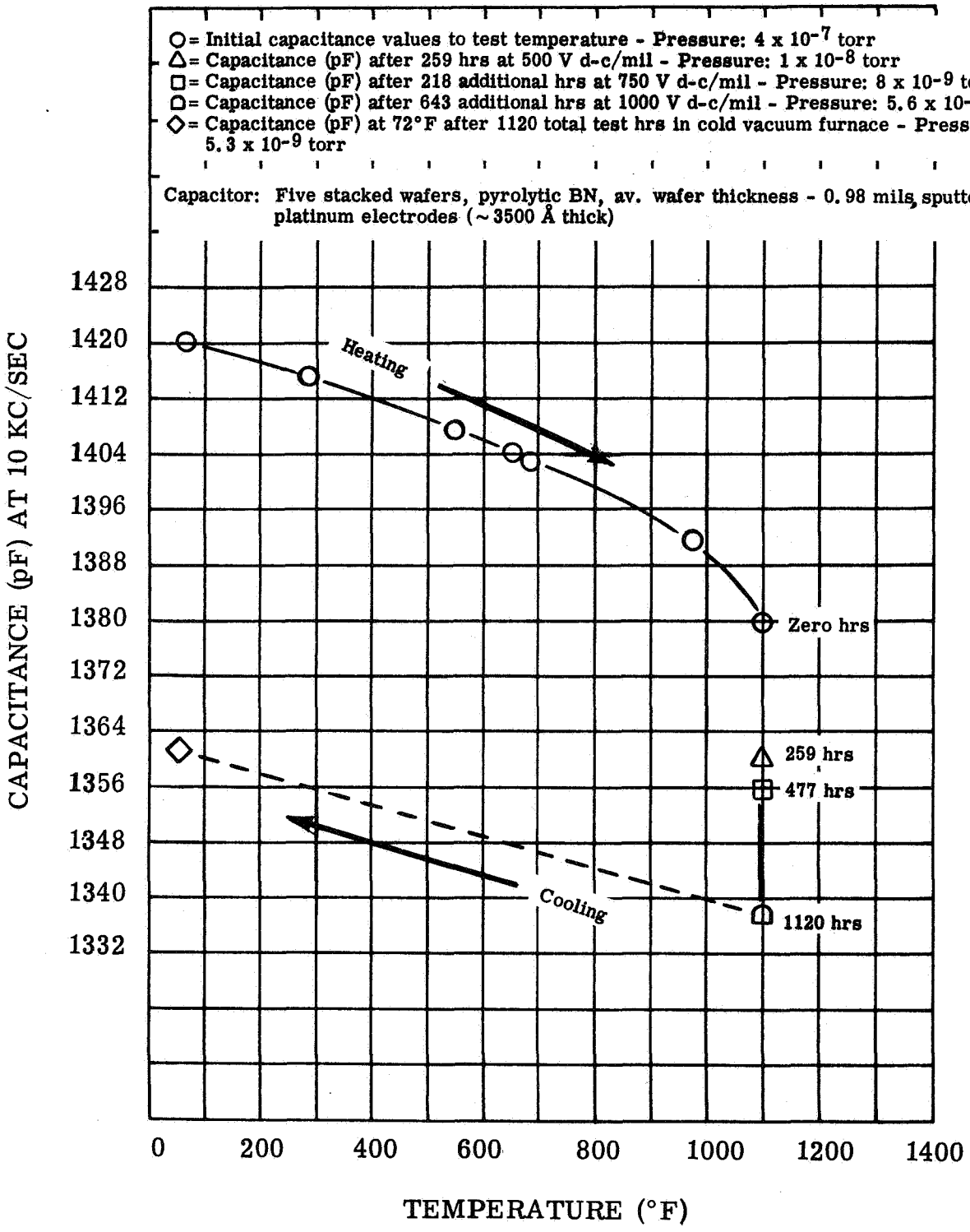

FIGURE III-4. Capacitance Versus Temperature and Time at Increased DC Energizing Voltages (Constant Temperature; 1100°F) in Vacuum for a Five Wafer Multi-Layer Pyrolytic Boron Nitride Capacitor

Figure III-4. Capacitance vs. Temperature and Time

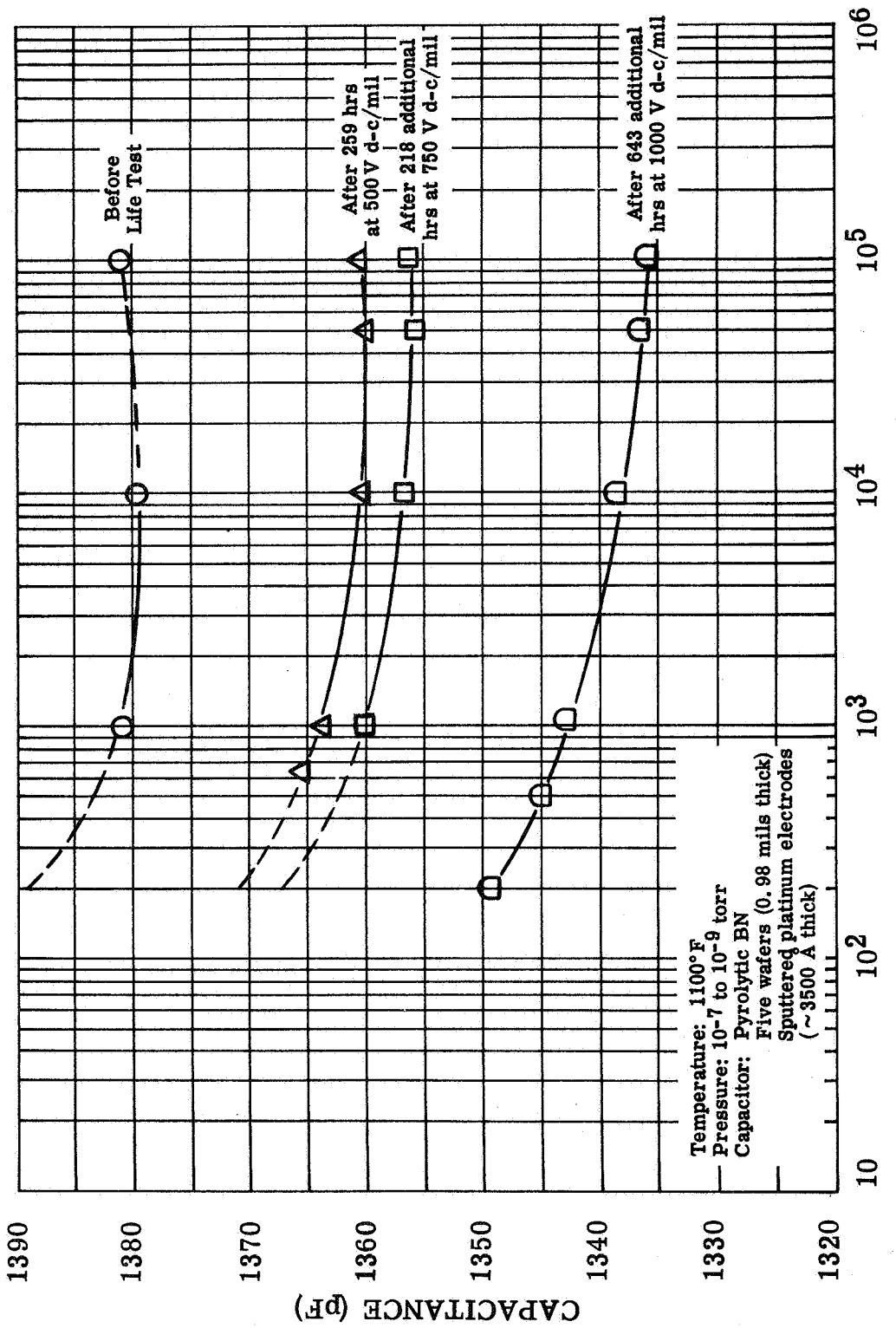

FIGURE III-5. Capacitance (pF) Versus Frequency at Several Time Intervals With Increasing Energizing Voltages for a 1120 Hour Life Test at 1100°F in Vacuum on a Five Wafer Multi-Layer Pyrolytic Boron Nitride Capacitor

Figure III-5. Capacitance vs. Frequency at Several Time Intervals

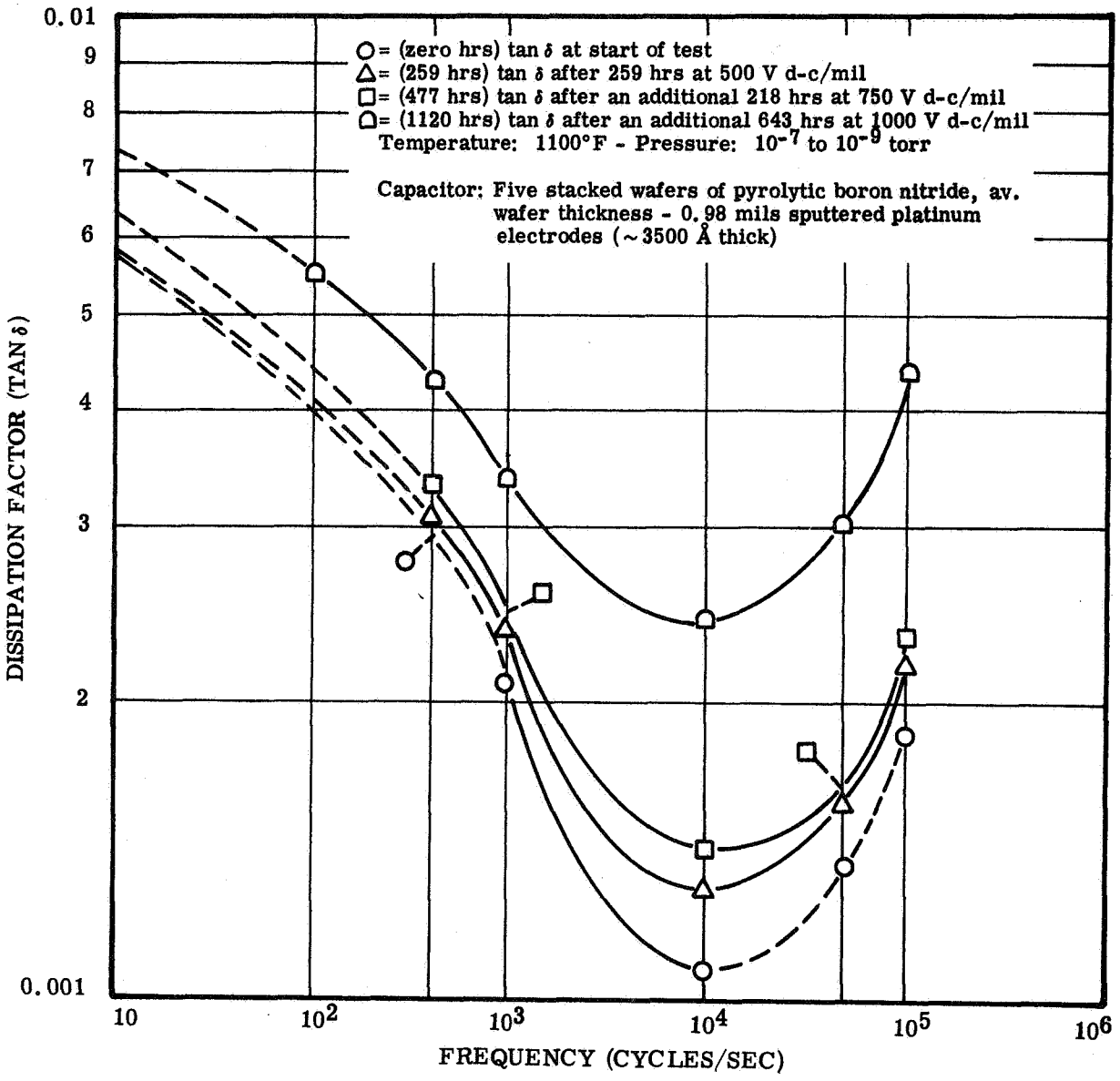

FIGURE III-6. Tan δ Versus Frequency at 1100°F in Vacuum at Different Time Intervals and Increased DC Energizing Voltages to 1120 Hours Total Test Time for a Five Wafer Pyrolytic Boron Nitride Capacitor

Figure III-6. Tan δ vs. Frequency at Several Time Intervals

Figures III-5 and III-6 show capacitance and tan δ as functions of frequency at 1100°F in vacuum during several time intervals (after 259, 477 and 1120 hours). The curves shown in figure III-5 indicate that most of the capacitance change occurred during the first 259 hours (at 500 V d-c/mil). Relatively little change occurred during the next 218 hours at 750 V d-c/mil. A detailed examination of these curves should reveal the relative changes in G and R as a function of test time using a modified form of equation (1):

$$\tan \delta = \frac{G}{2\pi fC} + 2\pi\ RC\, f^{3/2} \qquad (1)$$

where:

G = Conductance (dielectric losses of supporting insulators, solid dielectric between capacitor electrodes and d-c leakage conductance

R = Metallic resistance of leads, contacts and electrodes

f = frequency

C = Capacitance between electrodes

The curves in figure III-6 appear to follow the form of equation (1) if the conductance term (G), is modified so that tan δ decreases with frequency (in the lower frequency range) as the reciprocal of a fractional power of f($1/f^{1/2}$, $1/f^{1/3}$ etc.) rather than as 1/f.

The change in tan δ due to the series resistance term (R) which causes tan δ to increase with the 3/2 power of the frequency appears to fit the curves in figure III-6 reasonably well. Additional discussion of equation (1) and the equivalent circuit for a capacitor with series and parallel loss components can be found in the fourth quarterly report.

b. EXAMINATION OF THE FIVE WAFER LIFE TEST CAPACITOR

The five wafer pyrolytic boron nitride capacitor that successfully completed 1120 hours of test time at 1100°F was disassembled and examined. The pyrolytic boron nitride clamping fixture and the two uncoated (less sputtered platinum electrodes) wafers placed at the top and bottom of the five wafer capacitor stack

showed a slight amount of surface darkening together with several widely dispersed darkish spots. Vaporization and condensation of contaminates trapped within the layered structure of the pyrolytic boron nitride fixture may account for some of the darkening effect. In addition, contamination from the tantalum furnace element and the fixturing and capacitor (electrodes) may be another source of surface discoloration. In general, this effect could account for part of the increase in measured capacitor losses (tan δ) with time due to increased surface conductivities.

In attempting to separate the individual capacitor wafers in the stack, it was apparent that all of the wafers were bonded together via their electrodes. By carefully inserting a razor blade between two wafers it was found that adjacent electrodes were diffused into a single homogeneous foil. When the wafers were separated both electrodes adhered to one of the wafers and peeled away from the other. These results indicate that the initial electrode adherence decreased substantially under the combined driving forces of time, temperature, pressure, vacuum and the lower interface energies associated with metal to metal versus metal to oxide or nitride contact. The two outer electrodes on the end wafers in the stack did not show a loss of adherence apparently because they were in contact with boron nitride surfaces (high interface energies).

Thus it seems reasonable to conclude that a physical separation or air (vacuum) gap at the wafer electrode interface developed due to a decrease in electrode adherence. The width of this gap apparently increased with time, electrical stress and temperature fluctuations (furnace power interruptions).

Therefore, the decrease in capacitance and increase in tan δ (refer to figure III-1) after 1120 hours can be assigned to a parasitic series capacitance and its associated loss mechanisms produced by the air (vacuum) gap. If, for example, the gap has a width or thickness of 680 Å with a dielectric constant of one (for vacuum) a capacitance of about 30,000 pF would appear in series with one side of a standard capacitor wafer (calculated for an electrode area of 0.364 in^2). If a gap of equal thickness exists at the opposite electrode, another series capacitance is generated of equal magnitude. The effective capacitance is then 15,000 pF and will appear in series with the capacitance attributed to the bulk dielectric (pyrolytic boron nitride). A measured terminal capacitance would be about 294 pF or a 2 %

decrease in capacitance for a 300 pF (calculated capacitance less air gap) capacitor wafer. As the gap thickness increases, the series capacitance will decrease and the measured capacitance will also decrease.

To summarize, it appears that the instabilities in electrical properties with time and increasing d-c energizing voltages are primarily caused by electrode interface phenomenon and other extrinsic effects not necessarily associated with the bulk of the dielectric. Very satisfactory capacitor performance at 1100°F is indicated for a voltage stress up to 750 V d-c/mil. At 1000 V d-c/mil, accelerated degradation of tan δ and capacitance is evident but with further improvements in capacitor fabrication methods it appears that the degradation mechanism previously discussed can be significantly minimized.

C. PROGRAM FOR THE NEXT QUARTER

The final topical report will be completed.

SECTION IV

PROGRAM III - BORE SEAL DEVELOPMENT AND COMBINED MATERIAL INVESTIGATIONS UNDER A SPACE-SIMULATED ENVIRONMENT

The bore seal effort under task 1 will evaluate promising ceramic-metal sealing systems in potassium and lithium vapor at temperatures to 1600°F for 2000 hours. Elevated temperature seal strength and vacuum tightness will be determined. A 4-inch diameter bore seal loaded with potassium will be incorporated in a stator design and evaluated in a 5000-hour endurance test at temperature and in a high-vacuum environment. This test will confirm data determined on smaller geometries.

Two 5000-hour tests will be run under task 2 on a stator which typifies the construction of an inductor alternator or a motor. The first was run between 800° and 1100°F temperature. The second test will be run with a bore seal at temperatures between 1100° to 1600°F. All will be tested at a high-vacuum (less than 10^{-8} torr) under electric and magnetic stresses.

A transformer and two solenoids under tasks 3 and 4 will be similarly tested under high vacuum and at elevated temperature. The purpose will be to evaluate the combined effects of electric and magnetic stresses, and high vacuum on combinations of materials suitable for application to advanced space electric power systems. One solenoid test will be under d-c excitation and the other under intermittent excitation so the effects of an invariant electric stress can be investigated.

The design features incorporated into the stator, transformer and bore seal were defined in detail in Appendixes A, B, and C of the first quarterly report.

A. TASK 1 - BORE SEAL DEVELOPMENT

1. Summary of Technical Progress

a) Three 4-inch by 4-inch metal-beryllia bore seal capsules (Nos. 3, 4, and 5) were brazed during this quarter using the 60Zr-25V-15Cb alloy and evaporated molybdenum metallizing on the beryllia.

b) Bore seal capsule No. 1 was sectioned for metallographic examination and to obtain specimens for modulus-of-rupture strength and potassium compatibility. A 500-hour compatibility test of the specimens was completed at 1600°F. Bore seal capsule No. 2, which was leak-tight, will be used for mechanical tests.

c) Bore seal capsule No. 3 failed the vacuum leak test in the as-brazed condition.

d) Bore seal capsule No. 4 was loaded with potassium and sealed. It is now ready for the stator environmental compatibility test described under task 2 of this program.

e) Bore seal capsule No. 5 was loaded with potassium but the sealing weld was not completed because vaporized potassium shorted the electron beam welding coil.

f) Specimens were brazed, capsules were loaded, and the test started for a 2000-hour potassium compatibility run.

2. Discussion

The purpose of this program is to develop prototype bore seals for space electric power alternators in alkali metal Rankine cycle systems. Promising ceramic-to-metal seal systems are being evaluated with regard to manufacturing technique, mechanical and physical properties, and compatibility with high-purity potassium and lithium vapor.

Systems selected for evaluation have been narrowed to beryllia (65 ppm Si) joined to Cb-1Zr alloy with the following active metal brazes: Braze alloy No. 3(56Zr-16Ti-28V) with a brazing temperature of 2372°F and braze alloy No. 9(60Zr-25V-15Cb) with a brazing temperature of 2462°F utilizing molybdenum metallized beryllia.

High-purity yttria is being evaluated as a back-up ceramic. Properties to be measured include modulus-of-rupture, peel strength, high temperature tensile and creep rupture strength, vacuum tightness, and vibration and thermal shock resistance. Compatibility tests include exposure of selected seals and properties specimens to lithium and potassium at 1600°F for periods to 2000 hours.

Effort during this quarter was directed primarily toward fabricating and loading two potassium-filled 4-inch bore seal capsules, evaluating 4-inch bore seal capsule No. 1, and starting the 2000-hour potassium compatibility test of modulus-of-rupture bars. Priority was established in the order of listing. Problems were encountered in filling the bore seal capsule with potassium. As a result, the effort on properties of ceramic-to-metal seals was delayed.

a. PROPERTIES OF CERAMIC-TO-METAL SEALS

The vendor examined (ref. 1 and 2) the cracked 2-inch Thermalox 998 beryllia cylinders and backup rings which were returned to them. (See the sixth quarterly report.) Their records show that no cracks existed at the time of their preshipment inspection. An additional crack was found in one of the ceramic during their re-examination.

Packing for shipment appeared proper. Detailed consideration by the vendor of possible causes disclosed no likely cause in their production or handling. Re-examination of the receiving inspection procedures shows that the beryllia cylinders were handled along with many other ceramics and no likely time for breakage can be postulated. The cracks appear to be caused by internal stress.

One 2-inch by 2-inch BeO cylinder and three 2-inch by 0.2-inch BeO backup rings were received from the vendor to replace the returned, cracked ceramics.

b. ALKALI METAL EXPOSURE TESTS

Two groups of capsules were loaded with specimens and potassium and sealed for exposure at 1600°F. A 4-inch bore seal capsule was included for potassium-loading with each group of capsules. The first group (test 9.5) of capsules included two capsules containing sections cut from bore seal capsule No. 1 and a capsule containing yttria and alumina ceramics. The

second group (test 9.2) consisted of four capsules containing brazed specimens for 2000-hour vacuum and potassium compatibility tests at 1600°F.

(1) Preparation of Specimens

Eleven brazing runs were completed to prepare specimens as shown in table IV-1. Ceramics and metal parts were prepared as described in the fifth and sixth quarterly reports. Beryllia ceramics to be brazed with alloy No. 9 (60Zr-25V-15Cb) were metallized with evaporated molybdenum except for those in brazing run 9.5. Rejections of modulus-of-rupture assemblies indicated in the table (table IV-1 shows the fraction of assemblies accepted for testing) were due to movement of the ceramics after the brazing jig was assembled, resulting in misaligned assemblies. The yield of leak-tight vacuum leak test assemblies brazed with braze alloy No. 3 (56Zr-16Ti-28V) continued to be low.

(2) Exposure of Specimens from Bore Seal Capsule No. 1 to Potassium and Vacuum

Four capsules containing sections from bore seal No. 1 were subjected to 1600°F temperature in a furnace at an ultimate pressure of 2×10^{-9} torr. (See table IV-2.) The capsules had been prepared and loaded in a group which included bore seal capsule No. 4. A purity test capsule was also loaded with potassium in this group. Subsequent mercury amalgamation analysis of the potassium in this capsule by Mine Safety Appliance Research Corporation showed the oxygen content to be 22 ppm. The loaded capsules were exposed for a total period of 557 hours at 1600°F ± 35°F.

After completion of the test, capsules containing the bore seal sections were opened in the following manner: A 11/16-inch hole was drilled in the top of the capsule using silicone vacuum oil as the lubricant. The capsule was quickly submerged in a beaker containing methyl alcohol. After the reaction stopped, the capsule was rinsed with distilled water. The end of the capsule was then cut off using a carborundum wheel. The specimens were removed and rinsed in de-ionized water, methyl alcohol, and acetone in the listed order. The specimens were dried in vacuum at 200°F.

TABLE IV-1. Summary of Brazing Runs Made In Fabricating Ceramic-to-Metal Seal Assemblies for Alkali Metal Tests

Braze Run No.	Purpose (test No.)	Load Description			Conditions
		Brazing Alloy	Assemblies	Material and Lot No.	
9.1	9.2[d]	56Zr-28V-16Ti	2/5 MoR; 2/2 TP; 0/2, 1/2 VT[a]	BeO-B; Cb-1Zr-A	All Alloy 56Zr-28V-16Ti Specimens held at 2102°F for 10 min., brazed at 2372°F, 5 min. at a pressure of < 1 x 10^{-6} torr
9.2	9.2[d]	56Zr-28V-16Ti	3/5 MoR; 2/2 TP; 2/2, 2/2 VT	BeO-B; Cb-1Zr-A	
9.3	9.2[d]	60Zr-25V-15Cb[c]	5/5 MoR	BeO-B; Cb-1Zr-A	
9.4	9.2[d]	60Zr-25V-15Cb[c]	5/5 MoR; 2/2 TP; 2/2, 2/2 VT	BeO-B; Cb-1Zr-A	All Alloy 60Zr-25V-15Cb Specimens held at 2202°F for 10 min., brazed at 2462°F, 5 min. at a pressure of < 1 x 10^{-6} torr.
9.5	9.2[d]	60Zr-25V-15Cb[b]	5/5 MoR; 2/2 TP; 2/2, 2/2 VT	BeO-BA; Cb-1Zr-A	
9.6	9.2[d]	60Zr-25V-15Cb[c]	5/5 MoR; 2/2 TP; 2/2, 2/2 VT	BeO-BA; Cb-1Zr-A	
9.7	9.2[d]	56Zr-28V-16Ti	3/5 MoR; 2/2 TP; 0/2, 0/2 VT	MoR & TP with BeO-B, VT with BeO-BA; all with Cb-1Zr-A	
9.8	9.2[d]	56Zr-28V-16Ti	2/3 MoR; 2/2 TP	BeO-BA; Cb-1Zr-A	
9.9	9.2[d]	56Zr-28V-16Ti	2/2, 2/2 VT	BeO-BA; Cb-1Zr-A	
9.10	9.3[e]	60Zr-25V-15Cb[c]	4/5 MoR; 2/2 TP; 2/2, 2/2 VT	BeO-B, Cb-1Zr-A	
9.11	9.3[e]	60Zr-25V-15Cb[c]	5/5 MoR; 2/2 TP; 2/2, 2/2 VT	BeO-B, Cb-1Zr-A	

Notes: (a) MoR = Modulus of Rupture Assembly; TP = Tab Peel Assembly; VT = Vacuum Test Assembly. For MoR and TP, number before slash is number of acceptable (not bent or unevenly brazed); after slash is number of starts. For VT, number before slash is number of leak tight joints in an assembly containing the number of joints listed after the slash.
(b) Not metallized. Set aside for possible future evaluation.
(c) Metallized with evaporated Mo before brazing.
(d) Two thousand hour exposure test in potassium and vacuum at 1600°F.
(e) Two thousand hour exposure test in lithium and vacuum at 1600°F.

TABLE IV-2. Furnace Pressure Data on the 500 Hour 1600°F Potassium Exposure Test of Bore Seal Capsule No. 1 Sections

Time	Pressure (torr)
After weekend Pump-down furnace cold	1.5×10^{-8}
Maximum Pressure during heat-up time of 26 hours	2.0×10^{-6}
Start of test	7×10^{-7}
After 24 hours	2.6×10^{-8}
After 50 hours	1.7×10^{-8}
After 125 hours	1.0×10^{-8}
After 200 hours	9×10^{-9}
After 310 hours	6.5×10^{-9}
At end of test (at temperature) 557 hours	5×10^{-9}
At end of test (at room temperature)	2×10^{-9}

Inspection of the specimens revealed a gray cast to the potassium-exposed specimens; no change in the vacuum-exposed specimens. The modulus-of-rupture strength of as-fabricated, vacuum-exposed and potassium-exposed specimens will be reported in the next report. A seal section from bore seal capsule No. 1 was to be exposed to potassium with the ceramic MoR bars; however, the specimen was not prepared in time to include in this group so it was included in the following group in a capsule by itself numbered 9.2B. The capsule was loaded and ready to start the test run near the end of the quarter.

(3) Exposure of Ceramics and Ceramic-to-Metal Seal Assemblies to Potassium and Vacuum for 2000 hours at 1600°F (test 9.2)

Capsules were loaded with modulus-of-rupture assemblies (MoR), tab-peel assemblies (TP), and vacuum leak-test assemblies (VT) as shown in table IV-3.

The specimens were assigned to the capsules in a random manner. A number was assigned to each accepted, brazed assembly. Using a table of random numbers, the specimens were distributed among the capsules. The distribution of specimens from the different brazing runs is shown in table IV-4.

Capsules were handled and loaded in a group that also included capsule No. 9.2B. Four-inch bore seal capsule No. 5 was included in this group for loading with potassium. The capsules and specimens were vacuum fired at 1470°F for 5 minutes before reinserting them in the electron beam welding chamber for loading. The four capsules (9.4, 9.5, 9.7, and 9.8) were placed on test for 2000 hours at the end of this quarter.

c. BORE SEAL CAPSULE CONSTRUCTION

The scope of this task includes the manufacture of as many as six 4-inch by 4-inch model bore seal capsules from Mo metallized 99.8 percent beryllia and columbium-1% zirconium using braze alloy No. 9 (60Zr-25V-15Cb); loading two assemblies with potassium, and the destructive evaluation of one model seal. Three additional assemblies were brazed; one was loaded with potassium. It is now ready for environmental testing with an alternator stator.

TABLE IV-3. Specimen Distribution in Capsules

Capsule Number	Environment	Load Description
9.4	Potassium	5 MoR, 2 TP, 1 VT assemblies in vapor, 5 MoR assemblies in liquid. All 99.8% BeO to Cb-1Zr specimens brazed with alloy No. 9.
9.5	Potassium	5 MoR, 2 TP, 1 VT assemblies in vapor. All 99.8% BeO to Cb-1Zr specimens brazed with alloy No. 3.
9.6	Potassium	5 each of Y_2O_3, Lucalox Al_2O_3, and sapphire MoR bars in vapor; 3 each in liquid.
9.7	Vacuum	5 MoR, 2 TP, 1 VT assemblies. All 99.8% BeO to Cb-1Zr specimens brazed with alloy No. 9.
9.8	Vacuum	5 MoR, 2 TP, 1 VT assemblies. All 99.8% BeO to Cb-1Zr specimens brazed with alloy No. 3.

TABLE IV-4. Distribution of Specimens from Different Brazing Runs[a]

Capsule Number	Load Description
9.4	3 MoR, 2 TP, 1 VT from braze run 9.6; 4 MoR from braze run 9.5; 1 MoR from braze run 9.3
9.5	1 MoR from braze run 9.1; 1 MoR, 1 VT, 1 TP from braze run 9.2; 2 MoR from braze run 9.8; 1 MoR, 1 TP from braze run 9.7.
9.7	3 MoR from braze run 9.6; 2 MoR, 2 TP, 1 VT from braze run 9.5.
9.8	1 MoR, 1 TP, 1 VT from braze run 9.1; 2 MoR from braze run 9.2; 2 MoR from braze run 9.7.

(a) See table IV-1 for summary of brazing runs.

(1) Fabrication of 4-Inch Bore Seal Capsules Nos. 3 to 5

Three more model bore seals were constructed using the procedures outlined in the sixth quarterly report.

(a) Bore Seal Capsule No. 3

This bore seal was not vacuum-tight. The flange on one endbell had warped slightly after the brazing run. The flange had been flattened using the same procedure that had been used for the other flanges (see the sixth quarterly report) so the cause of the warpage is not known.

(b) Bore Seal Capsule No. 4

A good braze was obtained although an excess amount of alloy was indicated by the puddling on the inside surface of the backup ring. The assembly passed the cold vacuum/pressure test (see sixth quarterly report) with no leak detectable at a sensitivity of 10^{-9} atm-cc/sec.

(c) Bore Seal Capsule No. 5

The same results were obtained as for bore seal No. 4. The end bell was electron beam welded to the tubulation and not back brazed with alloy No. 9 as were the end bells for the other assemblies.

(2) Filling Bore Seal Capsules with Potassium and Sealing

Three assemblies were loaded with potassium but a successful closure weld was made on only one.

(a) Bore Seal Capsule No. 2

The bore seal was vacuum fired at 1472°F for 10 minutes before inserting into the electron beam chamber. Hot gettered potassium was loaded into the bore seal at $< 5 \times 10^{-6}$ torr. The assembly was then mounted in the motor-driven chuck for welding. The electron beam welding gun shorted and the filament was burned out before the closure

weld could be completed. The bore seal was removed from the chamber; the potassium dissolved with alcohol; the end of the tubulation cut off and remachined; and the assembly was set aside for possible future use.

(b) Bore Seal No. 4

The bore seal was vacuum fired at 1470°F for 10 minutes before inserting into the electron beam welding chamber. The bore seal was included with a group of capsules (section IV.A.2.b.(2)) for loading. About one gram of potassium was loaded into the bore seal and the closure weld was made. The loaded bore seal is now in place in a stator for environmental testing.

(c) Bore Seal No. 5

The bore seal was vacuum fired at 1470°F before inserting into the electron beam welding chamber. Difficulty was encountered in attaining the required vacuum so it was necessary to clean out the system and refire the bore seal. A fine stream of potassium which had passed into the fore pump during a series of loadings had corroded the pump. After replacing the pump and an alkali metal shut-off valve, the bore seal was loaded. During electron beam welding a power surge caused a blow-hole in the weld area. The bore seal was removed, cleaned, and held for future use.

(3) Evaluation of 4-Inch Bore Seal Capsule No. 1

A new subtask was started to evaluate the strength and potassium corrosion resistance of the ceramics used to manufacture the 4-inch bore seal capsules. This was motivated by the questionable visual appearance of the ceramics (discussed previously in the sixth quarterly report).

An outline of the subtask is given below:

a) Cut 20 MoR bars and 2 ceramic/metal seal samples from the bore seal.

b) Expose 5 MoR bars in a potassium compatibility capsule and 5 in a vacuum capsule for 500 hours at 1600 °F.

c) Break the 20 bars to determine the following:

   1) As-fabricated strength in radial direction.

   2) As-fabricated strength in circumferential direction.

   3) Effect of elevated temperature vacuum exposure

   4) Effect of elevated temperature potassium exposure.

d) Expose a seal sample in the above potassium compatibility capsule and compare the microstructure to the as-fabricated condition.

Bars were cut in an axial direction from the 0.1-inch-thick section of the 4-inch cylindrical ceramic tube. They were then diamond ground to a square cross section. Because of the radius of curvature of the cylinder, it was necessary that the finished bars be slightly smaller than the standard 0.1-inch by 0.1-inch bars normally used on this program. The bars were cleaned and clean-fired the same as other new bars. Ten bars were selected at random for loading into capsules and testing as described in section IV.A.2.b.(2). After testing, the five bars exposed to potassium vapor had turned gray in color but no other visible effects were noted. No change in the vacuum exposed samples was noted. All bars were ready for strength determination at the end of the quarter.

The two seal samples were cut and polished and one inserted into a capsule for potassium vapor exposure for 500 hours. A photomicrograph of the matching specimen is shown in figure IV-1. Four significant features were noted:

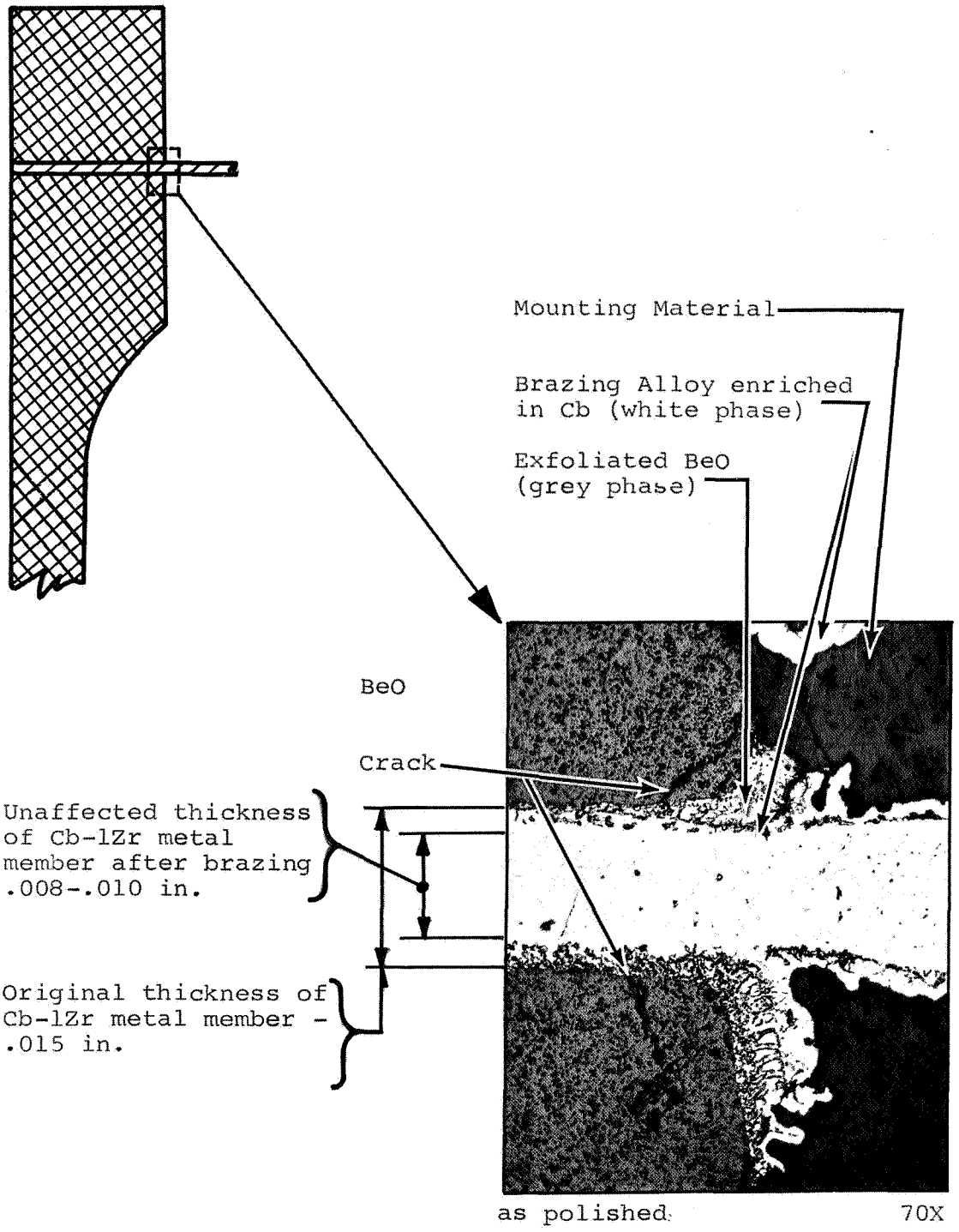

FIGURE IV-1. Cross-Section of Seal Area From 4 inch by 4 inch Bore Seal Capsule No. 1, 70X

1) The ceramic is cracked near the inside surface of the cylinder in a direction indicating radial tensile forces on the ceramic. The cracks apparently formed after cooling, since one crack in the specimen inserted into the capsule extended through the two phase exfoliated region and stopped at the edge of the (apparently) ductile, light-colored brazing alloy.

2) The ceramic has exfoliated at the corners where excess brazing alloy has flowed from the joint. The dark phase surrounded by the white brazing alloy appears to be a different shade from the base ceramic in the photomicrograph but visual examination at high magnification shows the same fine porous structure to exist in both places. No difference in shading was noted visually.

3) The ceramic has been eroded by the brazing alloy along the entire joint face and small particles of BeO are suspended in the reaction layer.

4) The Cb-1Zr has dissolved into the brazing alloy until the undisturbed sheet is only 8- to 10-mils thick at the inside edge of the ceramic.

It is apparent that an overbrazed condition exists but, despite that, a strong, vacuum-tight joint was made. The conditions listed above were not found in smaller brazed structures; this produces some insight into the problems that will exist when larger systems are needed.

Careful control of the amount of brazing alloy to prevent "puddling" or other formation of excess alloy at the inside surface is required. This will be very difficult to attain with the present alloy powder form until some method of controlling the amount per unit seal area is perfected. Reduced time and/or temperature in the liquid condition is required.

In order that findings obtained from small assemblies can be properly utilized, the brazing cycle needs to be programmed to resemble that obtainable with large structures in a larger vacuum furnace.

Until such time as the above improvements can be made, work to resolve the exfoliation or cracking is not warranted since both are presently judged to be associated with the overbrazed/excess brazing alloy condition.

d. CONCLUSION

It may be concluded from work in this task that the 4-inch bore seal capsules are suitable for preliminary testing and that scale-up to larger assemblies can be considered. However, it is clear that some limitations exist.

The brazing cycle for large assemblies is not yet optimum. The brazing alloy appears to have a wide latitude in time-temperature conditions above the melting point as far as the ability to produce strong, vacuum-tight joints is concerned, but no data exist on potassium compatibility and metallurgical stability of the structure obtained under the different brazing and exposure conditions.

The large ceramics appear to have uneven density and to have inadequate quality control during manufacture. The vacuum integrity of high purity beryllia tubes with thinner walls (< 0.100 inch) and/or larger diameters (>4 inch) would be uncertain if made by the same procedures.

3. Program for the Next Quarter

a) Continue the 2000-hour potassium exposure test at 1600°F.

b) Change over the electron beam welding chamber for lithium loading, complete fabrication of specimens, load capsules with lithium, and start the 2000-hour lithium test at 1600°F.

c) Complete brazing of specimens for elevated temperature testing and start the tests.

B. TASK 2 - STATOR AND BORE SEAL

1. Summary of Technical Progress

a) A total of 909 endurance test hours was accumulated during the quarter to complete a 5000-hour high vacuum test with a stator hot spot temperature of 1100°F.

b) Thermal vacuum chamber pressure at the beginning of this quarter was 4.2×10^{-9} torr. At the completion of the 5000-hour test, chamber pressure was 3.5×10^{-9} torr.

c) Manufacture of detail parts for a 1300°F hot spot temperature stator model was completed.

2. Discussion

a. STATOR INSTALLATION, CONSTRUCTION AND OPERATION AT 1100°F HOT SPOT TEMPERATURE

Figure IV-2 is a cutaway drawing of the thermal vacuum chamber which shows the stator installed in the furnace hot zone. The chamber is of double wall construction with baffles between the walls to channel cooling water flow. The chamber top cover is also double walled to provide a path for cooling water. Thermocouples were placed in position in the stator just prior to installation in the chamber. Stator winding leads were inserted into short lengths of hollow alumina tubing to insulate them as they passed through the top heat shields. Thermocouple and winding leads were then passes upward through perforations in the top heat shields as the shields were set in position. Winding leads were brazed to OFHC copper feedthrough bus bars inside the furnace, using a glass bell jar with supporting frame and foil curtains to maintain an argon atmosphere for the brazing operation. Thermocouples were passed through hollow Kovar tubes and brazed externally by induction methods in special glass fixtures which provided an inert gas atmosphere.

The stator main frame was made from a Hiperco 27 (27% Cobalt iron) alloy forging, and the laminations were held in place in the frame by a retaining ring which was also made from a Hiperco 27 alloy forging. The magnetic stack consisted of 244 Hiperco 27 alloy laminations 0.008-inch thick, with a sapphire-like insulation coating of plasma-arc sprayed Linde

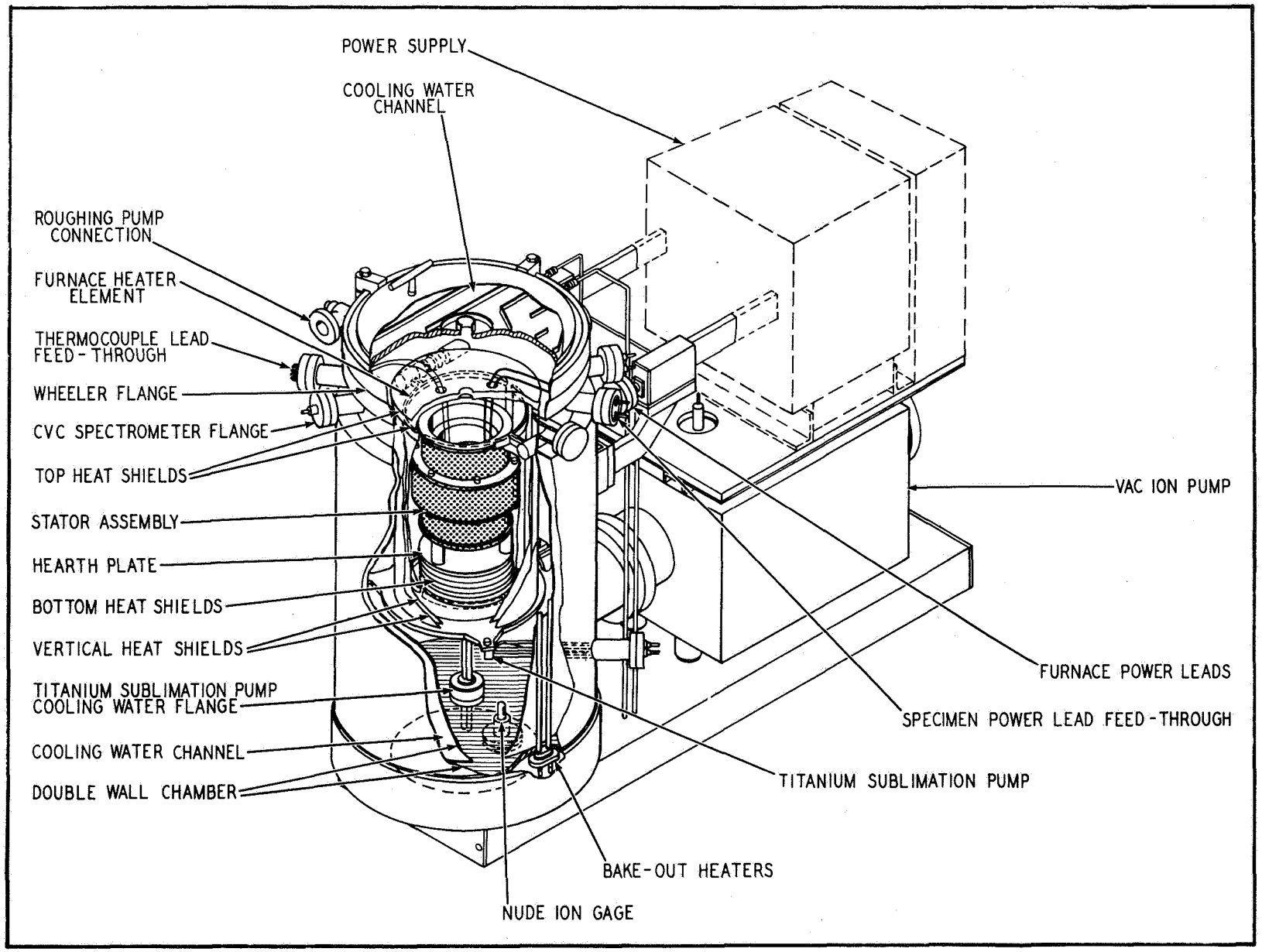

FIGURE IV-2. Cutaway View of Vacuum Furnace Showing the Stator Test Specimen Installed

A compound (Al_2O_3) on one side of each lamination. Conductor wire was rectangular nickel-clad silver (20% nickel cross-sectional area) coated with a 0.006-inch-thick layer of Anadur "E" glass, a refractory-oxide-filled glass fiber insulation. Coils were made in three segments and installed to be representative of a three phase winding. Slot insulation was provided by ceramic (99%Al_2O_3) U-shaped channels (slot liners), spacers, and wedges. Westinghouse W-839 potting compound (aluminum-orthophosphate-bonded zircon) was used to fill small voids between the slot liners and slots, and extended about 3/8 inch beyond the slot liner ends to provide winding support. Hollow Al_2O_3 tubes were used as thermocouple insulators in the slot and stack areas. Thermocouples were installed in pairs in slots of each winding, in the stack, between the stack outside diameter and frame, on the frame outside diameter and on winding end turns. The stator physical size is representative of a three phase 15 kVA generator or 12 hp a-c induction motor operating at 12,000 rpm. The stator conductor and insulation system is being tested at a current-voltage level (292 volts and 41 amps/phase) equivalent to a 36 kVA machine. Refer to the program fourth quarterly report for additional details on stator construction, preparations for installing the stator in the thermal vacuum chamber, and initiation of the test program.

Static electrical measurements covering conductor resistance, d-c insulation resistance, and insulation leakage current when subjected to an a-c voltage potential were taken once each week.

One minute titanium sublimation pump (TSP) bursts were used at intervals to note the effect on chamber pressure. At the start of the program quarter the chamber pressure would decrease into the 10^{-10} torr range when using TSP, and held there for several hours before returning to the 10^{-9} torr range. At the completion of the 5000-hour test, the pressure was staying in the 10^{-10} torr range overnight.

b. STATOR DATA AND DISCUSSION

Figure IV-3 is a log-log plot of chamber pressure in torr versus total endurance test time. The time scale does not necessarily show consecutive calendar days, as the logging of official endurance time occurred only when the stator had voltage and current applied and was at a stable hot spot temperature. Thus, time was not logged when the power supply generator was off the line for a preventative maintenance bearing change. During these periods the system was maintained

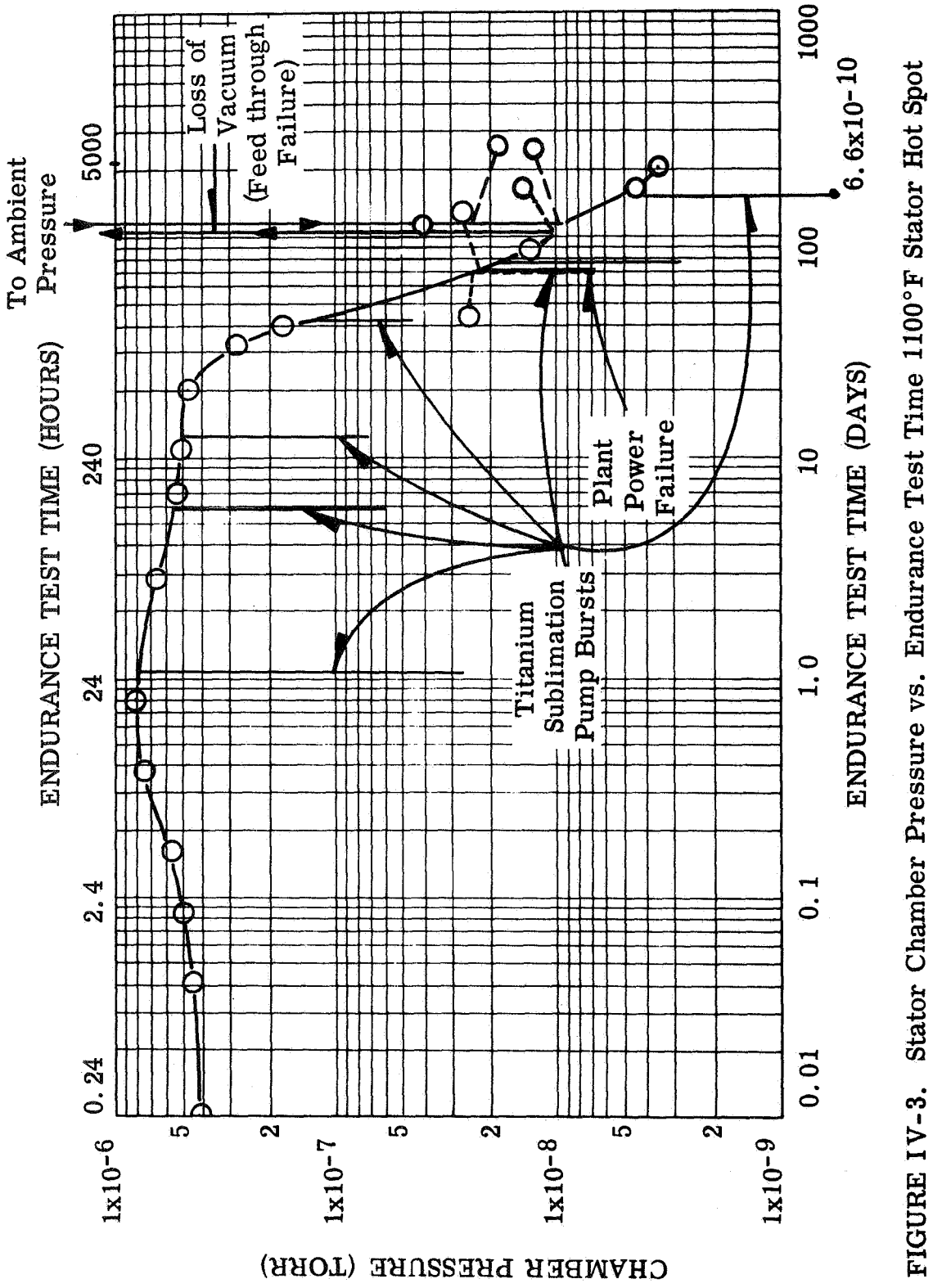

FIGURE IV-3. Stator Chamber Pressure vs. Endurance Test Time 1100°F Stator Hot Spot

Figure IV-3. Stator Chamber Pressure vs. Endurance Test Time

at an isothermal temperature of 1100°F. Time was not logged when a 12-hour plant-wide power failure occurred. The curve as plotted shows pressure values for steady state conditions. Titanium sublimation pump (TSP) burst pressure transients are shown as vertical lines in several places to indicate the magnitude of pressure reductions attained with titanium sublimation. Time was not logged during the period that loss of vacuum due to feed-through failure and subsequent repairs occurred during the sixth quarter but the plot has been expanded slightly at approximately 110 days to show pressure before the failure and the pressure that was attained within a few days after test conditions were re-established.

Figure IV-4 is a dimensionless plot showing conductor resistance during the course of the endurance test. Base line ρ_0 was 0.0134 ohms at 78°F. The effect of temperature on resistance is noted by the temperatures shown on the figure. Conductor resistance at a constant temperature has not indicated any change in 5000 hours.

Table IV-5 is a tabulation showing the stator insulation system performance as the test progressed. Readings were taken with 500 volts d-c potential applied between each pair of phases and each phase to ground. Hot spot temperature (stator slot) was maintained at 1100°F in part by the furnace heater element and in part by the current through the stator windings which developed resistive heating. Slot-liner temperatures began to decrease as soon as power was removed in order that static electrical readings could be taken. Data in the table has been corrected from actual temperatures to a reference slot temperature of 1100°F.

There was no degradation in the performance of the stator electrical insulation system as a result of 5000 hours test in a high vacuum environment with a hot spot temperature of 1100°F.

Figure IV-5 is a view of the stator test chamber taken after completion of the 5000-hour test. Stator winding leads and thermocouple leads have been clipped and the top heat shields removed to show the interior of the chamber. The chamber cleanliness and the complete lack of any deposits can be noted by the light reflections on the heating element and heat shields.

Figure IV-6 is an external view of the stator after removal from the test chamber. Stains on the winding lead ceramic

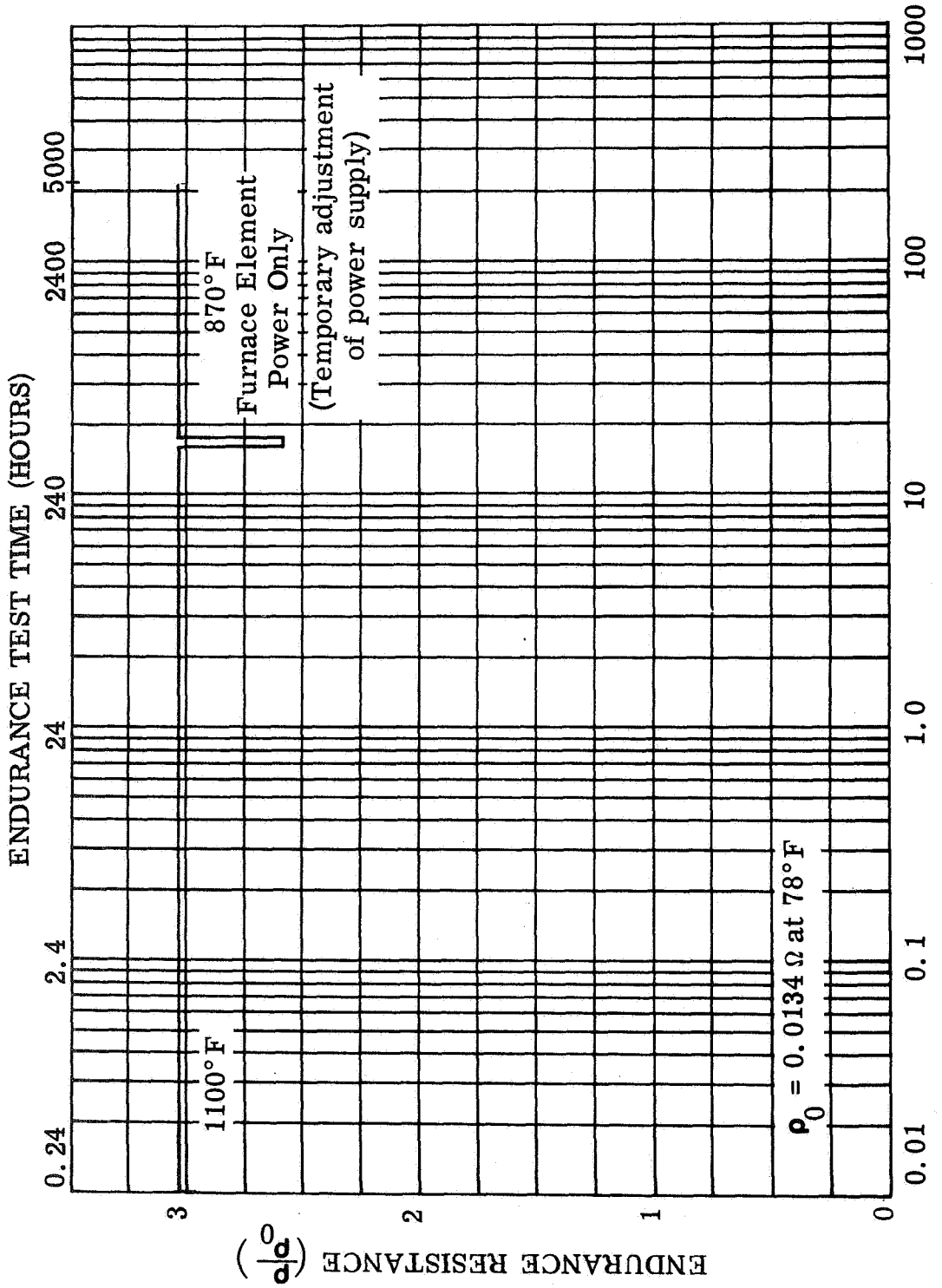

FIGURE IV-4. Stator Conductor Resistance vs. Endurance Test Time at Noted Conductor Hot Spot Temperatures

Figure IV-4. Stator Conductor Resistance vs. Endurance Test Time

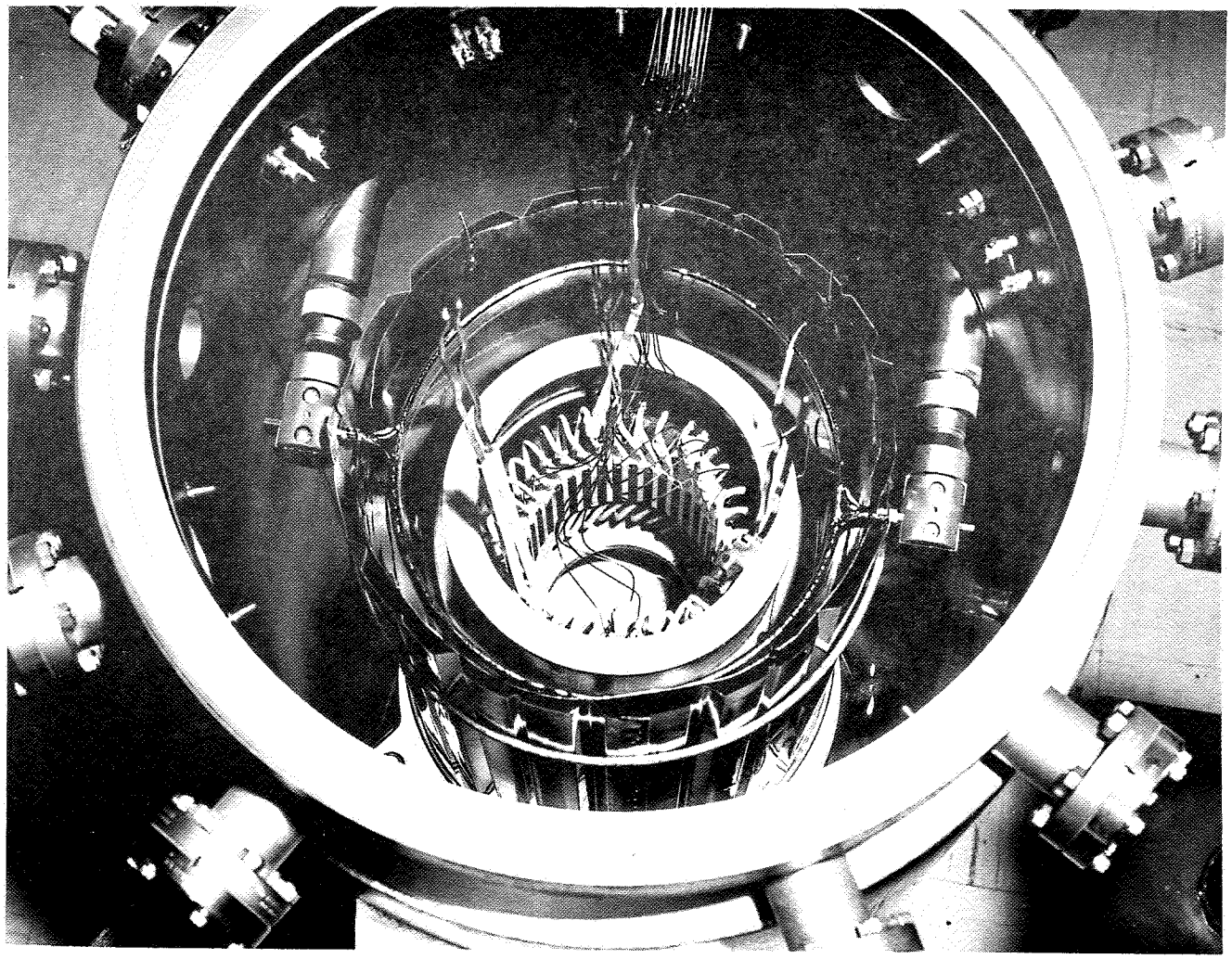

FIGURE IV-5. Stator in Test Chamber After Completion of 5000-Hour Test

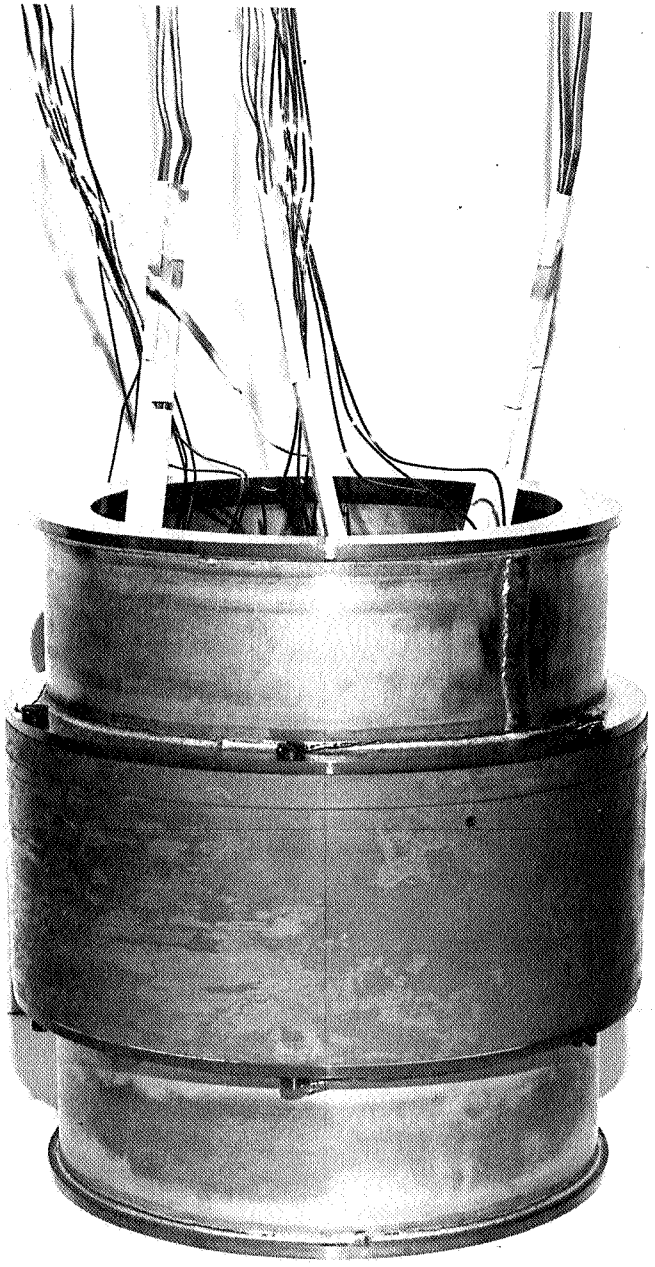

FIGURE IV-6. External View of Stator After Removal from Test Chamber

TABLE IV-5. Stator Insulation Performance in Vacuum With Slot (hot spot) Temperature at 1100°F

Endurance Test Time (hours)	0	2500	5000
Average Insulation Resistance (ohms) with 500 volts d-c Applied			
Phase to Phase	6.8×10^6	6.8×10^6	6.8×10^6
Phase to Ground	3.2×10^6	3.2×10^6	3.2×10^6

Note: Stator conductors are rectangular nickel-clad silver wire (0.091 inch by 0.144 inch) with Anadur E glass insulation. Slot insulation consists of 0.022-inch thick 99% alumina slot liners and 0.047-inch thick 99% alumina strips between phases.

insulating tubes indicate the location of the two chamber top heat shields. The investigation of such stains as well as the running of a vibration scan test on the stator assembly was postponed temporarily, as the program quarter was drawing to a close, and efforts were concentrated on completing a 1300°F hot spot temperature stator model to begin a second 5000-hour test at the higher temperature.

Figure IV-7 shows the stator stack, slot wedges, winding end turns and slot-end encapsulating compound. The compound shows some cracks but these occurred at points where the uncured compound had been grooved during installation to "direct" the formation of cracks.

Residual gas analysis scans of the stator test chamber environment were taken periodically during the test, and a final calibration was made after completion of the test with gases of selected mass number. These data must be fitted to an existing computer matrix solution to identify residual gas components and partial pressures. Data reduction has not been completed in time for inclusion in this report.

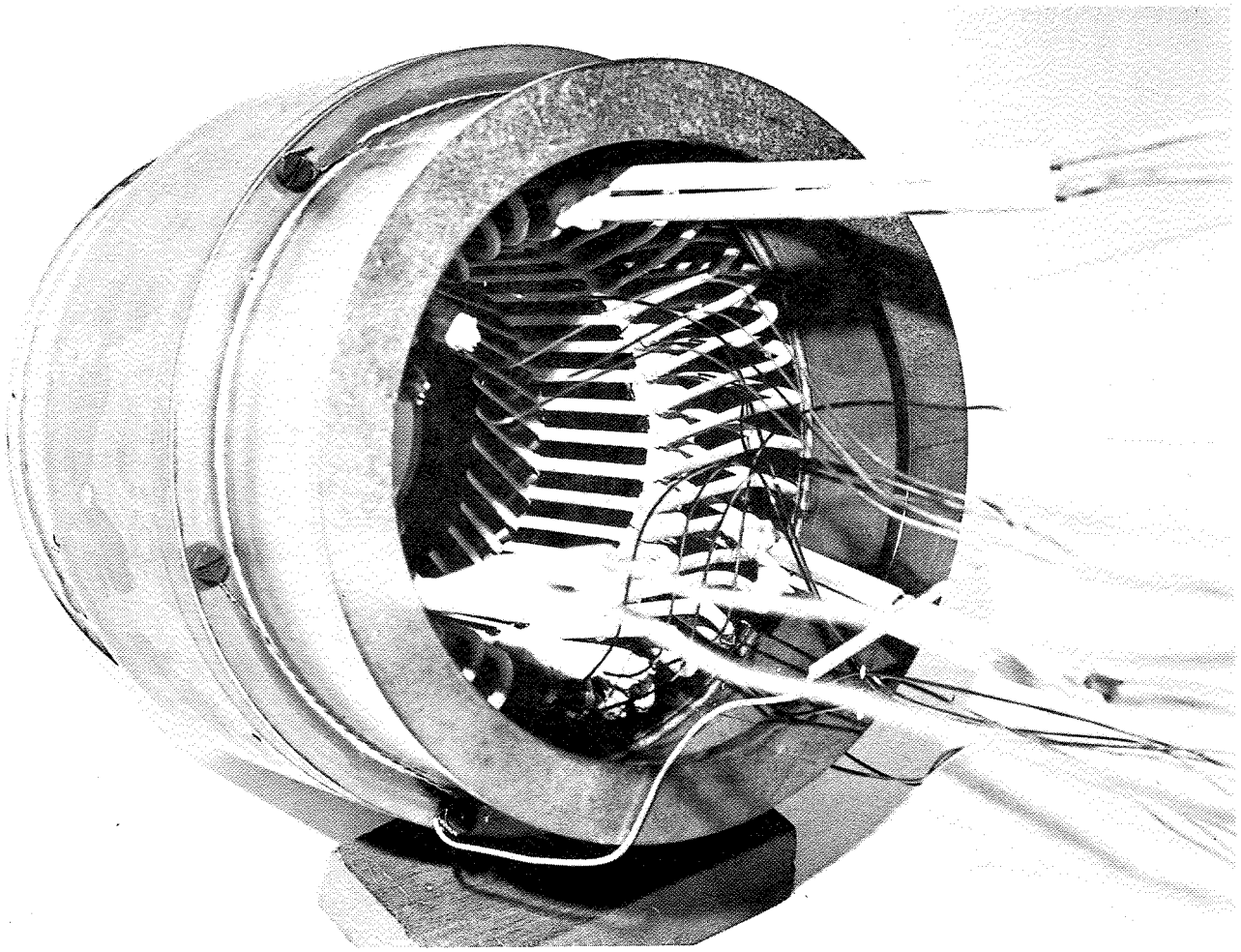

FIGURE IV-7. Post-test View of Stator Showing Stack, Windings, Slot Wedges and Encapsulating Compound

c. STATUS OF 1300°F STATOR MODEL - 2nd 5000-HOUR TEST

The 1300°F stator test model design is the same as the 1100°F model except for three materials changes. Nickel-clad silver wire is being replaced by Inconel-clad silver wire, to obtain greater mechanical strength at 1300°F temperatures. Conductor wire insulation is being changed from Anadur "E" glass to Anadur "S" glass, to provide increased insulation stability and increased retention of mechanical strength at temperature. "E" glass, which is a boro-silicate glass fiber, devitrifies and loses strength rapidly at temperatures above 1200°F. "S" glass is composed of over 99% silicon dioxide which is stable in the temperature range anticipated for this device. Presently available encapsulation compounds are not satisfactory for use at 1300°F because of outgassing characteristics and electrical insulation strength. W-839 encapsulation compound (aluminum-orthophosphate-bonded zircon) will be replaced by a cement consisting of chopped boron nitride fibers in a colloidal alumina binder fluid, which is an outgrowth of a Westinghouse independent program to develop a flexible boron nitride insulation system for the transformer model in task 3.

Figure IV-8 shows the 0.008-inch-thick Hiperco 27 alloy laminations assembled on the stacking fixture. After compression of the stack, it was electron beam welded in twelve places approximately 30 degrees apart. The second quarterly report presents core loss performance and magnetic destruction factors for electron beam welded Hiperco 27 alloy laminations.

3. Program for the Next Quarter

a) Place the 1100°F test stator through a vibration test scan and then complete post-test disassembly and inspection.

b) Complete assembly of the 1300°F hot spot stator test model.

c) Install the 1300°F model in a thermal-vacuum chamber and begin a 5000-hour high-temperature, high-vacuum endurance test.

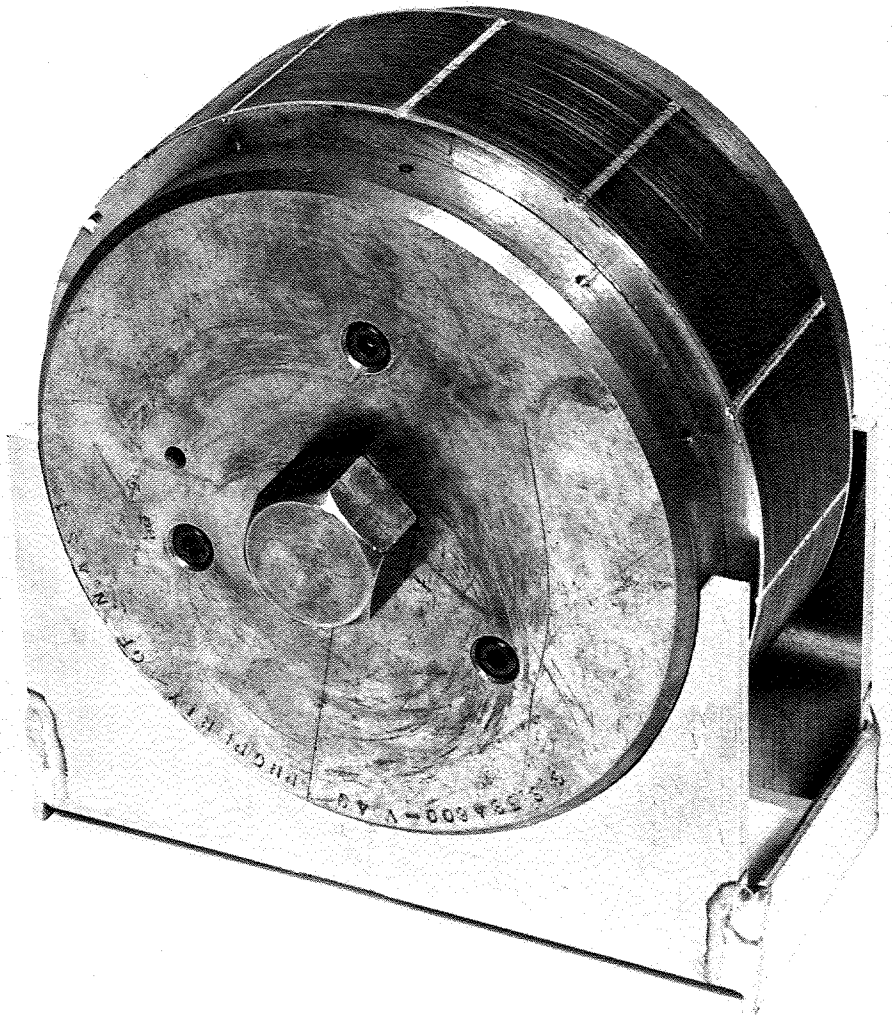

FIGURE IV-8. View of 1300°F Stator Stack Showing Electron Beam Welds

C. TASK 3 - TRANSFORMER

1. Summary of Technical Progress

a) A total of 985 endurance test hours at 1100°F was accumulated during the quarter to complete a 5000-hour high-temperature high-vacuum test.

b) Thermal-vacuum chamber pressure at the beginning of the period was 7.4×10^{-9} torr. At the completion of the 5000-hour test, chamber pressure was 6.1×10^{-9} torr.

c) Manufacture of detail parts for a 1300°F hot spot temperature transformer model was completed.

2. Discussion

a. TRANSFORMER INSTALLATION, CONSTRUCTION AND OPERATION AT 1100°F HOT SPOT TEMPERATURE

Figure IV-9 is a cutaway drawing of the thermal vacuum chamber showing the transformer and two solenoids installed in the furnace hot zone. Thermocouple and power leads were brought up through the top heat shields in the same manner as with the stator. Power leads were brazed to oxygen free high conductivity (OFHC) copper bus bar feedthroughs inside the chamber, and the thermocouples were passed through hollow Kovar tube feedthroughs and brazed to the tubes outside the chamber.

The transformer core was made from E-I style Hiperco 27 alloy laminations 0.008-inch thick, with a coating of plasma-arc sprayed Linde A compound (Al_2O_3) on one side of each lamination (same as stator laminations). The windings were formed around a ceramic spool (99.5% Al_2O_3) which provided insulation between the windings and the center leg of the core. Alumina (99.5%) end plates and channels provided insulation between the winding ends and sides and the laminations. Non-magnetic alloy strips (Hastelloy Alloy B) were used outside the laminations to provide lamination support. The laminations and support strips were held together by through-studs, ceramic washers, and lock nuts. The primary winding was made from No. 20 AWG (0.032 diam) nickel-clad silver wire (20% nickel cross-sectional area) coated with Anadur "E" glass insulation and consisted of 174 turns in five layers. Flexible insulation (Burnil CM-2) 0.010-inch thick was used to separate the layers.

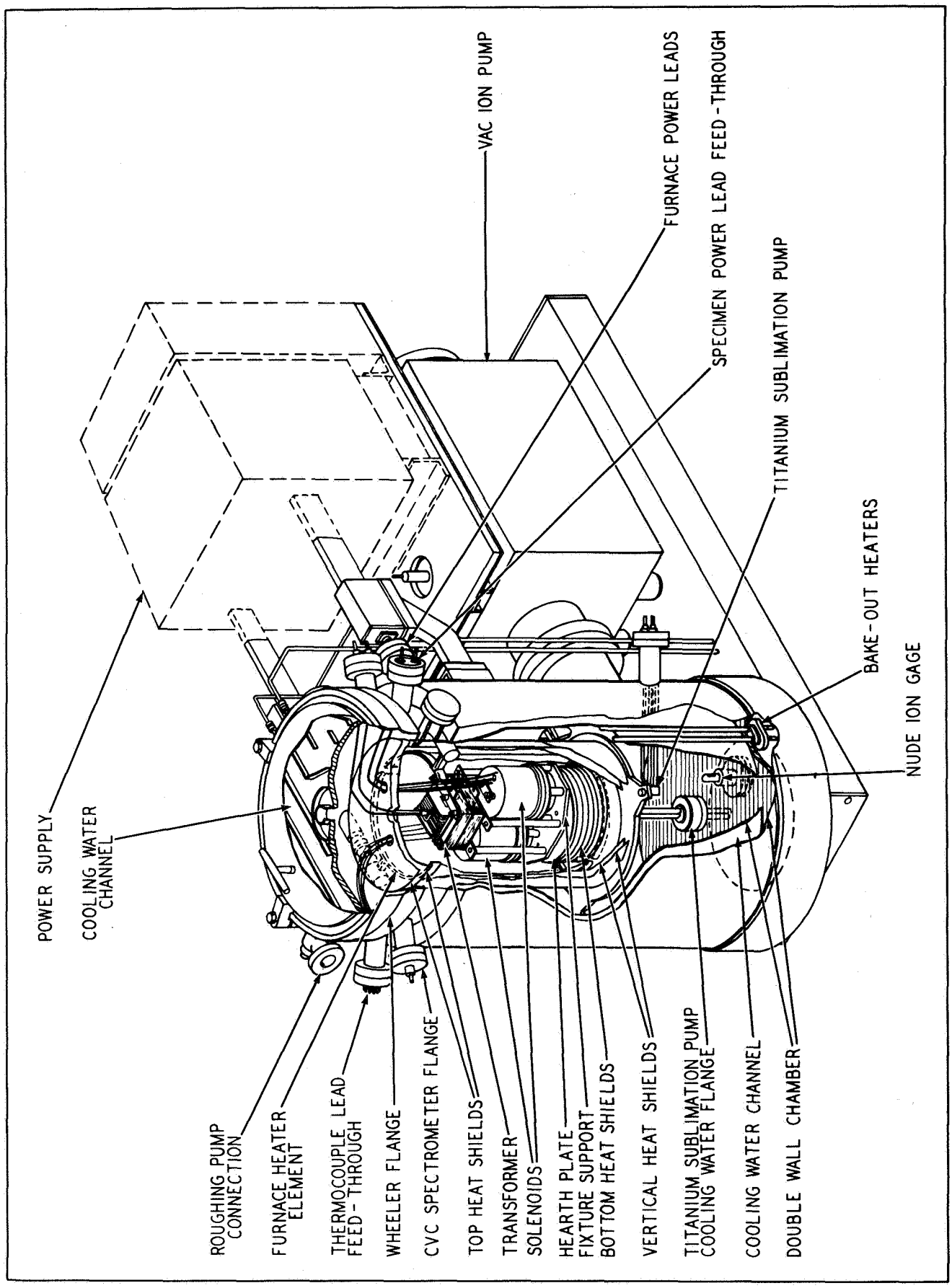

FIGURE IV-9. Cutaway View of a Vacuum Furnace Showing Installation of Two Solenoids and a Transformer

The secondary winding was a single layer 10-turn coil made from the same type wire and insulation but in No. 7 AWG size (0.144 diam). Four layers of 0.010-inch-thick Burnil CM-2 were installed between the outermost primary winding layer and the secondary winding. Pairs of thermocouples were installed between the primary winding and ceramic spool and between the primary and secondary windings. The stack was divided into two halves by ceramic strip spacers so that two thermocouples could be buried in ceramic tubes in the center of the core.

Refer to the fourth quarterly report for additional details on transformer construction, preparations for installing the transformer in the test chamber, and initiation of the test program.

Transformer test operation was routine during the program quarter. Both windings were connected in series and supplied by an a-c voltage source to maintain a 600-volt a-c potential between each winding and ground. This mode of test was adopted in the fourth quarter after the primary winding developed a layer-to-layer short circuit which prevented normal transformer operation. Details of this are covered in the fourth quarterly report. The 1100°F test hot spot temperature was established in the energized solenoid (task 4), which is installed in the same test chamber. Transformer temperature was maintained at an average value of 1035°F by heat radiated from the solenoid and test chamber heater element.

Static electrical measurements covering winding resistance, d-c insulation resistance, and insulation leakage current when subjected to an a-c voltage potential were taken once each week.

Titanium sublimation pump (TSP) bursts of one minute duration were used at intervals to evaluate the effect on the chamber base pressure. Early in the program quarter, the chamber pressure was reduced into the 10^{-10} torr range for several hours after each TSP burst. By the end of the program quarter a one minute TSP burst was holding chamber pressure in the 10^{-10} torr range overnight.

b. TRANSFORMER DATA AND DISCUSSION

Figure IV-10 is a plot of chamber pressure versus endurance test time. The power supply for the transformer is one phase

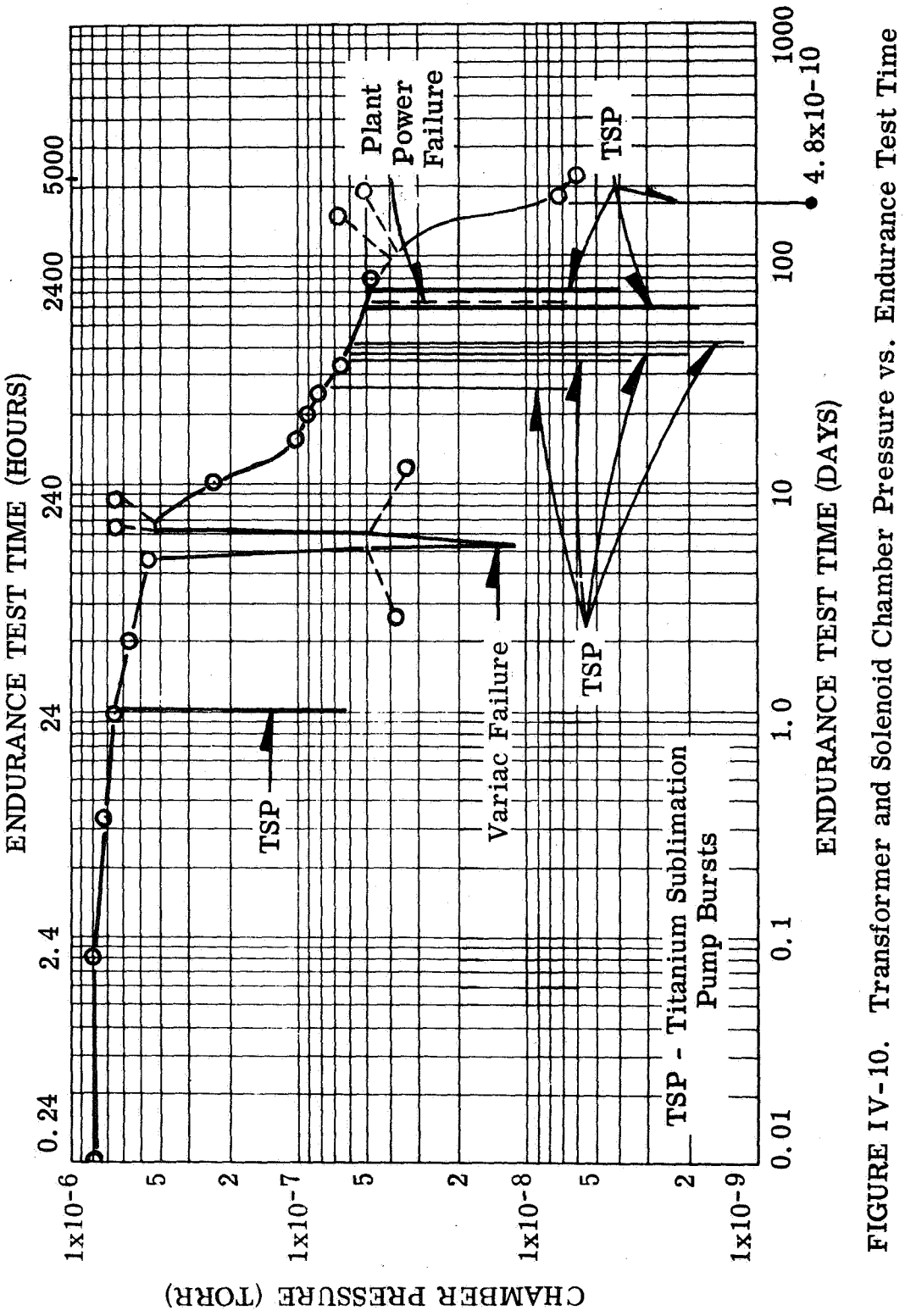

FIGURE IV-10. Transformer and Solenoid Chamber Pressure vs. Endurance Test Time

Figure IV-10. Transformer and Solenoid Chamber Pressure vs. Endurance Test Time

of the generator which supplied the stator. The curve shows the temporary pressure reductions that occurred when titanium sublimation pump bursts were applied. It also shows the pressure decreases which accompanied the removal of power when the primary winding shorted after 107 hours of test and during a plant-wide power failure which occurred in the fourth program quarter. Chamber pressure was read by a Bayard-Alpert type nude ion gauge.

Figure IV-11 is a dimensionless plot of the transformer primary and secondary conductor resistance as a function of endurance test time. Neither conductor showed any changes in resistance values at constant temperature from 200 hours to 5000 hours. An increase in secondary resistance noted after the fifth day of endurance testing is covered later in this section. The primary winding shows additional resistance loss between the fifth and eighth days following the shorting of the winding.

Table IV-6 tabulates transformer insulation system performance during the course of endurance testing. Initially the transformer was set up to operate at a rated load of 1 kVA with 600 volts on the primary winding, approximately 30 volts on the secondary winding, and a hot spot temperature of 1100°F (center of lamination stack). After 107 hours of endurance testing a layer-to-layer short circuit developed in the primary winding making it impossible to load the transformer. From that point on a 600-volt a-c winding-to-ground potential was applied to each winding. The test hot spot temperature (1100°F) was established in the energized solenoid and the transformer temperature was established by radiation from the solenoid and the chamber heating element. Data in the table is referenced to a stabilized (unpowered) transformer temperature of 1030°F.

Figure IV-12 shows the transformer and solenoid thermal-vacuum test chamber with the top cover removed after completion of the 5000-hour test. Test model and thermocouple leads are still attached to the chamber feedthroughs. The clean condition of the chamber interior can be noted by the light reflections. Figure IV-13 shows the chamber with leads clipped and the top heat shields removed. Figure IV-14 is a view of the interior of the hot zone after the test specimens had been removed. Figure IV-15 shows the transformer and two solenoids on their support fixture after being removed from the chamber. The model lead ceramic insulators show

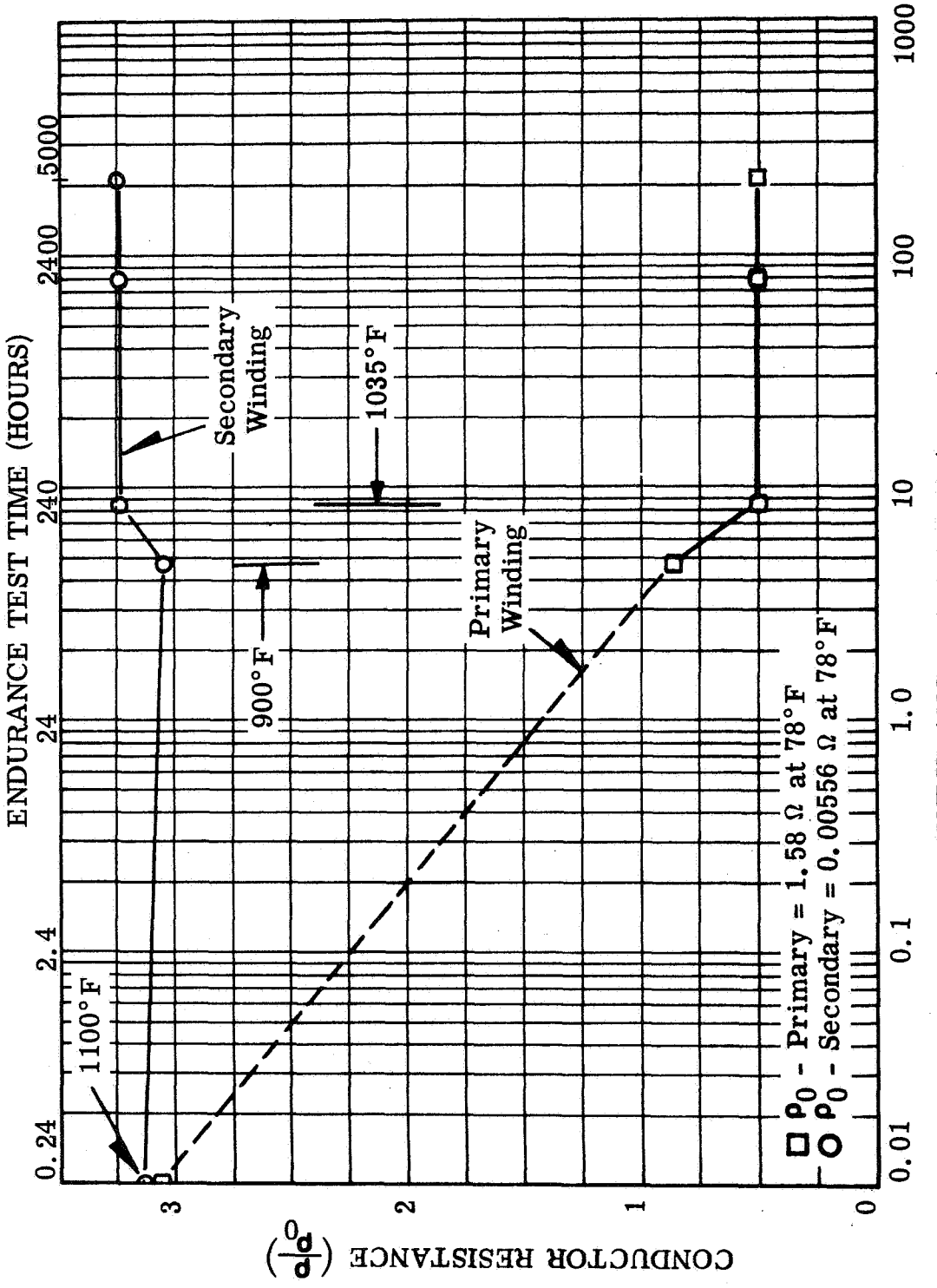

FIGURE IV-11. Transformer Winding Resistance vs. Endurance Test Time

Figure IV-11. Transformer Winding Resistance vs. Endurance Test Time

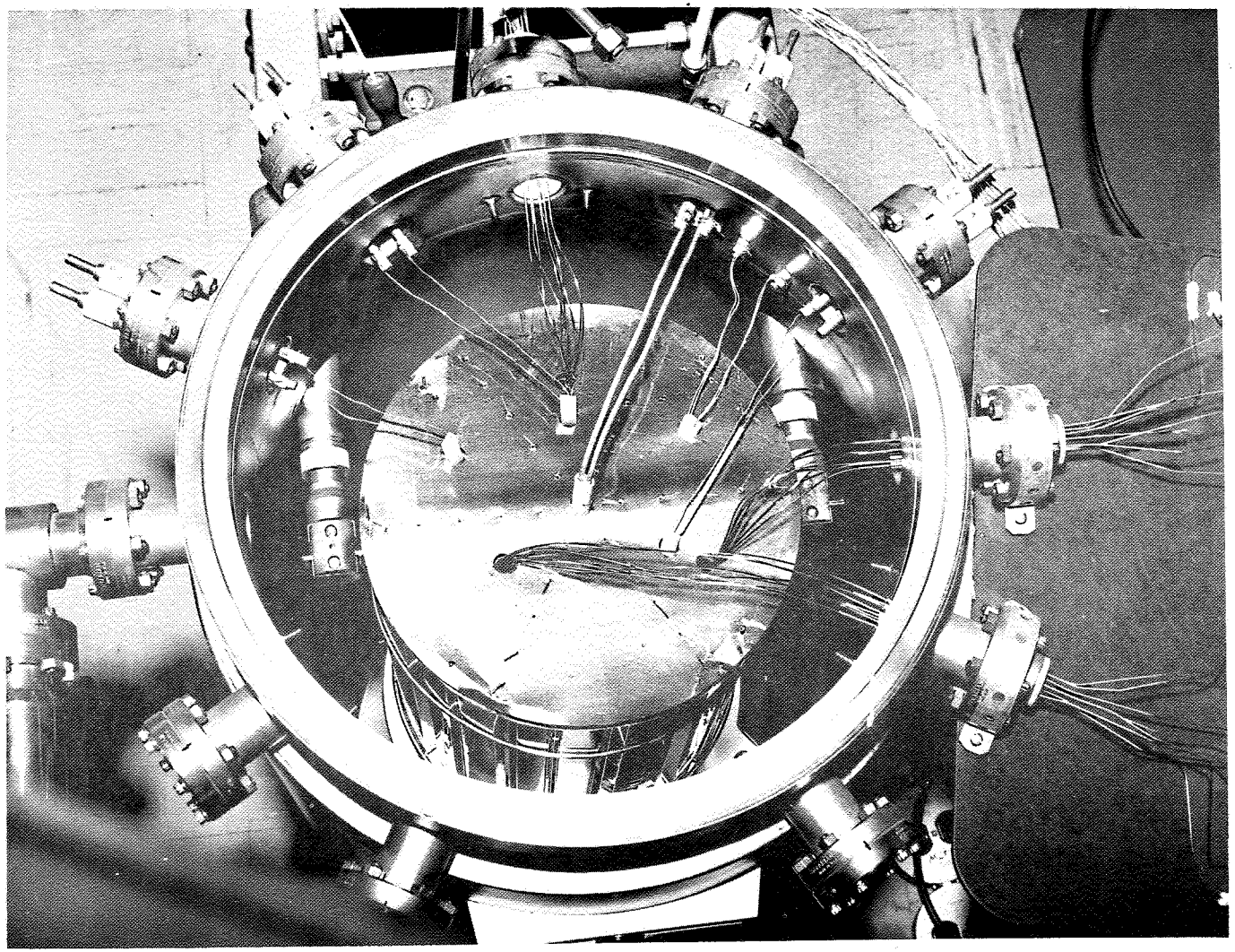

FIGURE IV-12. Transformer and Solenoid Test Chamber With Top Cover Removed

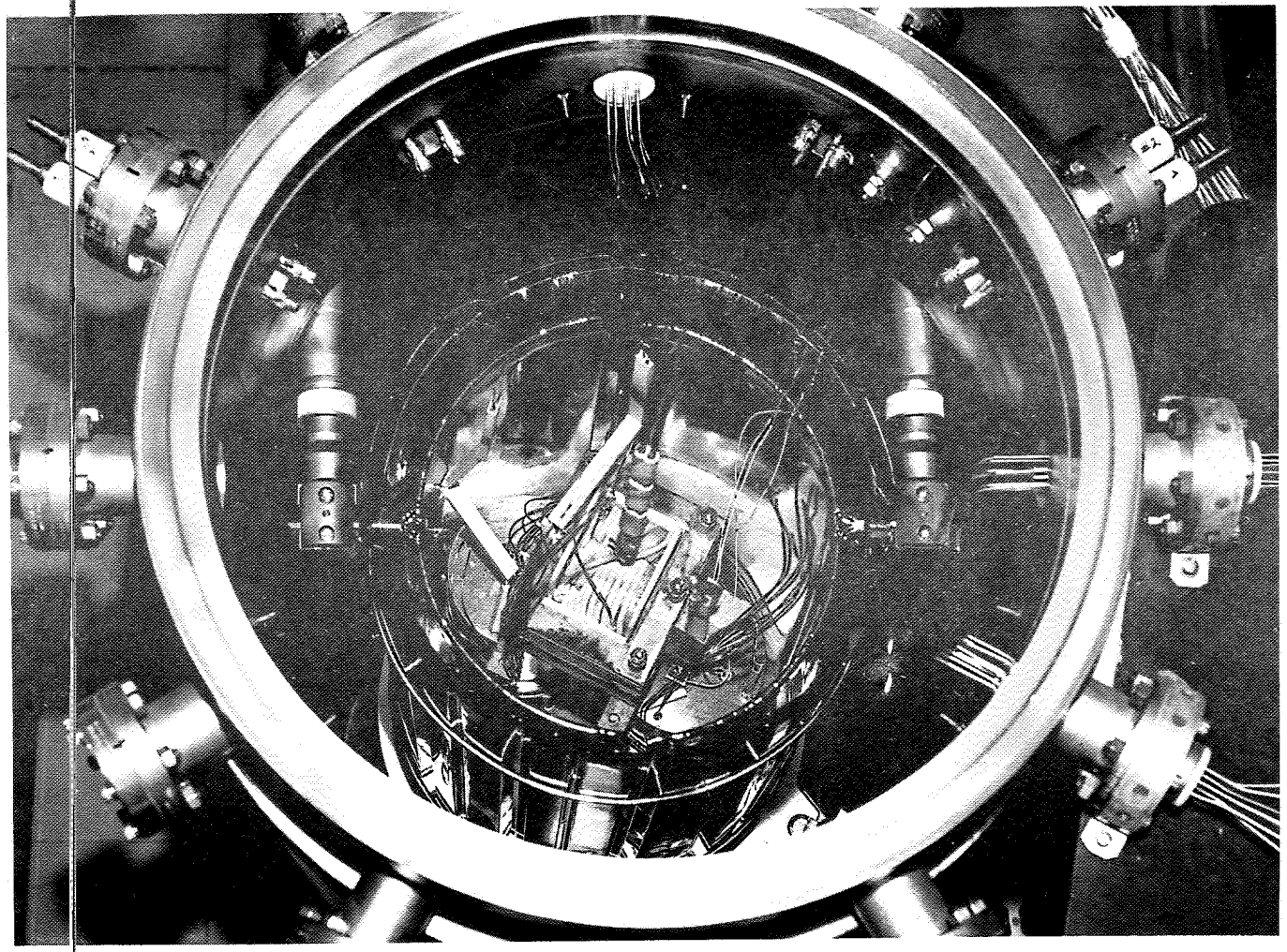

FIGURE IV-13. Transformer and Solenoids in Test Chamber With Top Heat Shields Removed

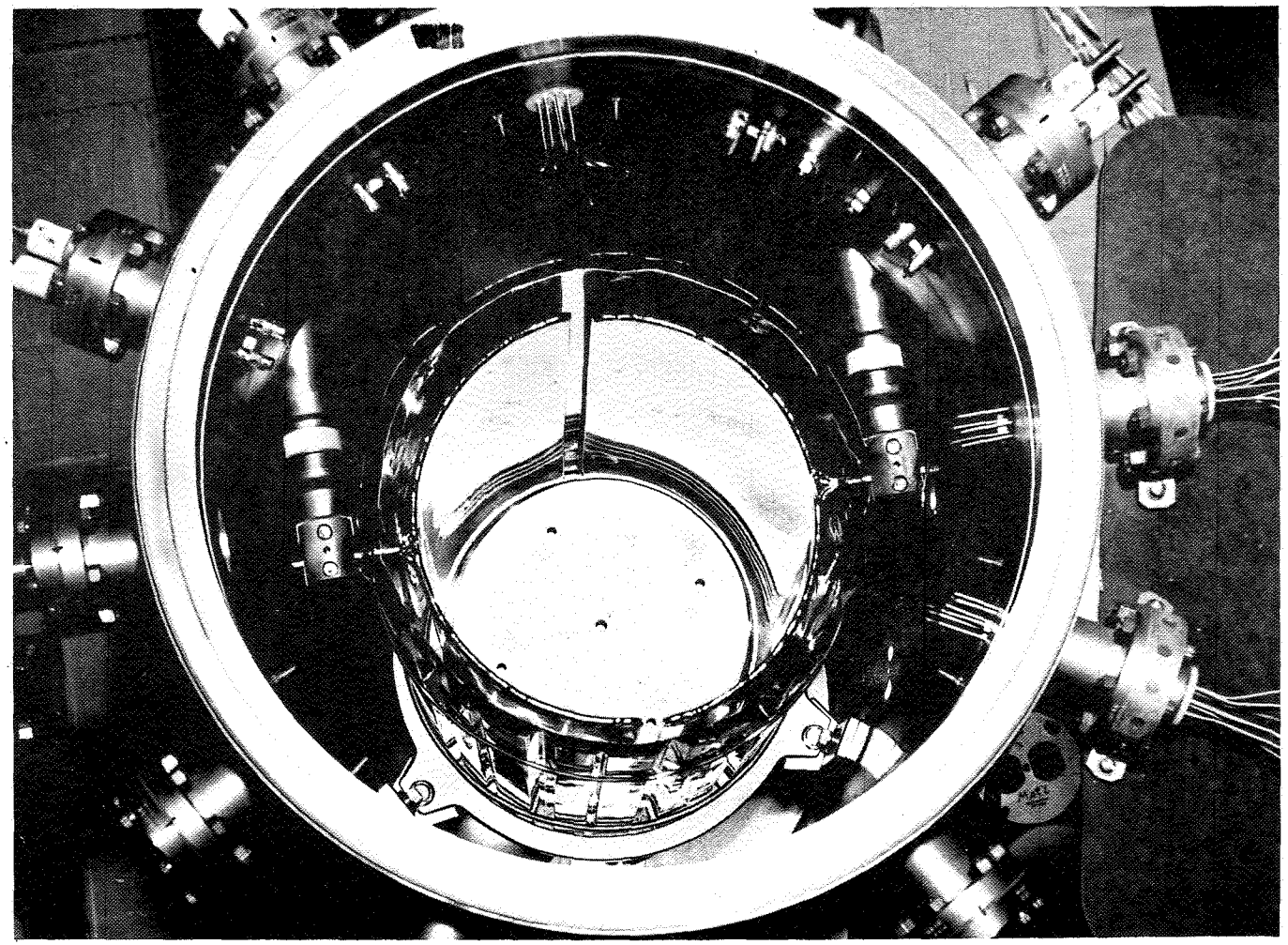

FIGURE IV-14. Test Chamber Hot Zone Interior With Transformer and Solenoids Removed

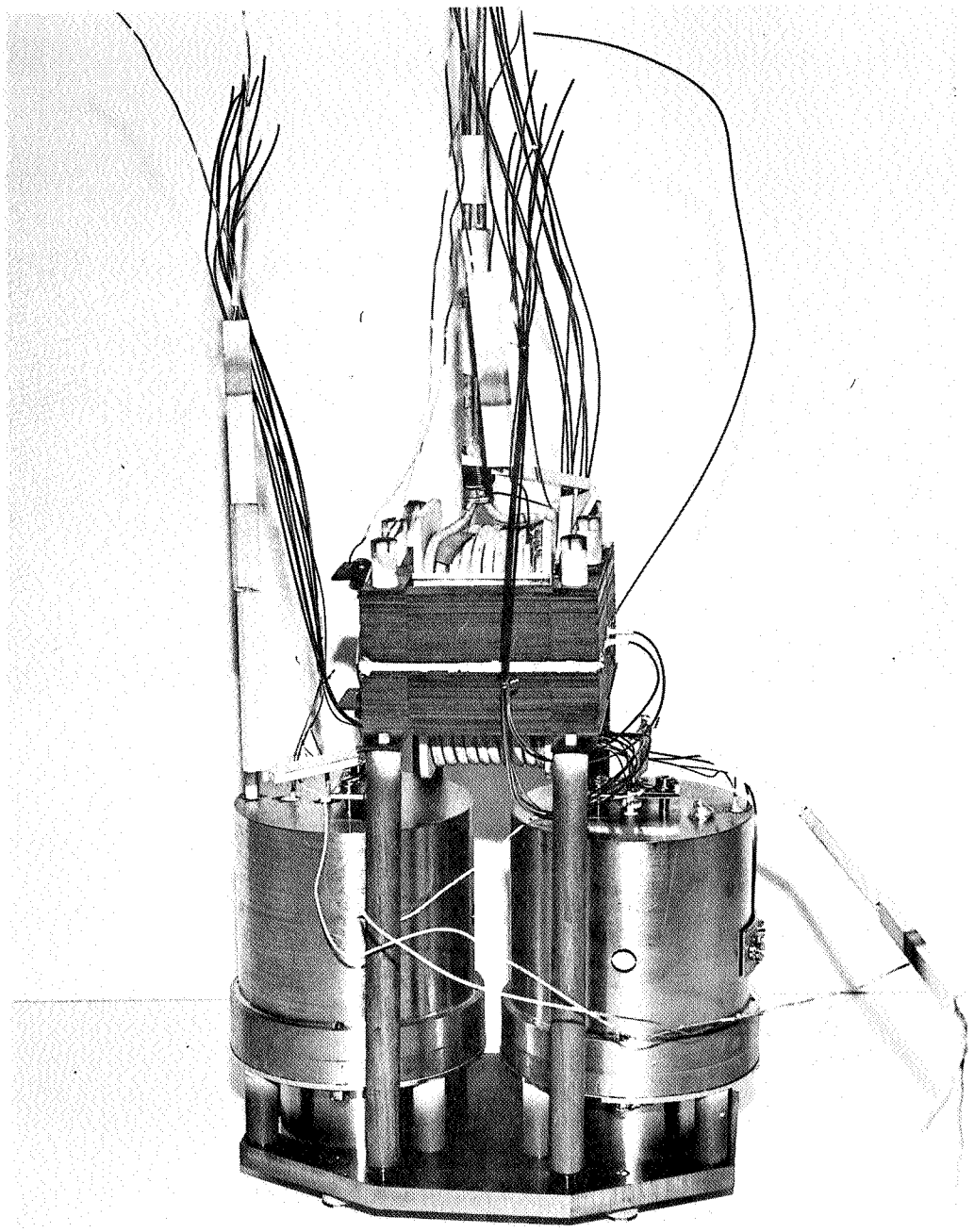

FIGURE IV-15. Transformer and Solenoids on Test Support Fixture After Removal From the Test Chamber

TABLE IV-6. Transformer Insulation Performance in Vacuum With a Stabilized (unpowered) Transformer Temperature of 1030°F

Endurance Test Time (hours)	0	2500	5000
Average Insulation Resistance (ohms) With 500 V d-c Applied:			
Primary to Secondary[a]	9×10^6	0.83×10^6	0.85×10^6
Primary to Ground[b]	17×10^6	16.8×10^6	17.0×10^6
Secondary to Ground[c]	15×10^6	14.6×10^6	14.7×10^6

(a) Primary winding developed a layer-to-layer short circuit after 107 hours of endurance testing.

(b) Primary Winding - 0.032-inch diameter nickel-clad silver wire with Anadur E glass insulation-0.010-inch thick synthetic mica between layers.

(c) Secondary Winding - 0.144-inch diameter nickel-clad silver wire with Anadur E glass insulation; four 0.010-inch layers of synthetic mica insulation between primary and secondary windings.

the same stains at the top heat shield passthroughs as were seen on the stator insulators. The right hand solenoid has been rotated on the fixture to show a bead of silver sitting on its top surface. The source of this bead is discussed below.

After 107 hours of endurance test on the transformer and solenoids, a malfunction occurred which initially was charged to a short between the variac and the voltmeter on the primary side of the transformer. Both pieces of equipment were damaged. Chamber heater and ion pump power were cut as part of the emergency shutdown procedure. When control power was restored a short time later the ion pump started normally, quickly dropping to a pressure of 1.2×10^{-8} torr (previous reading was 5.1×10^{-7} torr). Heater element power was reapplied to

maintain the models at approximately 900°F until wiring repairs could be completed. There was no evidence of trouble within the test chamber.

After the test hookup had been completed, power was applied to the primary winding with the secondary winding loaded. It was found that the primary winding would not support the secondary winding voltage or current. The symptoms were discussed with transformer designers, resulting in a diagnosis of one or more layer-to-layer short circuits in the primary winding caused by a voltage surge from the variac. This theory was supported by a reduction in primary winding conductor resistance from 4.85 ohms at 1100°F to 1.31 ohms at 900°F, and a further decrease to 0.8 ohms when readings were repeated seven days later. (Refer to figure IV-11 for a dimensionless plot of conductor resistance versus test time.) Insulation resistance between primary and secondary windings also showed a decrease (see table IV-6). Ground insulation data which had not been reduced for temperature differences did not show any significant change because a high purity alumina spool and end plates form the primary ground insulation system.

As a result of these findings both windings were wired to carry a 600-volt a-c potential to ground, to continue aging the insulation systems at high temperature and under electrical stress in vacuum.

Referring again to the conductor resistance parameter (figure IV-11), it will be noted that the secondary winding resistance at 900°F after the failure was not much less than the original value at 1100°F. When the winding temperature was increased to 1035°F, the resistance was greater than the initial 1100°F value. Since the winding consisted of a single layer having 10 turns which showed electrical continuity, there was no positive explanation for the resistance pattern.

Figure IV-16 is a close-up of the top of the secondary winding, showing that the furthermost turn has a cross-sectional segment of nickel-clad silver wire missing. Figure IV-17, which is a close-up of the bottom of one side of the transformer, shows a silver run at the port for the thermocouples between the primary and secondary windings. This port was located over the solenoid in Figure IV-15, which has a silver bead.

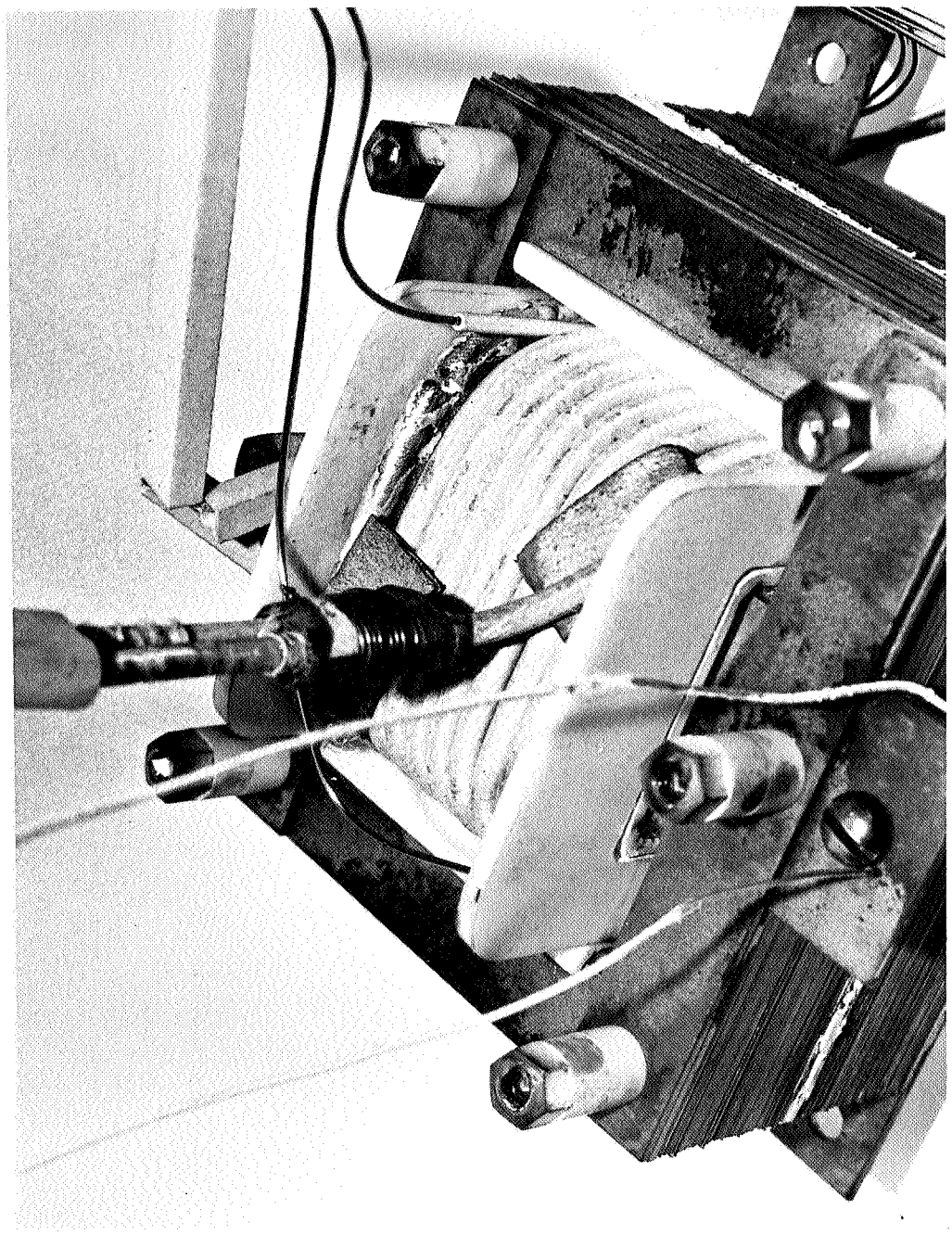

FIGURE IV-16. Close-up of Transformer Secondary Winding

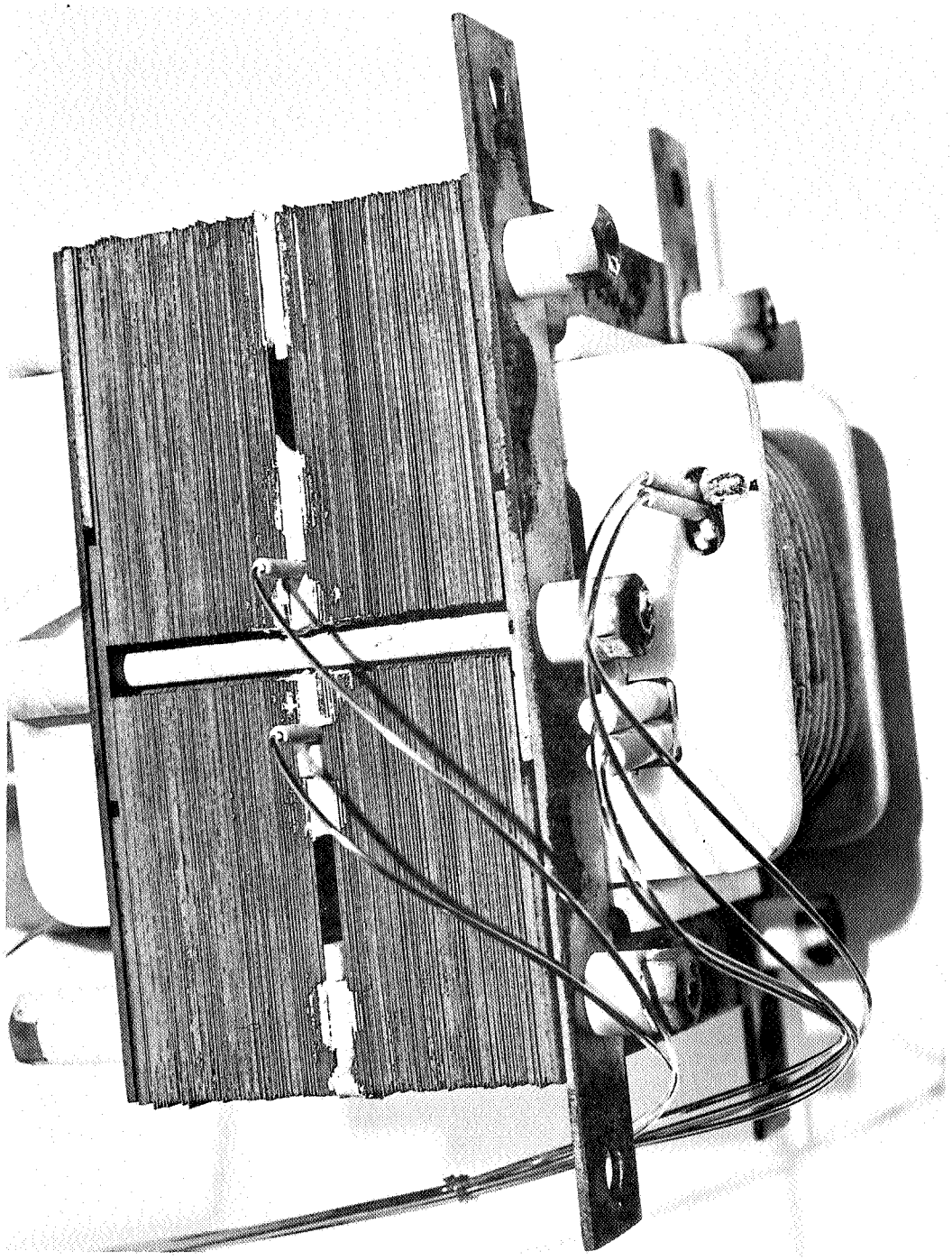

FIGURE IV-17. Side View of Transformer

Teardown of the transformer was postponed temporarily as the program quarter was coming to a close; and efforts were concentrated on completing the 1300°F stator, transformer, and solenoid models to begin new 5000-hour tests. Preliminary analysis of the secondary winding resistance behavior indicates that part of one turn is open, and that it is welded to the adjacent turn in a region that cannot be seen in the assembly. Apparently the weld resistance is somewhat higher than that of the open turn segment, resulting in a slight increase in winding resistance while maintaining electrical continuity. The physical condition of the primary winding is not known at this time. The transformer will be disassembled during the next program quarter and the results will be reported in the next report.

Residual gas analysis scans and a final calibration were obtained from the transformer and solenoid test chamber. As with the stator, data reduction has not been completed in time for inclusion in this report. It will be reported at a later date.

c. STATUS OF 1300°F TRANSFORMER MODEL - 2nd 5000-HOUR TEST

The 1300°F transformer test model design is the same as the 1100°F model except for four materials changes. Nickel-clad silver wire is being replaced by Inconel-clad silver wire to obtain greater mechanical strength at 1300°F temperatures. The winding wire insulation is being changed from Anadur "E" glass to Anadur "S" glass, for the same reasons that were described in the 1300°F stator model write-up. Very little W-839 encapsulation compound was used on the 1100°F model, but because of high-temperature outgassing characteristics, it is being replaced by a boron nitride fiber cement.

The Burnil CM-2 (3M Company) flexible sheet insulation, which was used between winding layers in the 1100°F model, does not have adequate electrical insulation capabilities at 1300°F. As an independent program, Westinghouse has been developing a flexible sheet insulation made from boron nitride fibers. This material will be used to replace the Burnil CM-2 in the 1300°F transformer model.

Manufacture of detail parts for the 1300°F hot spot transformer model was completed during the program quarter.

3. Program for the Next Quarter

a) Complete the manufacture and assembly of a transformer model rated for high-vacuum, high-temperature operation at a hot spot temperature of 1300°F.

b) Install the model in a thermal-vacuum chamber and begin a 5000-hour endurance test.

c) Disassemble the 1100°F hot spot transformer model for further analysis of the performance degradation during test.

D. TASK 4 - SOLENOID

1. Summary of Technical Progress

a) A total of 961 endurance test hours was accumulated during the quarter to complete a 5000-hour high-vacuum test with a solenoid hot spot temperature of 1100°F.

b) Thermal-vacuum chamber pressure at the beginning of the report period was 7.4×10^{-9} torr. Chamber pressure was 6.1×10^{-9} torr at the completion of the 5000-hour test.

c) Manufacture of detail parts for two 1300°F hot spot solenoid models was completed.

2. Discussion

a. SOLENOID INSTALLATION, CONSTRUCTION AND OPERATION AT 1100°F HOT SPOT TEMPERATURE

The transformer installation cutaway drawing, figure IV-9 also shows how the two solenoids were fitted into the chamber. All three components were installed at the same time.

The solenoid magnetic housing, cover and plunger are made from Hiperco 27 alloy forged material. The coil is wound on an alumina (99%) spool which provides insulation between the winding and the plunger and housing center core. Alumina end plates insulate the sides of the winding from the housing and cover. Bearing surfaces for the plunger consist of an alumina guide rod at one end of the plunger and an alumina bushing at the opposite end. The winding was formed from 1860 turns of No. 20 AWG (0.032 diam) nickel-clad silver wire with an Anadur insulation system. This is the same wire that was used for the transformer primary winding.

Pairs of thermocouples were installed between the winding inside diameter and the ceramic spool, at the radial mid-winding point, between the winding outside diameter and the housing and on the housing outside diameter. All except the housing outside diameter thermocouples were installed in 99% alumina tubes.

Each solenoid is rated at 1530 ampere-turns at 28 volts d-c

and a hot spot temperature of 1100°F. Refer to the program fourth quarterly report for additional details on solenoid construction, preparations for installing the solenoids in the test chamber, and initiation of the test program.

Solenoid test operation was routine during the program quarter. One solenoid was continuously energized with 13 volts d-c and 0.34 amperes, and the other was briefly energized periodically to verify movement of the plunger. The 1100°F hot spot test temperature was established in the continuously energized solenoid. One solenoid was energized continuously and one intermittently to investigate the effects of an invariant electric stress on conductor and insulation system performance.

Static electrical measurements covering winding resistance, d-c insulation resistance, and insulation leakage current when subjected to an a-c voltage potential were taken once each week. Pick-up and drop-out voltages and currents were also measured on each solenoid, to verify that the plungers were not immobilized in one position.

b. SOLENOID DATA AND DISCUSSION

Each solenoid accumulated 961 endurance test hours during the report period. One solenoid was energized continuously except during the taking of electrical readings. The other was unenergized except for periodic checks on plunger movability.

Figure IV-10 shows the chamber pressure versus test time curve which is also applicable to the solenoids. Pressure readings were taken with a nude ion gauge which is mounted in the bottom of the test chamber.

Figure IV-18 is a dimensionless plot of winding conductor resistance versus time for both solenoids. There was no change in resistance at constant temperature in either solenoid during the reporting period.

Table IV-7 is a tabulation of insulation performance for the energized and unenergized solenoids in terms of endurance test time. Readings were taken with a 500-volt d-c potential between each winding and ground. The temperature balance begins to change as soon as power is removed from the energized solenoid so that static readings can be made. Data in the table has been corrected from actual temperatures to a reference mid-

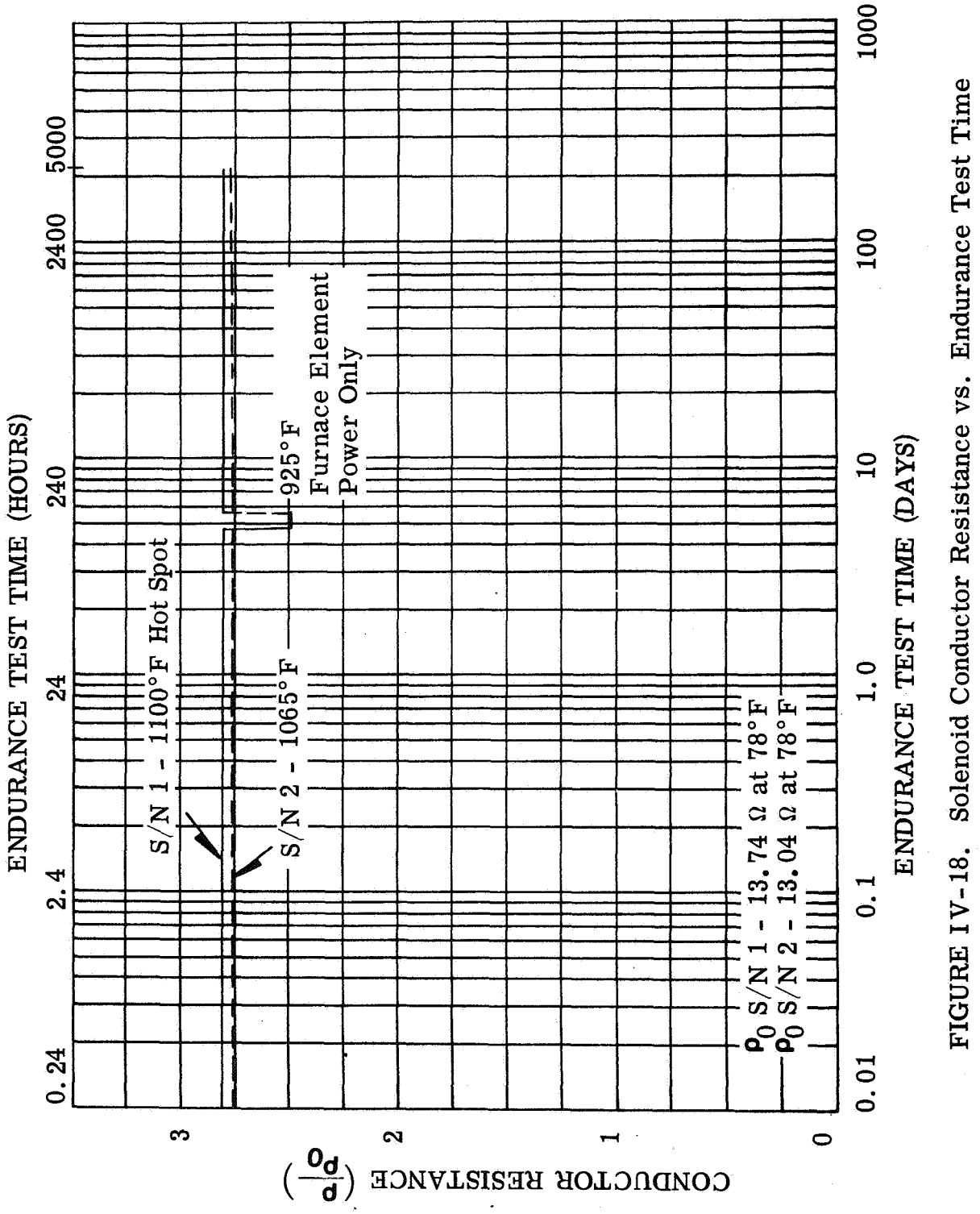

FIGURE IV-18. Solenoid Conductor Resistance vs. Endurance Test Time

Figure IV-18. Solenoid Conductor Resistance vs. Endurance Test Time

TABLE IV-7. Solenoid Insulation Performance In Vacuum With Midwinding (hot spot) Temperature at 1100°F

Endurance Test Time (hours)	0	2500	5000
Insulation Resistance (ohms) With 500 V d-c Applied:			
S/N 1 (energized)			
Winding to Ground	7×10^6	6.9×10^6	6.85×10^6
S/N 2 (not energized)			
Winding to Ground	8.5×10^6	8×10^6	8.4×10^6

Note: Conductor is 0.032-inch diameter nickel-clad silver wire with Anadur E glass insulation; 99% alumina winding spool and 99.5% alumina winding end plates.

winding temperature of 1100°F.

Figure IV-19 shows the two solenoids in the test chamber after the transformer had been removed from the support fixture following completion of the 5000-hour endurance test. The split inner sheet metal cylinder is the tantalum heating element. An image of one of the transformer support posts can be seen in each half of the cylinder, and also part of the support fixture platform. The brightness of the reflections on the heater element as well as the brightness of the tantalum heat shield cylinders is a good indication that the specimen materials which outgassed during the test did not include corrosive compounds as far as tantalum is concerned.

Figure IV-20 is a view of one solenoid partially disassembled after completion of the 5000-hour test. The weight has been removed from the plunger, the plunger stop plate and end bell removed from the housing, and the plunger extracted. W-839 potting compound was spread across the winding alumina end plate at assembly before the end bell was installed, to accommodate axial clearance between the winding assembly and the housing and end bell assembly. The potting compound apparently

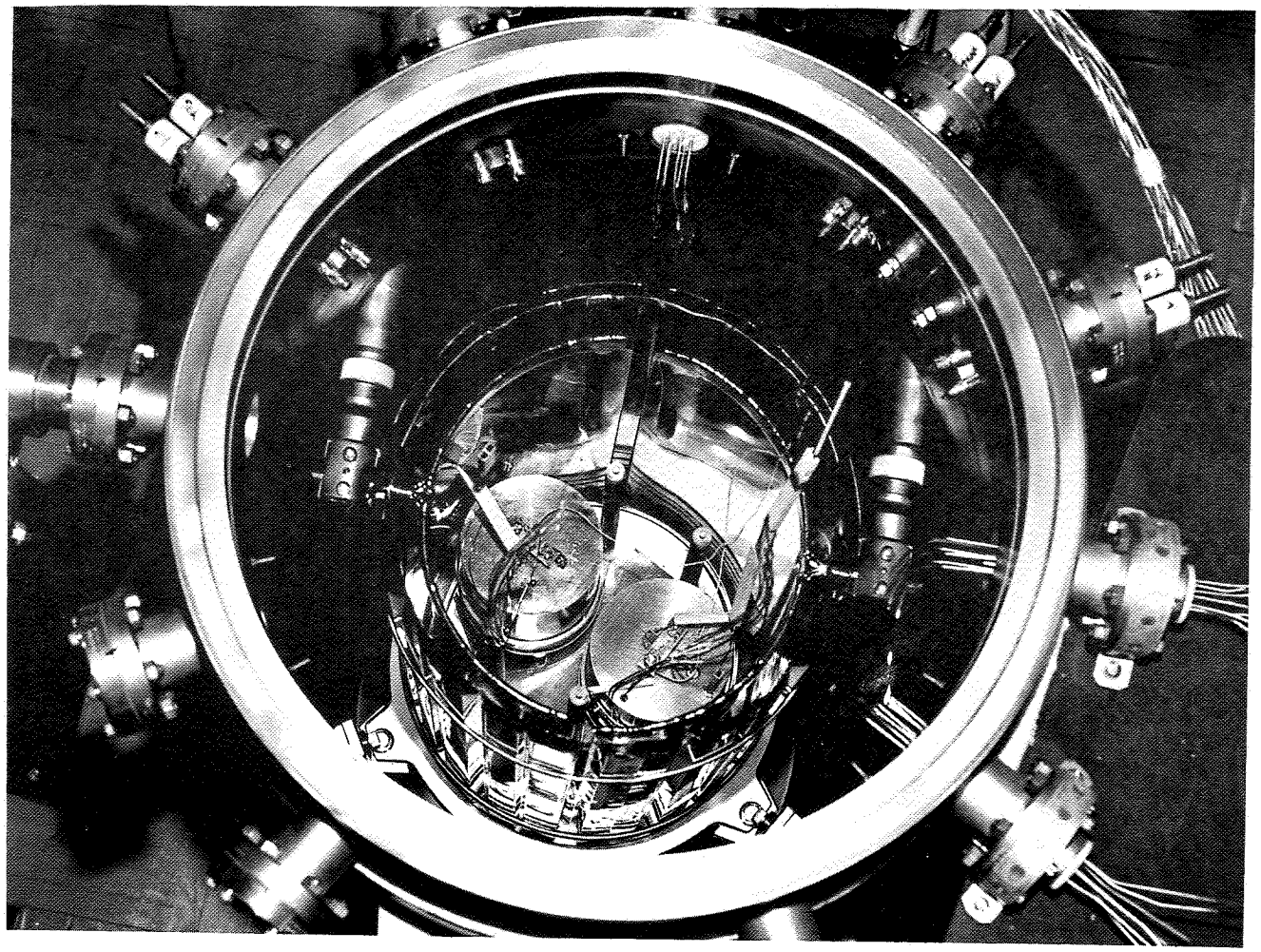

FIGURE IV-19. View of Solenoids in Test Chamber With Transformer Removed

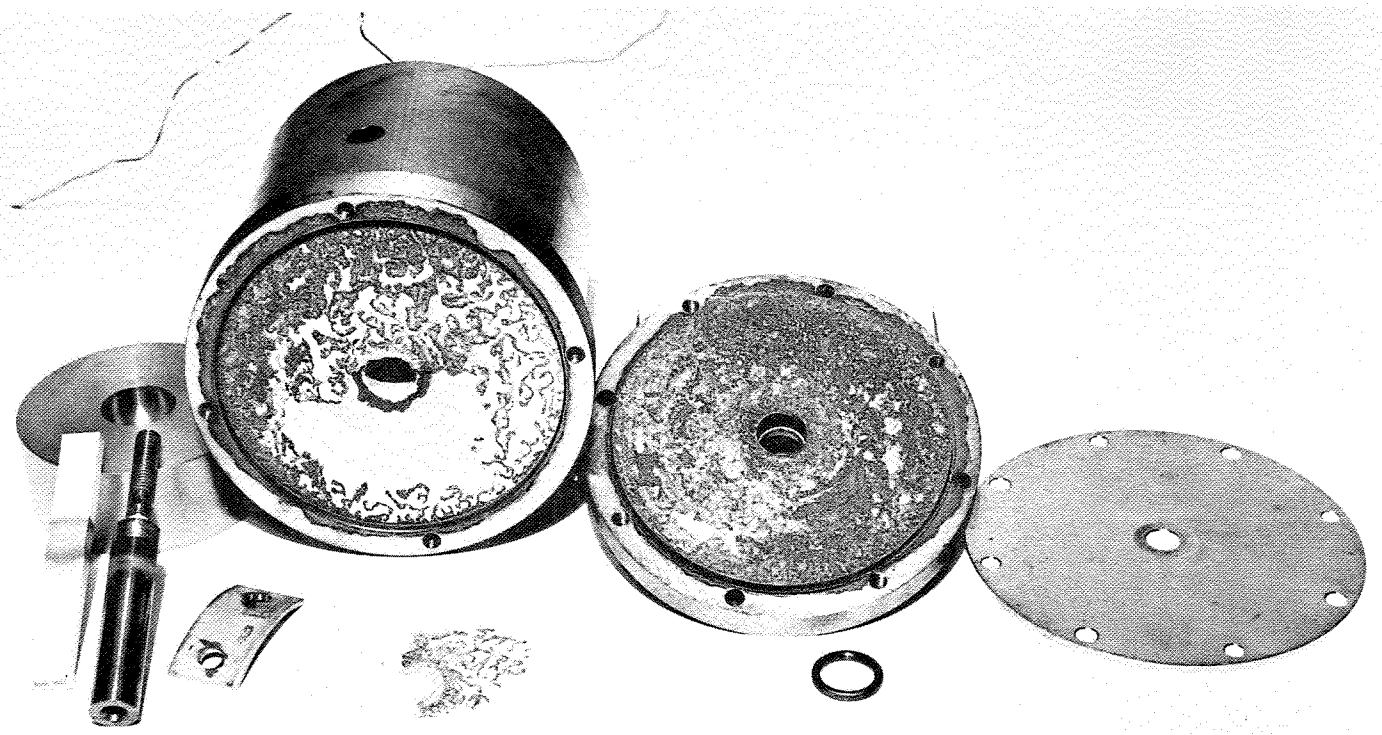

FIGURE IV-20. Solenoid S/N 1 Partially Disassembled After Completion of 5000-Hour Test

reacted with the cobalt in the Hiperco 27 alloy forged end bell during the course of the test. The dark areas showing on the end plate potting compound and the inside surface of the end bell are a dark blue in color. Some stains can be seen near the threaded end of the plunger, although there was no build-up on the shaft.

As with the other specimens, disassembly and analysis of the solenoid was postponed to concentrate on the next phase of the program. This activity will be continued in the next program quarter and reported in the next report. A vibration scan test will also be carried out on the other solenoid and the results reported in the next report.

c. STATUS OF 1300°F SOLENOID MODEL - 2nd 5000-HOUR TEST

The 1300°F solenoid test model design is the same as the 1100°F model except for three materials changes. Inconel-clad silver wire replaces nickel-clad silver wire and the Anadur insulation on the wire will be "S" glass in place of "E" glass. Boron nitride cement replaces W-839 encapsulating compound. The reasons for these changes are the same as those detailed in the 1300°F stator model write-up.

3. Program for the Next Quarter

a) Put one 1100°F test solenoid through a vibration scan and complete post-test disassembly and inspection as required.

b) Complete assembly of the 1300°F hot spot solenoid test models.

c) Install the two 1300°F models in a thermal-vacuum chamber and begin a 5000-hour high-temperature, high-vacuum endurance test.

SECTION V

REFERENCES

Reports published on this program are:

Kueser et al, P. E., "Development and Evaluation of Magnetic and Electrical Materials Capable of Operating in the 800° to 1600°F Temperature Range", First Quarterly Report, NASA-CR-54354, March 1965.

Kueser et al, P. E., "Development and Evaluation of Magnetic and Electrical Materials Capable of Operating in the 800° to 1600°F Temperature Range", Second Quarterly Report, NASA-CR-54355, June 1965.

Kueser et al, P. E., "Development and Evaluation of Magnetic and Electrical Materials Capable of Operating in the 800° to 1600°F Temperature Range", Third Quarterly Report, NASA-CR-54356, September 1965.

Kueser et al, P. E., "Development and Evaluation of Magnetic and Electrical Materials Capable of Operating in the 800° to 1600°F Temperature Range", Fourth Quarterly Report, NASA-CR-54357, December 1965.

Kueser et al, P. E., "Development and Evaluation of Magnetic and Electrical Materials Capable of Operating in the 800° to 1600°F Temperature Range", Fifth Quarterly Report, NASA-CR-54358, March 1966.

Kueser et al, P. E., "Development and Evaluation of Magnetic and Electrical Materials Capable of Operating in the 800° to 1600°F Temperature Range", Sixth Quarterly Report, NASA-CR-54359, June 1966.

References cited in this report follow and are grouped by Program and Task.

SECTION II

Program I - Magnetic Materials for High-Temperature Operation

References for Task 1 - Optimized Precipitation Hardened Magnetic Materials for Application in the 1000° to 1200°F Range.

1. Detert, K., Untersuchungen des Ausscheidungsverhaltens in Hochfesten Martensitaushärtenden Nickelstählen, Archiv Eisenhüttenw. V. 37, 1966.

2. Detert, K., Transformation and Precipitation in 15 percent N: Maraging Steel, Trans. ASM V. 59, p. 262, 1966.

3. Kueser, P. E., Magnetic Materials Topical Report, NASA-CR-54091, Contract NAS3-4162, 1964.

4. Detert, D., and Pohl, H., Untersuchungen über die Ausscheidungsvorgänge in Kobalt-Nickel-Legierungen mit Aluminium und Titan-Zusätzen, Z. Metallkunde, V. 57, P. 130, 1966.

5. Detert, K. and Pohl, H., Untersuchungen über die Ausscheidungsvorgänge in Nickel-und Nickel-Kobalt-Legierungen mit Aluminium-Titan-Zusätzen, Z. Metallkunde, V. 55, p. 36, 1965.

6. Hornbogen, E. and Kreye, H., Anomale Änderungen des spez. Elektrischen Widerstandes in Nickel-Aluminium-Legierungen, Z. Metallkunde, V. 57, p. 122, 1966.

7. Mihalisin, J. R. and Decker, R. F., Phase Transformations in Nickel-Rich Nickel-Titanium-Aluminium Alloys, Trans. AIME, V. 218, p. 507, 1960.

8. Mitchell, W. I., Über das Aushärtungsverhalten Einer Komplexen Legierung auf Nickel Basis. Z. Metallkunde, V. 55, p. 613, 1955.

9. Dragsdorf, R. D. and Forgeny, W. D., The Intermetallic Phases in the Co-Ta System, Acta. Cryst. V. 15, p. 531, 1962.

10. Hafley, W. L., Wilkinson, J. W., and Fardo, R., A Versatile Computer Program for Regression (curve fitting) Problems - II, Research Report 64-1C4-362-R1.

11. Peters, D. T. and Cupp, C. R., The Kinetics of Aging Reactions in 18% Ni Maraging Steels, Trans. AIME, in press.

SECTION IV

Program III - Bore Seal Development and Combined Material Investigation Under a Space-Simulated Environment

References for Task 1 - Bore Seal Development

1. Private Communication, R. J. Brown, Brush Beryllium Company to R. McRae, EIMAC, July 18, 1966.

2. Private Communication, L. A. Garling, Brush Beryllium Company to A. J. Manthos, EIMAC, July 11, 1966.